Differences between the last two glacial maxima and implications for ice-sheet, $\delta^{18}O$, and sea-level reconstructions

Eelco J. Rohling[1,2*], Fiona D. Hibbert[1*], Felicity H. Williams[1,2*], Katharine M. Grant[1], Gianluca Marino[1], Gavin L. Foster[2], Rick Hennekam[3,4], Gert J. de Lange[4], Andrew P. Roberts[1], Jimin Yu[1], Jody M. Webster[5], and Yusuke Yokoyama[6-8]

1. Research School of Earth Sciences, The Australian National University, Canberra, ACT, 2601, Australia.
2. Ocean and Earth Science, University of Southampton, National Oceanography Centre, Southampton SO14 3ZH, UK.
3. Department of Ocean Systems, Royal Netherlands Institute for Sea Research (NIOZ), and Utrecht University, P.O. Box 59, 1790 AB Den Burg, Texel, The Netherlands.
4. Department of Earth Sciences-Geochemistry, Faculty of Geosciences, Utrecht University, Utrecht, The Netherlands.
5. School of Geosciences, The University of Sydney, NSW, 2006, Australia.
6. Atmosphere and Ocean Research Institute, The University of Tokyo, 5-1-5 Kashiwanoha, Chiba 277-8564, Japan.
7. Department of Earth and Planetary Science, Graduate School of Science, The University of Tokyo, 7-3-1 Hongo, Bunkyoku, Tokyo 113-0033, Japan.
8. Department of Biogeochemistry, Japan Agency for Marine-Earth Science and Technology, 2-15 Natsushimacho, Yokosuka 237-0061, Japan.

* = joint first authors

Abstract. Studies of past glacial cycles yield critical information about climate and sea-level (ice-volume) variability, including the sensitivity of climate to radiative change, and impacts of crustal rebound on sea-level reconstructions for past interglacials. Here we identify significant differences between the last and penultimate glacial maxima (LGM and PGM) in terms of global volume and distribution of land ice, despite similar temperatures and radiative forcing. Our analysis challenges conventional views of relationships between global ice volume, sea level, seawater oxygen isotope values, and deep-sea temperature, and supports the potential presence of large floating Arctic ice shelves during the PGM. The existence of different glacial 'modes' calls for focussed research on the complex processes behind ice-age development. We present a glacioisostatic assessment to demonstrate how a different PGM ice-sheet configuration might affect sea-level estimates for the last interglacial. Results suggest that this may alter existing last interglacial sea-level estimates, which often use an LGM-like ice configuration, by several metres (likely upward).

Keywords

Last Glacial Maximum, Penultimate Glacial Maximum, sea level, ice volume, $\delta^{18}O$, Arctic ice shelf, Last Interglacial, glacioisostatic adjustment

1. Introduction

The volume and spatial distribution of continental ice masses during ice ages over the last 3 million years have been the focus of much research for several reasons. First, temporal changes in the radiative balance of climate are important because ice masses have high albedo and reflect incoming solar radiation (e.g., Hansen et al., 2007, 2008; Köhler et al., 2010, 2015; Rohling et al., 2012; PALAEOSENS project members, 2012; Martínez-Botí et al., 2015; Friedrich et al., 2016). Second, temporal development of ice-age cycles provides critical information about the nature of long-term climate cooling over the past few million years, in response to CO_2 reduction and interactions among ice, land cover, and climate (e.g., Clark et al., 2006; Köhler and Bintanja, 2008; de Boer et al., 2010, 2012; Hansen et al., 2013). Third, variable amplitude of individual ice ages helps to determine the relationship between climate change, astronomical climate forcing cycles, and climate feedbacks on timescales of 10s to 100s of kiloyears (e.g., Oglesby, 1990; Imbrie et al., 1993; Raymo et al., 2006; Colleoni et al., 2011, 2016; Ganopolski and Calov, 2011; Carlson and Winsor, 2012; Abe-Ouchi et al., 2013; Hatfield et al., 2016; Liakka et al., 2016). Fourth, the size and spatial distribution of land ice during past glacials determines crustal rebound processes when ice masses melt, which in turn affects sea-level reconstructions for subsequent interglacials. The latter are key to investigations of sea-level changes above the present level during warmer-than-present interglacials (e.g., the Last Interglacial, LIG, ~130-118 kyr ago (ka); Hibbert et al., 2016; Hoffman et al., 2017; Hansen et al., 2017), which can reveal ice-sheet disintegration processes of relevance to the future (e.g., Dutton and Lambeck, 2012; Dutton et al., 2015a,b; Yamane et al., 2015; DeConto and Pollard, 2016).

Despite the relevance of these issues, we lack detailed information about ice volumes and their spatial extent during glacial maxima. Based on intervals of maximum global ice volume (lowest sea level), the Last Glacial Maximum (LGM) spanned the ~26.5–19 ka interval (Clark et al., 2009), while the Penultimate Glacial Maximum (PGM) spanned ~155–140 ka, comprising two sea-level minima separated by a minor rise centred on ~145 ka (Grant et al., 2014). In general, we know most about the LGM, and information decreases markedly for older glacial maxima. Even for the PGM, information is so limited that studies often invoke an LGM-like ice volume (e.g., Lambeck and Chappell, 2001; Yokoyama and Esat, 2011). Initial assessment of Red Sea glacial sea-level lowstands seemed to support that view (Rohling et al., 1998), but only constrained the LGM sea-level drop to have been at least as low as that of the PGM, without giving a maximum value. Here we show that subsequent improvements to the Red Sea record firmly indicate a greater sea-level drop during the LGM than during the PGM. Independent evidence from western Mediterranean palaeo-shorelines also suggests that the LGM sea-level drop exceeded the PGM sea-level drop by about 10 m (Rabineau et al., 2006).

Robust quantitative assessment of sea-level differences between the last two glacial maxima is especially important because their spatial ice-mass distributions were markedly different (Table 1 summarises previously modelled ice-volume changes, relative to the present). Geological data and numerical modelling strongly suggest that the Eurasian ice sheet (EIS) covered a larger area during the PGM than during the LGM (Svendsen et al., 2004; Colleoni et al., 2011, 2016) (Figure 1), with most estimates suggesting a PGM EIS volume equivalent to a 33-53 m global sea-level fall (sea-level equivalent, SLE) (Table 1); this is approximately twice the size of the LGM EIS (14-29 m_{SLE}; Table 1 and Clark and Tarasov, 2014). Such contrasting ice-mass distributions between successive glacial maxima highlight significant complexity in the processes that drive glaciation into different 'modes' (e.g., Liakka et al., 2016). The difference also has repercussions for glacioisostatic adjustment (GIA) studies of sea-level history during the LIG, which was about 1 °C warmer than the Holocene (Clark and Huybers,

2009; Turney and Jones, 2010; McKay et al., 2011; Hoffman et al, 2017; Hansen et al., 2017), with sea levels that reached 4 to 10 m higher than today (Rohling et al., 2008; Dutton and Lambeck, 2012; Grant et al., 2012; Stocker et al., 2013; Dutton et al., 2015a, 2015b). Dendy et al. (2017) investigated the sensitivity of the predictions of the last interglacial highstand to uncertainties in the configuration of the major northern hemisphere ice sheets during MIS 6. They focused on the sensitivity of the GIA correction to three major components of sea-level uncertainty during the MIS 6/5 transition: the age model and duration of deglaciation; the number of glacial cycles modelled during the GIA analysis; and the relative distribution of ice volume between the North American and Eurasian ice sheets, assuming that total ice volume for these complexes remained the same at MIS 2 and MIS 6. A key result is that sensitivity to different ice-sheet configurations is in the ~5 m range (relative to the +4 to +10 m observed for LIG sea level). This calls for exploration of further total ice-volume and ice-mass distribution scenarios for the MIS 6/5 transition.

Little evidence exists regarding the PGM North American Ice Sheet complex (NAIS), because the LGM advance obliterated virtually all PGM glaciomorphological evidence (we use EIS and NAIS to refer to all Eurasian and North American ice sheets, respectively, rather than separating all ice masses). For example, even when assuming an LGM-like (~130 m_{SLE}, Clark et al., 2009) or smaller total PGM sea-level drop, with comparable Antarctic ice volume (Table 1) and a 33 to 53 or even 71 m_{SLE} EIS (Table 1), it follows that the NAIS must have been smaller than during the LGM. There is GIA modelling support for a smaller PGM NAIS to account for sea-level observations in Bermuda (Potter and Lambeck, 2003; Wainer et al., 2017), and climate modelling results agree best with global environmental proxy data in scenarios that combine a large EIS with a small NAIS (~30 m_{SLE}) (Colleoni et al., 2016). The lack of glaciomorphological evidence for the PGM NAIS also qualitatively supports a larger NAIS at the LGM than at the PGM.

Here we compile highly resolved data from multiple mutually independent sea-level reconstruction methods to gauge PGM sea level relative to the LGM. All have methodological and glacioisostatic uncertainties, and chronological uncertainties affect comparisons between records. But within individual records from the same method, high coherence is commonly achieved. Hence, confidence is higher for PGM–LGM comparisons within individual records than for relative sea-level comparisons among records. We use our PGM–LGM sea-level compilation in conjunction with a glaciogeomorphological synthesis of the PGM EIS and NAIS extent (Figure 1, Appendix I; see acknowledgements for data access), as well as information from published ice-sheet modelling studies, to test the small-NAIS hypothesis. We then consider the implications of PGM–LGM differences in ice volume and extent, with respect to: 1) concepts of glacial inception; 2) glacioisostatic corrections to last interglacial sea levels; and 3) global sea-level/ice-volume/$\delta^{18}O$ relationships.

2. PGM–LGM sea-level comparison

We use five primary data sources to quantify PGM *versus* LGM ice volume/sea level (Figure 2, Table 2). The first two are (near) continuous relative sea-level records derived from surface-water $\delta^{18}O$ residence-time effects in the highly evaporative Red Sea and Mediterranean Sea (Siddall et al., 2003; Rohling et al., 2014). The third source is a (near) continuous time-series of past ice volume/sea level from deep-sea seawater $\delta^{18}O$, hereafter named δ_{sw} (e.g., Martin et al., 2002; Sosdian and Rosenthal, 2009; Elderfield et al., 2012). The fourth source for our assessment of a PGM–LGM sea-level offset concerns fossil coral position data (Z_{cp}) from a comprehensive database that has been harmonised in terms of dating and uplift-correction protocols (Hibbert et al., 2016). The fifth source consists of western Mediterranean palaeo-shorelines (Rabineau et al., 2006). The latter was discussed before, while the other four sources are detailed below.

2.1. Red Sea and Mediterranean records

The marginal-sea method for sea-level reconstruction relies on the fact that water residence time in the highly evaporative, semi-enclosed Red Sea and Mediterranean Sea is a function of sea-level change because of the narrow and shallow straits that connect the basins with the open ocean. In today's Red Sea, the Bab-el-Mandab Strait is only 137 m deep, mean annual evaporation is ~2 m y^{-1}, and the basin has a narrow catchment with no major river systems or other hydrological complications (Siddall et al., 2004). For the Mediterranean, the Strait of Gibraltar is 284 m deep, mean annual evaporation is ~1 m y^{-1}, and large river systems provide considerable hydrological complications. Thus, relative sea-level reconstructions have a higher signal-to-noise ratio at Bab-el-Mandab than at Gibraltar. Accordingly, 1σ precision of individual Red Sea values from this method is about ±6 m (Siddall et al., 2003, 2004), compared with ±9 m to ±14 m for individual Mediterranean values at interglacial to glacial conditions, respectively (Rohling et al., 2014). Near-continuous records can be evaluated probabilistically, accounting for both age uncertainties and sea-level uncertainties. These assessments identify probability maxima and their 95% probability bounds (Grant et al., 2012, 2014; Rohling et al., 2014), which we use here. The two basins are independent; they are not connected, and link with separate oceans with different climate and ocean circulation dynamics (Schott et al., 2009; Buckley and Marshall, 2016).

A data-gap exists in the Red Sea LGM record due to an indurated layer without planktonic foraminifera (e.g., Fenton et al., 2000 and references therein); only a few sea-level values could be recovered from this "aplanktonic" layer (Figure 2b). However, sparse LGM data from bulk carbonate are supported by other Red Sea records that indicate a 5-5.5 ‰ change in foraminiferal $\delta^{18}O$ between the LGM and present (Arz et al., 2003, 2007), compared with 4 ‰ between the PGM and present (Rohling et al., 2009). Moreover, the aplanktonic LGM Red Sea conditions offer strong independent evidence that LGM sea level was lower than in the PGM. It formed under extreme salinities (S = ~50 to ~70) due to near-isolation of the Red Sea from

145 the world ocean by the shallow Hanish Sill, Bab-el-Mandab Strait (~137 m deep, relative to an
146 LGM global mean sea-level drop of ~130 m); such extreme conditions were not reached
147 during the PGM (Rohling et al., 1998; Fenton et al., 2000; Siddall et al., 2003). This implies
148 either that: (*a*) the sill was uplifted between the PGM and LGM; and/or (*b*) sea level dropped
149 more during the LGM than the PGM. Sill uplift has been quantified at 0.02 to 0.04 m kyr^{-1},
150 which gives at most 5 m of uplift from PGM to LGM (Rohling et al., 1998; Siddall et al., 2003).
151 This is insufficient to explain the large LGM-to-PGM environmental contrast, so we conclude
152 that sea level dropped much more during the LGM than in the PGM.
153
154 Our new Mediterranean $\delta^{18}O$ stack-based RSL record (Figures 2a, 3) includes $\delta^{18}O$ data from
155 four cores: LC21 (35° 40' N, 26° 35' E, 1522 m water depth) (Grant et al., 2012); MS21
156 (32°20.7'N, 31°39.0'E, 1022 m water depth) (Hennekam, 2015); M40-67 (34.814167°N,
157 27.296000°E, water depth 2157 m), and M40-71 (34.811160°N, 23.194160°E, water depth
158 2788 m) (Weldeab et al., 2003a,b). $\delta^{18}O$ records include data for the surface-dwelling
159 planktonic foraminifer *Globigerinoides ruber* (white) for all cores, and for the subsurface-
160 dwelling planktonic foraminifer *Neogloboquadrina pachyderma* (dextral) for core LC21
161 (habitats after Rohling et al., 2004), and we use conversions to sea level after Rohling et al.
162 (2014). The age model for each core is based on tuning to the Soreq Cave (Israel) speleothem
163 $\delta^{18}O$ record (Bar-Matthews 2003; Grant et al., 2012; Hennekam 2015), and recalibrating
164 original ^{14}C datings with the most recent ^{14}C calibration curve (Reimer et al., 2013) using a ΔR
165 value of 35±70 years (Siani et al., 2000).
166
167 In the Mediterranean, the marginal-basin method has limitations at times of strong northern
168 hemisphere insolation maxima, when African monsoon intensification led to large-scale
169 freshwater flooding into the basin from the Nile and other (now dry) North African river
170 systems (e.g., Rohling et al., 2002, 2004, 2014, 2015; Larrasoaña et al., 2003; Scrivner et al.,

2004; Osborne et al., 2008; Hennekam, 2015). Such times are identified in Mediterranean sediment cores based on sharply delineated intervals of low surface-water oxygen isotope ($\delta^{18}O$) anomalies (Fig. 3), increased sediment organic-matter accumulation under low-oxygen to anoxic deep-water conditions, and sediment barium enrichments (for a review, see Rohling et al., 2015). These organic-rich intervals are known as sapropels. Some sapropels have been oxidised after deposition (ghost sapropels), or organic carbon burial remained limited due to continued deep-water ventilation (missing sapropels), but in those cases the intervals can still be identified using other characteristic signals (Rohling et al., 2014). Hence, sapropel intervals are easily identified, and they do not affect our Mediterranean-based RSL values for the LGM or PGM (Figures 2, 3).

For both the Red Sea and Mediterranean records, individual data values (with uncertainties in both age and sea-level value) are not instructive for determining the PGM–LGM difference. Instead the overall structure of the records needs to be used, which accounts for covariations and autocorrelations within the record (systematic elements in the uncertainties). For this, we use Monte-Carlo-style probabilistic evaluations of the highly resolved data series that determine the probability maximum (modal value) and its 95% probability interval. Here we use published results for the Red Sea (Grant et al., 2012) and new results from the same method for our new Mediterranean stack (Figures 2a,b). Good signal agreement exists between the Mediterranean and Red Sea records, except during the sharply delineated Mediterranean sapropel intervals. In those intervals, freshwater-induced low-$\delta^{18}O$ surface-water conditions (e.g., Rohling et al., 2002, 2004) yield spurious (high) sea-level extremes in the Mediterranean reconstruction (Figures 2b, 3), which can be discarded when identified using associated sapropel indicators (Rohling et al., 2014, 2015).

2.2. Deep-sea seawater $\delta^{18}O$

Highly resolved time-series of past sea-level variability can also be obtained from δ_{sw} data (e.g., Sosdian and Rosenthal, 2009; Martin et al., 2002; Elderfield et al., 2012). These are derived

198 from benthic foraminiferal carbonate $\delta^{18}O$ data (δ_c) that are corrected for temperature
199 changes using Mg/Ca analyses of the same benthic foraminifera (Martin et al., 2002; Sosdian
200 and Rosenthal, 2009; Elderfield et al., 2010, 2012). Variations in δ_{sw} primarily represent
201 global ice-volume changes that are related to global sea-level changes via isotope mass-
202 balance calculations. But deep-sea temperature changes are relatively small (~3 °C between
203 glacials and interglacials), and the Mg/Ca method cannot resolve them to better than about
204 ±1 °C (1σ). Note that the deep-sea δ_{sw} method also involves assumptions about the ice-$\delta^{18}O$
205 value when converting δ_{sw} into ice-volume estimates (this is further discussed on the basis of
206 results from this study, in section 4.3). Overall, the deep-sea δ_{sw} method yields individual sea-
207 level estimates with uncertainties of about ±30 m. Again, probabilistic assessment of highly
208 resolved, coherent δ_{sw} records from single cores with strictly constrained stratigraphy allows
209 recovery of the overall structure of changes with narrower uncertainties. Therefore, we use
210 the results from a probabilistic assessment of a single coherent δ_{sw} record of SW Pacific
211 abyssal waters that likely presents a well-integrated global signal (Elderfield et al., 2012).
212 Specifically, we use a probabilistic assessment of that record, which highlights the overall
213 signal structure, and accounts for both chronological and sea-level uncertainties (Rohling et
214 al., 2014) (Figure 2c).

215 ## 2.3. Fossil coral data

216 Fossil corals provide valuable insights into past changes in sea level. However, they are
217 discrete rather than continuous estimates and are associated with several locational (tectonic
218 and glacio-isostatic) as well as biological (e.g., palaeo-water depth) assumptions. For coral-
219 based evidence of past sea levels, we extract fossil coral position data (Z_{cp}) from the
220 methodologically harmonised database of Hibbert et al. (2016), with 2σ uncertainties (Figure
221 2d). We consider only samples that pass the following screening criteria: (*a*) % calcite < 2; (*b*)
222 ^{232}Th concentration < 2 ppb; and (*c*) $\delta^{234}U_{initial}$ = 147 ±5 ‰ (ages <17 ka and 71 to 130 ka),
223 $\delta^{234}U_{initial}$ = 142 ±8 ‰ (ages 17 to 71 ka), and $\delta^{234}U_{initial}$ = 147 $^{+5}/_{-10}$ ‰ (ages >130 ka).
224

225 It is difficult to use fossil corals to determine sea-level lowstands of glacial maxima before the
226 LGM because the evidence is hidden at poorly accessible water depths, buried under younger
227 sediments, or overgrown by corals from subsequent lowstands. Consequently, no site
228 currently has both LGM and PGM coral sea-level estimates. Drill cores from Tahiti, however,
229 have corals from the PGM (Thomas et al., 2009) as well as corals 'bracketing' the LGM (Bard et
230 al., 1996, 2010; Thomas et al., 2009; Deschamps et al., 2012). Tahiti is also unusual in that it
231 has independently constrained subsidence rates (based on radiometrically dated lava flows;
232 Bard et al., 1996; Le Roy, 1994), which – when assumed to be constant through time – help in
233 obtaining good tectonically corrected elevations. A drill core from Tiarei (Tahiti; Thomas et al.,
234 2009) has in-growth-position corals of the same genus (*Porites* sp.) for the PGM and the end of
235 Marine Isotope Stage 3 (end of MIS 3; ~29 ka). While taxonomically similar, these corals are
236 from different assemblages and have been assigned different palaeo-waterdepth estimates,
237 with the MIS 3 samples likely representing a deeper, fore-reef setting (Montaggioni, 2005).
238 The same site (Tiarei) also has a taxonomically different in-growth-position coral at a similar
239 tectonically corrected elevation as the MIS 3 corals, dated to ~16 ka (*Pocillopora* sp.,
240 Deschamps et al., 2012). Taken together, the corals dated at ~29 ka and 16 ka provide a
241 minimum estimate of the LGM sea-level drop, given that LGM sea level likely fell below the
242 elevation of these 'bracketing' corals. Based on this minimum LGM sea-level-drop estimate,
243 we infer a coral-based minimum estimate for the PGM–LGM sea-level difference of ~14 m. If
244 the mean Z_{cp} values for the end-of-MIS 3 and PGM corals are taken at face value (taking the
245 end-of-MIS 3 as indicative of the LGM), then the inferred PGM–LGM sea-level difference is ~27
246 m (Figure 2d). Note that comparison with Barbados LGM data (also *Porites*; Bard et al., 1990;
247 Fairbanks et al., 2005) suggests a potentially greater PGM–LGM offset (~41 m), but this
248 estimate is subject to differences between the geological and glacioisostatic settings of
249 Barbados and Tahiti. We therefore concentrate on the 'face-value' estimate from Tahiti as the
250 most representative coral-based estimate (Figure 2d, Table 2).
251

We do not suggest that the data in Figure 2d represent a finished coral-based sea-level record because that would require – most importantly – additional high-quality coral data for both the LGM and PGM, and additional study-specific considerations that include stratigraphic and biological assemblage arguments, and glacioisostatic corrections among sites (for discussion, see Hibbert et al. (2016) and references therein). Given the current limited availability of (screened) data, such a complete assessment is not yet feasible. Instead, we merely use the data to show amplitude agreement between coral data and other reconstructions, and then focus on the PGM–LGM difference.

2.4. Synthesis of PGM–LGM sea-level contrasts

The depth difference (Δz) between PGM and LGM sea-level estimates is highlighted in Figure 2 for each method considered, including the western Mediterranean palaeo-shoreline evidence of Rabineau et al. (2006) (see also Table 2). We find that all five methods (six with two coral options) reveal a coherent PGM–LGM sea-level offset with mean Δz = 21 ±14 m (95% probability). In IPCC terminology (Stocker et al., 2013), therefore, it is virtually certain for the PGM–LGM that Δz exceeds 0 m, and extremely likely that Δz falls between 7 and 35 m. The fact that the five methods are independent of each other is strong validation of our Δz observations. Furthermore, a lower LGM global sea level (hence a larger global ice volume), relative to the PGM, agrees qualitatively with glacial-cycle model results driven by astronomical cycles and greenhouse gas (CO_2) fluctuations (Δz = ~10 m) (Abe-Ouchi et al., 2013), and with the aforementioned Red Sea aplanktonic-zone observations.

To test the sensitivity of our approach for detecting sea-level differences, we also compare sea levels for the PGM with those for MIS 4 (Table 3, Figure 2). Observed $\Delta z_{PGM-MIS4}$ values are both positive and negative. Even if the anomalous value with negative $\Delta z_{PGM-MIS4}$ is omitted, the 95% probability bounds for mean $\Delta z_{PGM-MIS4}$ still overlap with zero. At 95% probability,

277 therefore, PGM and MIS 4 sea levels cannot be distinguished, whereas PGM and LGM sea level
278 were clearly different.

279 # 3. PGM–LGM contrasts in ice extent and volume

280 ## 3.1. Synthesis of PGM ice-sheet extents, mapping and dating

281 Extensive mapping of glacial features (moraines, till and glacial outwash sequences, etc.)
282 suggests that the southern limit of the EIS extended much further to the south during
283 the Saalian maximum, relative to the LGM (see compilation of Svendsen et al. (2004),
284 updated in Ehlers et al. (2011a) and references therein). The Saalian complex of
285 glaciogenic landforms and sediments includes multiple glacial episodes between the
286 Holsteinian and Eemian interglacials (Gibbard and Cohen, 2008), including the PGM. The
287 maximum extent of each of these glaciations was not necessarily reached at the same
288 time along the entirety of the ice margin; effectively they were spatially variable and
289 diachronous glacial maxima. The PGM limits are well-documented only for the SW
290 margins of the EIS (e.g., Netherlands, Busschers et al., 2005, 2008; Laban and van der
291 Meer, 2004, 2011 and references therein; Germany, Ehlers et al., 2011b; Litt et al., 2007;
292 Poland, Marks, 2011 and references therein). Reconstructions for the eastern sector are
293 more tentative (e.g., Astakhov, 2011, 2013; Velichko et al., 2011; Möller et al., 2015;
294 Astakhov et al., 2016), and much of the literature is restricted to Russian sources (for
295 reviews, see Astakhov, 2013, Astakhov et al., 2016).
296
297 The record of the PGM glaciation in North America is more fragmentary than that for
298 Eurasia. In general, the Laurentide LGM ice limits are the most extensive (e.g., Dyke et
299 al., 2002), except for some protrusions of older glacial material, e.g., in Illinois (type
300 section for the pre-LGM Illinoian glaciation that includes the PGM, Curry et al., 2011),
301 where several glacial till members and glacial ridges extend beyond the Wisconsinan
302 (LGM) limits, with OSL constraints that suggest three advances within MIS 6 (McKay and

303 Berg, 2008; McKay et al., 2008; Webb et al., 2012). More extensive pre-LGM (including
304 Illinoian) ice limits have also been reported in Ohio (e.g., Pavey et al., 1999; Szabo and
305 Totten, 1995; Szabo et al., 2011; Fugitt et al., 2016), Pennsylvania (Braun, 2011 and
306 references therein), Missouri (e.g., Rovey and Balco, 2011), and Wisconsin (Syverson
307 and Colgan, 2011), but age control and correlations are problematic. For the Cordilleran
308 Ice Sheet (contributing to our broad NAIS interpretation), continental-ice presence is
309 documented in NW Canada and Alaska only for the Late Pleistocene (i.e., post-PGM). The
310 sedimentary record captures a succession of plateau/montane glaciations (often
311 successively less extensive than the previous), but only a single continental glaciation
312 (Liverman et al., 1989; Jackson et al., 1991; Young et al., 1994; Duk-Rodkin et al., 1996;
313 Harris, 2005; Barendregt and Duk-Rodkin, 2011; Clague and Ward, 2011; Jackson et al.,
314 2011; Demuro et al., 2012; Turner et al., 2013). Uncertain, and often inconsistent age
315 control again hinders correlation of these pre-LGM glaciations (e.g., Stroeven et al., 2010,
316 2014).
317
318 Marine records offer a (potentially) continuous record of PGM ice-sheet dynamics. The
319 input of ice-rafted debris (IRD) allows reconstruction of ice sheet dynamics, ice source,
320 and iceberg-melt location (Ruddiman, 1977; Bond and Lotti, 1995; Hemming, 2004). The
321 marine record of Eurasian glacial episodes (e.g., Spielhagen et al., 2004; Sejrup et al.,
322 2005; Toucanne et al., 2009; Obrochta et al., 2014; Löwemark et al., 2016) and
323 geophysical mapping (e.g., Polyak et al., 2001, 2004; Jakobsson et al., 2010; Niessen et
324 al., 2013; Dove et al., 2014), indicate differences between the LGM and PGM glaciations,
325 with suggestions that the PGM/MIS 6 glaciation was one of the more extensive glacial
326 episodes. Conversely, IRD from North America (Hudson Strait) does not seem to have
327 reached the North Atlantic IRD belt during the penultimate glacial cycle (Obrochta et al.,
328 2014), while it still occurred in the Labrador Sea, in close proximity to the eastern North
329 American margin (Channell et al., 2012). This contrasts with large quantities of North

American IRD in the IRD belt during the last glacial cycle (e.g., Ruddiman, 1977; Hemming, 2004), which suggests likely differences in ice-mass distribution and ice-stream dynamics between the PGM and LGM NAIS.

Robust correlations and chronology of mapped pre-LGM ice advances have proven elusive, not least due to difficulties in continental-scale correlation of glacial features/stratigraphic units and the proliferation of stratigraphic terminology. These difficulties are compounded when comparing terrestrial records of glaciation with marine records (e.g., Mix et al., 2001). For example, the last glacial interval in the marine record, MIS2 (Imbrie et al., 1984; Martinson et al., 1987; Lisiecki and Raymo, 2005), represents an interval of maximum global ice volume, which does not necessarily correspond to the timing of maximum mapped glacial extents on land, which are themselves globally asynchronous (e.g., Ehlers and Gibbard, 2007). Correlations between glacial units, and correlations to the marine record are also affected by methodological constraints of the various absolute dating methods. The PGM falls outside the range of the radiocarbon method, and for other absolute methods (optically stimulated luminescence (OSL) and cosmogenic nuclide dating) care must be taken with both sampling and interpretation because of inherent methodological assumptions (e.g., Aitken, 1998; Gosse and Phillips, 2001) and geological uncertainties (e.g., erosion, prior exposure and shielding issues associated with cosmogenic nuclide dating, Fabel and Harbor, 1999; Putkonen and Swanson, 2003; and incomplete bleaching of quartz and feldspar grains in glacial settings for OSL dating, e.g., Gemmell, 1988). Relative age control for some glacial sediments has been achieved using the stratigraphic position of glacial deposits relative to interglacial sediments (e.g., peats, the ages of which are occasionally constrained by U-series dating), and tephra (e.g., the Old Crow tephra that provides a youngest age limit for underlying glaciogenic sediments in North America; e.g., Ward et al., 2008). Available PGM terrestrial evidence for the EIS with currently

357 available dating constraints is summarised in Figure 1. Note that we make no judgement
358 regarding the reliability of ages, and include sites only where the original authors
359 specifically attribute glacial sediments/features to the PGM, where this is either
360 identified as MIS 6 or the youngest Saalian/Illinoian glacial episodes. Our database for
361 these PGM-specific data is available at the URL listed in the acknowledgements.
362
363 The mapped extents in Figure 1 help to constrain the maximum PGM ice-sheet area, but
364 are not indicative of ice-sheet thickness (i.e., topography, volume). Instead, model
365 inversion techniques with varying assumptions and input datasets (e.g., Peltier, 2004;
366 Lambeck et al., 2006; Abe-Ouchi et al., 2015) are needed to provide dynamic ice
367 histories with volume, extent, and topographic constraints (see Stokes et al., 2015 for an
368 overview on modelling past ice sheets). Ice-sheet extent, form, and thickness result from
369 interactions between glaciological and climatological factors on local, regional, and
370 global scales. Limits to ice-sheet extent include ice rheology (Glen, 1958) and ice-flow
371 mechanisms driven by ice-elevation gradients, including the ice-thickness/basal-melting
372 negative feedback (Payne, 1995; Marshall and Clark, 2002), and variations in basal
373 conditions such as topography, sub-glacial till rheology (e.g., Clark and Pollard, 1998;
374 Licciardi et al., 1998), and geothermal heat flux (e.g., Pattyn, 2010). Regional ice
375 thickness depends primarily on near-surface temperatures and rates of snow
376 accumulation and ablation (e.g., Seguinot et al., 2014). In addition, the mass balance of
377 an ice sheet can be affected by factors such as: dust deposition that alters snow and ice
378 albedo (e.g., Krinner et al., 2006; Bar-Or et al., 2007); albedo feedbacks from changes in
379 vegetation cover around the ice sheet (e.g., Gallimore and Kutzbach, 1996); and changes
380 in the sources and pathways of moisture advection. Differences in these factors may
381 account (partly) for the different spatial EIS extents between the PGM and LGM. For
382 example, dust transportation is thought to have been more intense during the LGM than
383 the PGM (e.g., Naafs et al., 2012). In addition, the PGM EIS was affected by large pro-

glacial lakes, which (because of large heat capacities) can cool regional summer climates, and which also modify precipitation through meso-scale atmospheric feedbacks (e.g., Krinner et al., 2004; Colleoni et al., 2009). No geological evidence exists for such lakes during the LGM (Mangerud et al., 2004).

Even under favourable conditions for glaciation, other controls such as topographic (including ice-sheet) barriers may block moisture advection, limiting ice-sheet growth above a certain height (e.g., Kageyama and Valdes, 2000; Ullman et al., 2014; Liakka et al., 2016). Ice-sheet orography by itself affects local weather systems – e.g., lee-side cyclogenesis by increasing the advection of cold air, with impacts on precipitation – in addition to altering atmospheric stationary-wave patterns over the ice topography (e.g., Cook and Held, 1988; Roe and Lindzen, 2001; Abe-Ouchi et al., 2007; Löfverström et al., 2014). Such influences affect ice-sheet ablation and elevation through temperature changes at both local and regional scales (e.g., Roe and Lindzen, 2001; Liakka et al., 2012). For example, NAIS-elevation changes during the last glacial cycle altered both the position and strength of the North Atlantic jet stream (e.g., Kageyama and Valdes, 2000; Abe-Ouchi et al., 2007). This caused changes in North Atlantic storm tracks and European precipitation (Liakka et al., 2016): a higher NAIS results in a more zonal jet stream (Roe and Lindzen, 2001; Löfverström et al., 2014), with drier (wetter) conditions in northern (southern) Europe (Löfverström et al., 2014). Conversely, a small NAIS has limited impact on European precipitation (Liakka et al., 2016). Other impacts on the storm track relate to sea-ice and sea-surface temperature distributions (Kageyama and Valdes, 2000): during the LGM, for example, extensive Arctic/North Atlantic sea-ice cover is thought to have caused considerable southward storm-track displacement (e.g., Kageyama et al., 1999). These various influences likely account for the significant difference in EIS distributions between the PGM and LGM (e.g., Liakka et al., 2016), given that (*i*) the PGM had less extensive and seasonally open sea-ice conditions, relative to

411 extensive and severe sea-ice conditions during the LGM (e.g., Spielhagen et al., 2004;
412 Nørgaard-Pedersen et al., 2007; Polyak et al., 2010; de Vernal et al., 2013; Arndt et al.,
413 2014; Löwemark et al., 2016), and (*ii*) the NAIS was smaller/lower during the PGM than
414 during the LGM (e.g., Svendson et al., 2004; Ehlers et al., 2011a).
415
416 Stationary wave patterns also affect the southernmost boundary of the NAIS, by
417 enhancing or decreasing local ablation (Cook and Held, 1988; Roe and Lindzen, 2001;
418 Liakka et al., 2012). Certain configurations induce warming in the northwest of North
419 America, cooling over the central continent, and a warm anomaly in the east; this
420 pattern facilitates southward ice-sheet expansion over the central continent, and
421 poleward deflection of the ice margin in the east (Liakka et al., 2012). A reduced
422 wavelength of the stationary wave – a function of differences in the zonal-mean
423 background state, latitude, and size of the NAIS (Cook and Held, 1988; Ringler and Cook
424 1997; Liakka et al., 2012, 2016) – tends to shift the centre of mass eastward, which
425 facilitates southward penetration of a NAIS lobe along the eastern continental boundary
426 (Roe and Lindzen, 2001). Ice-volume hysteresis may also be (partly) related to
427 variations in the latitudinal extent of the Laurentide ice sheet (Abe-Ouchi et al., 2013).
428 Overall, differences between PGM and LGM reconstructions of the NAIS likely reflect
429 differences in the zonal-mean atmospheric circulation and the induced temperature
430 anomalies (e.g., Liakka et al., 2012).
431

432 ### 3.2. PGM ice-volume estimates

433 We now use our PGM–LGM Δz of 21 ±14 m to calculate ranges of PGM ice volumes for the EIS
434 and NAIS, based on published ice-sheet reconstructions (Table 1). Relative to an LGM sea-
435 level drop of about 130 m, our Δz suggests a PGM sea-level drop of 109 ±14 m. A selection of
436 recent ice-volume estimates for the PGM and LGM ice sheets is given in Table 1, with a focus
437 on models that are constrained by geological or sea-level evidence, which illustrates the

evolution of estimates within the last decade (notably, a reduction in LGM EIS estimates). Comparisons between estimates may be complicated by differing methods (e.g., whether estimates are constrained by glacio-geomorphological observations), the assumptions made when calculating m_{SLE} (e.g., choice of water/ice densities, and whether the modern ocean area is used or a reduced value due to sea-level lowering), and incremental model development, which can lead to differences between originally published values and those from subsequent modelling.

Assuming a PGM sea-level drop of 109 ±14 m, a PGM EIS volume of 33 to 53 m_{SLE}, and comparable Antarctic excess ice volume between the PGM and LGM (assuming ~17 m_{SLE} as an upper bound, based on geologically constrained glaciological modelling; Table 1), the inferred values imply a North American NAIS volume as small as 59 to 39 m_{SLE} (±14 m_{SLE}), respectively. A caveat applies with respect to attribution of component contributions to the overall sea-level drop, namely that various indicators for the maximum EIS extent may represent different glacial advance phases at different locations (Svendsen et al., 2004; Lambeck et al., 2006; Hughes et al., 2013; Colleoni et al., 2016) (Figure 1). In that case, PGM EIS volume may have been overestimated; a conservative limit may be calculated for the PGM NAIS by assuming a 29 m_{SLE} limit for the PGM EIS, similar to the upper limit for the LGM EIS and in agreement with ice-sheet models that suggest a maximum EIS of 40 m_{SLE} (Bintanja et al., 2005; Abe-Ouchi et al., 2015) (which conflicts with data-driven estimates of 50 to 71 m_{SLE}; Table 1). This conservative limit for PGM NAIS volume is 63 ± 14 m_{SLE}, so that we infer a PGM NAIS ice-volume range of 39-63 m_{SLE} (±14 m_{SLE}) from our Δz assessment, while previous PGM NAIS reconstructions infer a volume of 30-84 m_{SLE} (Table 1). In contrast to our PGM NAIS ice-volume range of 39-63 m_{SLE} (±14 m_{SLE}), LGM NAIS estimates range over 51-94 m_{SLE} (Table 1).

Overall, our analysis indicates that PGM global land-based ice volume was smaller than LGM global land-based ice volume; more robust analysis requires improved individual component

ice-volume estimates. A strong case exists for a small PGM NAIS, from a combination of climate and ice-sheet modelling (Colleoni et al., 2014, 2016; Wekerle et al., 2016), GIA modelling (Potter and Lambeck, 2003; Lambeck et al., 2006, 2010, 2017, Wainer et al., 2017), and North Atlantic IRD observations (Obrochta et al., 2014), in addition to our sea-level assessment (this study).

4. Implications of PGM–LGM ice-volume differences

4.1. Implications for concepts of glacial inception

To provide a wider climatic context to the PGM–LGM ice-volume differences documented in this study, we also determined PGM–LGM contrasts in other key climate parameters (Table 4). For this analysis, we performed Monte-Carlo-style probabilistic assessments (n = 10,000 simulations) based on the uncertainties associated with the various records. For CO_2, CH_4, and Antarctic temperature records (Monnin et al., 2001, 2004; Loulergue et al., 2008; Lourantou et al., 2010; Stenni et al., 2010; Schmitt et al., 2012; Schneider et al., 2013; Landais et al., 2013; Parrenin et al., 2013; Ahn and Brook, 2014), we account for uncertainties associated with chronology (AICC2012, Veres et al., 2013; Bazin et al., 2013) and proxy measurement in each record to determine the 68% (16^{th}–84^{th} percentile) and 95% (2.5^{th}–97.5^{th} percentile) probability intervals, the median (50^{th} percentile), and the probability maximum (modal value) with its 95% probability interval (e.g., Grant et al., 2012; Rohling et al., 2014; Marino et al., 2015). We probabilistically calculate greenhouse gas (GHG) components of Earth's radiative balance (ΔF_{CO2}, ΔF_{CH4}, and ΔF_{GHG}) from ice-core time series of CO_2 and/or CH_4, referencing radiative forcing estimates to the values at AD1000 (cf. Rohling et al., 2012). This probabilistic analysis accounts for (*i*) chronological and measurement uncertainties for CO_2 (Monnin et al., 2001, 2004; Schmitt et al., 2012; Schneider et al., 2013; Landais et al., 2013; Ahn and Brook, 2014) and/or CH_4 time series (Loulergue et al., 2008), and (*ii*) uncertainties associated with conversion of CO_2 and/or CH_4 to ΔF_{CO2}, ΔF_{CH4}, and ΔF_{GHG}. Input data for the Monte Carlo routines are the ice-core 'gas ages' with uncertainties of the AICC2012

chronology (Veres et al., 2013; Bazin et al., 2013) and CO_2 and/or CH_4 data with analytical uncertainties (Monnin et al., 2001, 2004; Loulergue et al., 2008; Schmitt et al., 2012; Schneider et al., 2013; Landais et al., 2013; Ahn and Brook, 2014). Each data point was separately and randomly sampled *n* times within its uncertainties and converted to ΔF values, using the equations of Köhler et al. (2010) with their uncertainties. Each iteration was interpolated linearly and the probability distribution was assessed at each time step to determine probability intervals and probability maxima. Finally, minima in the median and probability maximum of each climate parameter (with 95% probability bounds) were determined within the 19-26.5 kyr ago (cf. Clark et al., 2009) and 138-155 kyr ago intervals for the LGM and PGM, respectively. LGM and PGM minima for summer insolation and energy at 65°N were determined directly from the original datasets (Laskar et al., 2004; Huybers, 2006) through the same time intervals. In our analysis we also considered deep-sea benthic foraminiferal carbonate $\delta^{18}O$ from a stack of 57 globally distributed global records (Lisiecki and Raymo, 2005): PGM and LGM maxima are reported as anomalies ($\Delta\delta^{18}O_{benthic}$) with respect to the mean of the most recent 2 kyrs.

Our assessment reveals similar values of commonly used key climate parameters between the two glacial maxima (Table 4), in contrast to the significant sea-level difference between the PGM and LGM (section 2.4). The identified contrasts between the PGM and LGM highlight a need for future research to unravel the causes of ice-age development into either a PGM-like, or an LGM-like mode. Different PGM and LGM ice distributions between North America and Eurasia imply different moisture fluxes over the continents between these glacial cycles, partly due to interactions between NAIS size and atmospheric dynamics (e.g., Colleoni et al., 2016; Liakka et al., 2016), and partly due to complex interacting processes that drive glaciations toward large- or small-NAIS sizes (e.g., Colleoni et al., 2011). For example, not only summer insolation and GHG forcing (Table 4), but also ice-albedo feedbacks, vegetation-albedo feedbacks, dust deposition on snow/ice, sea-ice expansion, and sea surface

518 temperature reduction need to be considered (e.g., Oglesby, 1990; Calov et al., 2009; Clark et
519 al., 2009; Colleoni et al., 2011; Abe-Ouchi et al., 2013; Liakka et al., 2016). Moreover, ice-sheet
520 accumulation may not be related directly to the commonly used summer insolation at specific
521 latitudes, but may also be affected (more) by insolation in other seasons, particularly spring
522 (Colleoni et al., 2011; Jakobsson et al., 2014a). Ice-sheet nucleation may, in addition, depend
523 on chaotic aspects of the weather/climate system; for example, successive winters with heavy
524 snowfall may – almost randomly – cause some locations to receive an initial snow cover with
525 enough volume and albedo feedback to ensure its survival and subsequent growth potential
526 (e.g., Oglesby, 1990). Finally, modelling studies (e.g., Abe-Ouchi et al., 2013) indicate that
527 glacial culminations like the PGM and LGM reflect the outcome of temporal developments in
528 forcings and feedbacks through the preceding glacial cycle that include insolation (e.g., Laskar,
529 2004; Colleoni et al., 2011), CO_2 and CH_4 concentrations (Monnin et al., 2001; Loulergue et al.,
530 2008; Schmitt et al., 2012; Schneider et al., 2013; Landais et al., 2013), and sea level/ice
531 volume (e.g., Waelbroeck et al., 2002; Rohling et al., 2009, 2014; Elderfield et al., 2012; Grant
532 et al., 2014), and also in state variables such as surface and deep-sea temperature (e.g., Stenni
533 et al., 2010; Elderfield et al., 2012; Parrenin et al., 2013; Rohling et al., 2012, 2014; Martínez-
534 Botí et al., 2015; Snyder, 2016a,b). Climate simulations by Colleoni et al. (2014) suggest that
535 orbital and greenhouse-gas changes for the penultimate glacial cycle were more favourable
536 for glacial inception over Eurasia than over North America, relative to the last glacial cycle.
537 Targeted high-resolution, coupled modelling of full glacial cycles on a global scale may further
538 improve understanding of differences between the PGM and LGM, and other glacial maxima,
539 and use of stable O-isotope-enabled models may then help to explore the major issue
540 highlighted in section 4.3.

541 ### 4.2. Glacioisostatic corrections to Last Interglacial sea level

542 Proxy-based sea-level reconstructions generally refer to a location-specific relative sea level
543 (RSL). This is related to global mean sea level (GMSL) via a glacial isostatic correction: GIA
544 correction = GMSL – RSL. Different PGM and LGM ice-mass distributions may critically affect

545 last interglacial glacioisostatic corrections, and therefore reconstructions of LIG GMSL. We
546 present an exploration of this influence using several hypothetical scenarios (Figures 4-7;
547 Table 5). We solve the sea-level equation using the Kendall et al. (2005) method, which is
548 adapted to account for feedback from Earth's rotational vector (Mitrovica et al., 2005). The
549 model takes into account self-gravitational feedbacks, moving shorelines, and marine-
550 terminating ice sheets, and the sea-level equation is solved in an iterative, pseudo-spectral
551 manner (Mitrovica et al., 2005; Tamisiea, 2011; Williams, 2016) that incorporates a
552 spherically symmetric Earth representation.
553
554 We use three model outputs: *(a)* a global grid of RSL values generated for a suite of earth-
555 model parameterisations; *(b)* an RSL curve for several key reconstruction sites; and *(c)* a
556 GMSL curve where ocean volume and area are corrected for GIA effects at each modelled time
557 step. We model GIA for representative sites for key fossil-coral locations at Barbados
558 (13.116 °N, 59.542 °W), Tahiti (17.567 °S, 149.58 °W), Western Australia (22.32 °S, 113.8 °E),
559 and the Seychelles (4.67 °S, 55.5 °E) (e.g., Fairbanks, 1989; Stirling et al., 1995; Bard et al.,
560 1996; Israelson and Wohlfarth, 1999 – as early examples from the extensive literature
561 summarised by Hibbert et al., 2016). Hanish Sill, Bab-el-Mandab Strait (13.733 °N, 42.533 °E),
562 is the control point for Red Sea reconstructions, as is Camarinal Sill, Strait of Gibraltar
563 (35.92 °N, 5.72 °W), for Mediterranean Sea reconstructions (Siddall et al., 2003; Grant et al.,
564 2012, 2014; Rohling et al., 2014). Finally, we model a point for the easternmost
565 Mediterranean, at Rosh Hanikra (33.093 °N, 35.105 °E), for which a detailed LIG coastal
566 stratigraphic sequence has been published (Sivan et al., 2016).
567
568 GIA assessment requires an ice history, which is a series of time-point files with ice-height
569 data on a global grid (here a 512 x 256 Gauss-Legendre grid). We developed four hypothetical
570 ice histories based on the arguments in this study, in 2-kyr time steps (Table 5, Figure 5). We
571 emphasise that these are idealised hypothetical scenarios, designed to test the GIA response

572 at each key location. For more conclusive GIA corrections, extensive reconstruction is needed
573 of the time development of total ice mass and its distribution between continental locations,
574 at discrete time steps through entire glacial cycles.
575
576 Our hypothetical "ICE-1" ice history (Figure 5a) is a version of the ICE-5G model (Peltier,
577 2004) that is extended to cover 2 identical glacial cycles, placed before and after a 14-kyr
578 interglacial highstand between 130 and 116 ka (Dutton and Lambeck, 2012). Because of the
579 way this is constructed by copying the last glacial cycle, the peak amplitude for the PGM
580 happens to fall on 152 ka. Our further hypothetical scenarios keep timing-structure the same,
581 and only change total ice-volume amplitudes and relative NAIS:EIS ice-mass distributions as
582 explained below. Amplitude changes prior to 26 ka are scaled according to the SPECMAP
583 curve (Imbrie et al., 1984). Note that our scenarios are hypothetical and use arbitrary values
584 from within ranges outlined above, to investigate the potential sense and scale of impacts;
585 more definitive reconstructions are contingent upon future research to determine ice-mass
586 distributions, Antarctic contributions, and GIA model developments (e.g., allowing for
587 incorporation of inhomogeneous Earth models), etc.
588
589 In our hypothetical "ICE-2" ice history (Figure 5b), the impact of reduced ice mass at the PGM
590 is compared with the LGM, while keeping constant the NAIS:EIS mass-distribution
591 proportionality. ICE-2 features a 16% sea-level change for the PGM, from an LGM-like –130 m
592 to a reduced value of –109 m. A 16% total ice-volume reduction at maximum glaciation
593 represents ~21 m_{SLE} of change when applied to the ICE-5G model. Change to an ice history
594 requires adjustment over a sequence of time steps. To create ICE-2 by changing the PGM of
595 ICE-1 (152 kyr ago), we also scaled the surrounding 154, 152, 150, 148, 146, 144 and 142 ka
596 time points: 154 ka has a 14% ice reduction; 152, 150, and 148 ka have 16% reduction; 146
597 ka has 10% reduction; and 144 and 142 ka have 8% reduction, relative to ICE-1.
598

599 Hypothetical ice history "ICE-3" (Figure 5c) was designed to investigate how a changed PGM
600 ice-mass distribution (i.e., smaller NAIS, larger EIS) affects RSL histories at our study sites. We
601 constrained the NAIS to 32 m_{SLE} between 200 and 140 ka, and EIS to a 60 m_{SLE} maximum
602 between 152 and 142 ka, and left the interglacial to present day identical to ICE-1 and ICE-2.
603 Temporal scaling for the EIS through the penultimate glacial cycle is applied as follows
604 (Figure 5c): between 236 and 198 ka, we scaled the EIS volume of ICE-2 by a factor of 1.25,
605 between 196 and 162 ka we scaled it by a factor of 3, from 160 to 154 ka we scaled it by a
606 factor of 3.2, from 140 to 136 ka we scaled it by a factor 5.5, and from 152 to 142 ka we held
607 the ice volume at 60 m_{SLE}. All these adjustments were made within the geographical
608 boundaries set out by ICE-5G. Within the extended ICE-1 glacial history, the NAIS reached a
609 greater ice volume early in the penultimate glacial cycle. To accommodate this in ICE-3, we
610 allowed initial penultimate glacial variation to the NAIS (up to 36 m_{SLE}), but when its ice
611 volume would have increased further we capped it at 32 m_{SLE}. The required variation for total
612 global volume was then distributed into the EIS, and any remnant required volume was
613 pushed into the East and West Antarctic ice sheets (Figure 5c).
614
615 In a hypothetical ice history "ICE-4" (Figure 5d), impacts of allowing the EIS to occupy a larger
616 area are assessed (cf. Figure 1). In ICE-3, the EIS remained within its ICE-5G boundaries
617 despite giving it greater mass. In ICE-4, we used the EIS distribution of de Boer et al. (2014),
618 and spliced it into ICE-3 instead of the ICE-5G extent (EIS only). This new penultimate glacial
619 EIS was scaled to match ICE-3 volume variations, with the same rule as applied to NAIS
620 volume. Resulting ice-volume variations are identical to ICE-3 for all ice sheets; the only
621 difference is the EIS spatial distribution.
622
623 All ice histories were run using a range of 495 Earth models that comprise 3 parameters for
624 lithosphere thickness (71, 96, and 120 km), 11 parameters for upper mantle viscosity (1×10^{20}
625 to 1×10^{21} Pa s), and 15 parameters for lower mantle viscosity (2×10^{21} to 5×10^{22} Pa s). Results

626 at each location are compared with an LGM-like PGM (ICE-1) (Table 6). Appendix Ic provides
627 a global representation of the range in peak (maximum) RSL results within the LIG across all
628 495 Earth models, for each of our ice histories. While results for the LIG (Figure 7) and for the
629 wider interval of 160-110 ka (Figure 6) are – for clarity – only shown for a VM2-like Earth
630 model (with lithosphere thickness of 96 km, and upper and lower mantle viscosities of 5×10^{20}
631 and 2.5×10^{21} Pa s, respectively), they can be compared to Figure 8 to understand the range of
632 response possible across our wide suite of Earth parameters (Table 6).
633
634 Reviewing the RSL response at the LIG onset (~130 ka), we find that key differences in
635 sensitivity (to Earth model) and amplitude of RSL differences between a small (ICE-1, 2) or
636 large EIS (ICE-3, 4) are systematic across locations. Some sites have relatively low sensitivity
637 to, and small amplitude offset for, this change (Western Australia, Barbados). Others have
638 intermediate impact (2-6 m difference, with Earth-model sensitivity characterised in the
639 range of 1-2.5 m; Hanish Sill, Tahiti, Seychelles), and some have even larger impacts, with
640 additional sensitivity to ice-sheet configuration and Earth model (Camarinal Sill, Rosh
641 Hanikra) (Figure 7, Table 6).
642
643 Our results are explored in a global context for three different representative Earth models
644 (Figure 8 and Table 7). Each panel in Figure 8 represents the difference between peak
645 (maximum) RSL within the last interglacial for two ice histories: ICE 1 for an LGM-like PGM,
646 and ICE 3 for a PGM with reduced total ice volume, larger EIS, and smaller NAIS, albeit with
647 constant geographical ice-sheet boundaries. Figure 8a, b, and c represent data generated
648 using Earth models E1, E2, and E3, respectively (Table 7). All three panels indicate that a
649 variation in PGM ice volume and distribution is likely to result in a change to the GIA
650 correction during the interglacial period, and that the magnitude of this GIA correction
651 depends strongly on the choice of Earth model. Variation in LIG peak RSL between ICE-1 and
652 ICE-3 for E1 ranges from –2 to +4 m for the sites considered here (Figure 8a) and corresponds

653 to 0 to +2.9 m changes in the GIA correction between the two scenarios. Repeating this
654 exercise for the seven locations considered for all Earth models – given that peak RSL varies
655 markedly between Earth models (Figure 8b, c) – the difference between GIA corrections for
656 ICE-1 and ICE-3 ranges between –0.6 and +7.2 m (average values for each location over the
657 full suite of Earth models). This range of likely adjustments is of the same order of magnitude
658 as the existing range of GMSL estimates for the LIG (i.e., +4 to +10 m above present), and
659 therefore cannot be ignored. We infer that considering alternate ice-sheet configurations for
660 the PGM will cause adjustments of several metres in GIA corrections, even at far-field sites
661 (Figure 8; Table 6). More precise PGM ice-volume and mass-distribution reconstructions, and
662 improved GIA models, will be needed to obtain more conclusive LIG GMSL estimates. For
663 example, Dendy et al. (2017) highlighted the inadequacy of constructing past ice histories by
664 replicating the same glacial cycle. They quantified the scale of the sensitivity by comparing
665 results from a MIS 6/ 5 deglaciation based on a particular age model (Waelbroeck et al., 2002;
666 Shakun et al., 2015) with a deglaciation that replicated the most recent one. This uncertainty
667 is likely to be refined further as constraints on age models for the MIS 6 deglaciation continue
668 to evolve (Marino et al., 2015).
669
670 Our initial assessment with hypothetical scenarios indicates a high probability that LIG GMSL
671 estimates will need to be altered significantly. One caveat applies, namely that the inferred
672 adjustments are partly due to the selection of sites used, given that none seems to sample the
673 major regions of negative adjustment in Figure 8. This suggests that these commonly used key
674 sites for LIG sea-level study may not be the most representative sampling for determining
675 GMSL, and that sound LIG estimates will need a denser suite of sites at which LIG RSL
676 observations are made. Then, the same exercise performed here for 7 sites should be
677 performed for a wider suite, to evaluate the impact of different ice-mass distributions.

4.3. The global $\delta^{18}O$:sea-level/ice-volume relationship

The PGM–LGM value of Δz estimated from δ_{sw} (Elderfield et al., 2012) appears less well defined and less conclusive than that estimated from the other sea-level records (Table 2). Ice-volume/sea-level reconstructions from seawater $\delta^{18}O$ records have so far either assumed a temporally invariant relationship, or one in which ice became isotopically more negative with increasing ice volume within a glacial cycle (e.g., Duplessy et al., 2002; Waelbroeck et al., 2002; Bintanja et al., 2005; Siddall et al., 2010; de Boer et al., 2014). Potential seawater $\delta^{18}O$ bias among glacial cycles due to different ice-volume to ice-$\delta^{18}O$ relationships would therefore affect all ocean-$\delta^{18}O$-based methods, including the Red Sea and Mediterranean sea-level methods. However, the relative impact of this bias depends on the signal-to-noise ratio of each record, and specifically on the strength of the marginal-sea residence-time effect in the Red Sea and Mediterranean. Relative to open-ocean deep-sea glacial-interglacial $\delta^{18}O$ gradients (~1 to 1.5 ‰), Mediterranean and Red Sea $\delta^{18}O$ gradients are 2-3 times and 5-6 times as large, respectively. A global seawater $\delta^{18}O$ bias of, for example, ~0.2 ‰ would therefore have limited impact in Red Sea or Mediterranean sea-level reconstructions, but would substantially affect the open-ocean δ_{sw} method.

With this in mind, we note that global deep-sea benthic foraminiferal carbonate $\delta^{18}O$ records (δ_c) commonly have PGM and LGM values that are identical within uncertainties (Table 4). Such records represent combined ice-volume and deep-sea temperature influences, in a proportional relationship of ~22 ±3 m $°C^{-1}$ (1σ) (Adkins et al., 2002; Martin et al., 2002; Sosdian and Rosenthal, 2009; Elderfield et al., 2012). Thus, our mean Δz of 21 m implies ~1 °C lower deep-sea temperatures during the PGM than the LGM (see also Rohling et al., 2014). SW Pacific Mg/Ca-based deep-sea temperature estimates suggest 1 ±0.5 °C lower values during the wider PGM interval (160-140 kyr ago) than the LGM (Elderfield et al., 2012). Another Mg/Ca study also suggests that Pacific PGM deep-sea temperatures were ~1 °C lower than for the LGM (Martin et al., 2002). These anomalies fall well within the uncertainties of Mg/Ca

705 calibrations, which remain poorly constrained at these low temperatures, especially because
706 near-freezing temperatures require extrapolation outside the present-day calibration window
707 for the method (Martin et al., 2002; Elderfield et al., 2010). More importantly, it is difficult to
708 imagine how deep-sea temperatures could have been much lower than in the LGM because
709 (pressure-corrected) conditions are thought to have been close to freezing in much of the
710 LGM deep sea already (Adkins et al., 2002). Deconvolution of deep Pacific δ_c into temperature
711 and sea-level related δ_{sw} components suggests similar deep-sea temperatures for the PGM and
712 LGM (Siddall et al., 2010). Finally, Antarctic temperature reconstructions – from the continent
713 adjacent to locations where abyssal ocean temperatures are acquired – indicate similar PGM
714 and LGM temperatures (Table 4), which indirectly suggests similar deep-sea temperatures.
715
716 If PGM and LGM deep-sea temperatures were similar (within about 0.5 °C), then a
717 fundamental PGM–LGM offset is implied in the relationships between mean global-ocean δ_{sw}
718 and sea level or ice volume. This might arise from: *(a)* ocean circulation differences among
719 glacial cycles, filling different volumes of the deep sea with waters of different mean δ_{sw}
720 values, although such contrasts are thought to be averaged over multi-millennial periods (e.g.,
721 Siddall et al., 2010); *(b)* different moisture pathways feeding contrasting glacial configurations
722 (e.g., Ullman et al., 2014; Colleoni et al., 2016), with impacts on atmospheric vapour isotopic
723 fractionation and, hence, ice $\delta^{18}O$; or *(c)* potential development of massive, largely floating
724 Arctic ice shelves during certain glacials (e.g., PGM), and not during others (e.g., LGM) – these
725 would cause negligible sea level change, but considerable mean ocean $\delta^{18}O$ change (Niessen et
726 al., 2013; Jakobsson et al., 2016). Below, we discuss these three options in turn.
727
728 Variations in δ_{sw} arise from: the waxing and waning of ice sheets (i.e., changes in global ice
729 volumes); changes in the balance of evaporation and precipitation (e.g., Duplessy et al., 1991,
730 1992); changes in the balance between advection and mixing between water masses (e.g.,
731 Curry and Oppo, 2005); and changes in the processes and intensity of deep-water formation,

where varying contributions of melt-water, entrained water, and brine to the newly formed deep waters may impose regional δ_{sw} anomalies. For example, pore-water δ_{sw} measurements are different in the deep Pacific, and northern and southern Atlantic between the LGM and today (Adkins et al., 2002); the inferred changes suggest a large freshwater imbalance in the northern convecting regions during the LGM, with an important role for increased sea-ice formation and export. Given the great difference in Arctic sea-ice conditions that has been inferred between the PGM (less extensive and seasonally open) and LGM (extensive and severe sea-ice conditions) (Knies et al., 2000; Polyak et al., 2010; de Vernal et al., 2013; Niessen et al., 2013; Arndt et al., 2014; Jakobsson et al., 2010, 2014b; Löwemark et al., 2015), a difference in both the isotopic composition and volumetric contribution of northern-sourced deep waters might be expected between the two glacial periods. There are some hints of local δ_{sw} differences between the two glacial intervals (e.g., Skinner and Shackleton, 2006), with a shoaled hydrographic gradient separating northern- and southern-sourced deep waters and a potentially weaker North Atlantic overturning cell during the PGM. Oxygen-isotope tracer models may help to unravel varying changes in source δ_{sw} as well as different volumetric source-contributions to the deep sea in different locations.

Decoupling of the δ_{sw}:ice-volume relationship could also occur if the moisture pathways of ice growth change between different glacial intervals (option *b* above). Vapour sourced from surface waters records the initial surface-water δ_{sw} (source-water effect), so that regional variations in source δ_{sw} have some initial impact on ice-sheet $\delta^{18}O$. More importantly, ice $\delta^{18}O$ also changes with the intensity of Rayleigh distillation, as accumulation changes from warm, low-elevation to colder, higher-elevation environments as glaciation progresses. Similarly, longer air trajectories with more Rayleigh distillation lead to accumulation of ice with lower $\delta^{18}O$. As a result, each ice sheet will have a different isotopic time-"evolution" (e.g., Mix and Ruddiman, 1984) depending upon their volume/height and the latitudinal range over which they expand. As discussed before, the different configurations of the NAIS and EIS during the

PGM, relative to the LGM, strongly suggest that their processes of glacial inception and ice-sheet growth were also different (e.g., Colleoni et al., 2011). Thus, differences in atmospheric circulation – and hence moisture supply and degree of isotopic fractionation – as induced by a lower PGM NAIS may have affected the isotopic composition of globally integrated ice volume, leading to potential misrepresentations of both amplitude and timing of the ice-volume signal (e.g., Mix and Ruddiman, 1984; Clark and Mix, 2002). So far, even the LGM isotopic compositions of various ice sheets (and their time-evolution) remain poorly constrained (e.g., Duplessey et al., 2002; Ferguson and Jasechko, 2015), and even less information is available for the PGM. Again, isotope-enabled models may help to characterise the potential impact of different moisture-transport pathways and fractionation effects in the δ_{sw}:ice-volume difference between the PGM and LGM.

Contributions from options *(a)* and *(b)*, outlined above, cannot be excluded. But option *(c)*, which involves potential development of massive, largely floating Arctic ice shelves during the PGM and not during the LGM, may be particularly important given the large size and longstanding character of the PGM δ_c:sea-level discrepancy relative to the LGM. Evidence of past floating ice shelves can be elusive or equivocal because, by their nature, they preserve few traces. However, ice-grounding features (e.g., parallel streamlined submarine landforms and ploughmarks) may be preserved in seafloor sediments, and their occurrence on bathymetric highs, in conjunction with regions devoid of glaciogenic seabed disturbance, has been used to suggest evidence of past floating ice (e.g., Polyak et al., 2001, Jakobsson et al., 2008). In the Arctic, erosional features have been found at depths of ~1 km on the Lomonosov Ridge, Chukchi Borderlands, Yermak Plateau, East Siberian Margin, Baffin Bay, and Hovgaard Ridge (Fram Strait) (e.g., Polyak et al., 2001; Kuijpers et al., 2007; Dowdeswell et al., 2010; Gebhardt et al., 2011; Niessen et al., 2013; Arndt et al., 2014), while other portions of the Lomonosov and Mendeleev Ridges are largely devoid of glaciogenic features, which may suggest ice-free conditions (Jakobsson et al., 2010). Bathymetric highs in the Arctic may have

786 acted as pinning points, allowing ice-rise formation that stabilised and facilitated ice-shelf
787 thickening (Vogt et al., 1994; Grosswald and Hughes, 1999; Jakobsson et al., 2016).
788
789 (Largely) floating Arctic ice shelves during glacial intervals were proposed in the 1970s and
790 1980s (Mercer, 1970; Hughes et al., 1977; Broecker, 1975; Grosswald, 1980; Denton and
791 Hughes, 1981; Williams et al., 1981; Chappell and Shackleton, 1986), but then were
792 overlooked due to difficulties in obtaining data from the region and a lack of direct evidence
793 for such shelves during the LGM (for an overview, see Jakobsson et al., 2016). Recent
794 geophysical mapping in the Arctic, however, has led to a re-evaluation of large floating Arctic
795 ice shelves during the Pleistocene. Various mechanisms have been proposed to account for
796 the mapped submarine features, including the drifting of ice-shelf remnants or mega-bergs
797 trapped in multi-year sea ice, or a transient surge or brief grounding of a floating ice shelf
798 (Polyak et al., 2001, 2009; Engels et al., 2008; Dowdeswell et al., 2010; O'Regan et al., 2010;
799 Gebhardt et al., 2011; Niessen et al., 2013; Dove et al., 2014). Age control for many of the
800 features remains enigmatic, often relying on stratigraphic correlation and biostratigraphy; for
801 example, identification of diagnostic MIS 5e nannofossils gives a likely, or minimum, MIS 6 age
802 estimate for features on Morris Jesup Rise, Lomonosov Ridge, Yermak Plateau, Hovgaard
803 Ridge, Mendeleev Ridge, and Arlis Plateau (Jakobsson, 1999; Polyak et al., 2001; Matthiessen
804 and Knies, 2001; Kristoffersen et al., 2004; Spielhagen et al., 2004; Jakobsson et al., 2008,
805 2010, 2016; Arndt et al., 2014; Löwemark et al., 2016). Debate continues not only about the
806 age of the submarine features (e.g., Flower, 1997; Niessen et al., 2013), but also about the
807 scale of any ice shelves, from Arctic-wide as proposed by Hughes et al. (1977) and more
808 recently by Jakobsson et al. (2016), to (much) more limited extents (Engels et al., 2008;
809 Jakobsson et al., 2010; Niessen et al., 2013; Stein et al., 2017).
810
811 The potential presence of an Arctic ice shelf raises questions about regional oceanography.
812 Seasonally open waters (leads in the ice) are thought to have been continually present in

portions of the Arctic throughout the last two glacial-interglacial cycles, albeit to a lesser degree during glacial periods (Hebbeln and Wefer, 1991; Lloyd et al., 1996; Spielhagen et al., 2004; Knies and Spielhagen, 2016). Such open waters may have provided an important moisture source for ice growth in Eurasia (Spielhagen et al., 2004). In order to reconcile the presence of a large ice shelf with continued warm-water advection into the Arctic (Lloyd et al., 1996; Kneis et al., 2000; Spielhagen et al., 2004), deepening of the cold halocline and advection of Atlantic waters at greater depth than present have been proposed (e.g., Jakobsson et al., 2010; Cronin et al., 2012). Lomonosov Ridge may have acted as a topographic barrier to Atlantic water circulation in the Amerasian Basin, possibly promoting ice-shelf growth in this region (Jakobsson et al., 2010). Extensive MIS 6 ice-shelf/shelves covering the central Arctic (e.g., Hughes et al., 1977; Jakobsson et al., 2016) suggest partial contact with warmer Atlantic waters in cavities under the ice shelf, analogous to modern Antarctic ice shelves (e.g., Kirschner et al., 2013), with a potential for continued exchange of warmer waters across Lomonosov Ridge below the grounded ice shelf. Alternatively, Kristoffersen et al. (2004) suggested that advection of warmer Atlantic waters to Lomonosov Ridge during MIS 6 was associated with surges or collapses of Saalian ice-sheets, which may have facilitated northward drift of deep-draft icebergs across Lomonosov Ridge from their discharge areas in the northern Barents-Kara region.

Overall, the above discussion indicates that evidence for grounded ice in the Arctic is unequivocal, and some seabed features have been attributed to ice-shelf processes (e.g., Polyak et al., 2001; Jakobsson et al., 2010, 2016; Niessen et al., 2013). However, the age and extent of any Arctic ice-shelves remains elusive, and the existence of Arctic (or even pan-Arctic) ice shelves remains an open and ongoing field of research. We investigate what a sea-water-displacing Arctic ice mass/shelf might imply for the δ_{sw}:ice-volume relationship for the PGM. First, assuming a modern Arctic Ocean area at about 800 m depth (5.3×10^{12} m^2) and a world-ocean surface area of 362×10^{12} m^2, our inferred sea-level discrepancy between the

LGM and PGM (~ 21 m_{SLE} ±14 m at 95% probability) would produce an ice shelf of the correct thickness (~1.4 ±0.9 km) to account for the observed glacial erosional features in the Arctic. Massive Arctic ice shelves that consist of continental ice with low $\delta^{18}O$ values – largely floating, but also as water-displacing grounded ice – would alter the relationship between δ_{sw} and sea level (and hence, land-based/grounded ice volume) relative to the LGM, even if the relationship between δ_{sw} and total (land-based + floating/water-displacing) global ice volume remained constant. It has been estimated that PGM Arctic ice shelves may have caused a 0.14 ±0.03‰ increase in global δ_{sw} (and δ_c), with only a 0.4 m sea-level impact (Jakobsson et al., 2016). If we use the LGM land-ice-based ratio of 0.009 ±0.001 m per ‰ (1σ) (Adkins et al., 2002; Schrag et al., 2002), then such a δ_{sw} anomaly would equate to 16 ±10 m of sea-level change, at 95% probability. This again suggests that our observed Δz = 21 ±14 m (with indistinguishable deep-sea $\delta^{18}O$) may be largely accounted for by the presence of massive PGM Arctic ice shelves, and by their absence during the LGM. Contribution of both land-based and floating/water-displacing ice volume to PGM δ_{sw} (and δ_c) results in a smaller sea-level drop, while contributions of only land-based ice to LGM δ_{sw} (and δ_c) gives a larger sea-level drop.

5. Conclusions

We provide independent evidence that continental ice volumes on North America (NAIS) and Eurasia (EIS) differed between the PGM and the LGM. During the PGM, the EIS likely reached 33-53 m_{SLE} and the NAIS 39-59 m_{SLE}. This compares with LGM values of 14-29 and 51-88 m_{SLE} for the EIS and NAIS, respectively. Our results provide independent support for the inference that Arctic-wide ice shelves existed during the PGM and not the LGM, with a previously estimated volume of ~16 m_{SLE} (actual sea-level impact was negligible because the ice was displacing seawater). The existence of different ice-sheet configurations between Eurasia, North America, and the Arctic implies that complex ice-sheet nucleation processes and growth processes can lead to different glacial modes and that one glacial cycle cannot be used as an

analogue for another. Among glacial cycles, we infer distinctly different relationships between mean global seawater $\delta^{18}O$ and global continental ice volume/sea level, and/or between deep-sea and Antarctic temperatures. New research using PGM and LGM glaciation 'modes' may improve understanding of the controls on ice-mass distribution and on Arctic ice-shelf development during glacial inception. Comparison of the last two glacial cycles with older glacial cycles is needed to test if there are only two fundamental modes, or many. Finally, we infer that sea-level studies for the last interglacial – which was warmer and had higher sea levels than modern pre-industrial times – may contain considerable bias from erroneous assumptions about PGM ice volume and distribution. Depending on the global location of a given site of relative sea-level reconstruction, the adjustment to GIA correction as inferred here for different ice configurations can be several metres in a positive or negative direction. Results across three representative Earth models suggest that – if a global assessment were made based on the sites of LIG sea-level reconstruction considered here – LIG global mean sea level would be estimated ≥2 m higher than conventional estimates (from the same sites) with GIA correction based on an LGM-like PGM ice distribution. This requires validation by more complete assessments because it has ramifications for studies of potential ice-reduction processes that are being used to evaluate sea-level risk in our warming future.

884 **Acknowledgements.** This work was supported by Australian Laureate Fellowship
885 FL120100050 (E.J.R.), UK Natural Environment Research Council (NERC) consortium project
886 iGlass (NE/1009906/1 and NE/1008365/1; E.J.R., F.D.H., F.H.W., A.P.R.), Australian Research
887 Council (DP1094001) (J.M.W.), and Japan Society for the Promotion of Science KAKENHI
888 projects JP26247085, and JP15KK0151 (Y.Y.). F.H.W. acknowledges constructive discussions
889 with Mark Tamisiea regarding the GIA modelling and results. We thank Tony Purcell (ANU)
890 for providing LGM and PGM ice-volume estimates reported in Table 1, using the model
891 detailed in Lambeck et al. (2006, 2010, 2017). Our study uses two databases, one on the coral
892 sea-level markers (published in 2016), and the other on glaciomorphological evidence (this
893 study). Both are available via http://www.highstand.org/erohling/ejrhome.htm, where they
894 will be regularly updated. The glaciomorphological dataset in a fixed form precisely as used in
895 this study is also archived at doi: 0.6084/m9.figshare.5131963.

References

Abe-Ouchi, A., Segawa, T., Saito, F., 2007. Climatic conditions for modelling the Northern Hemisphere ice sheets throughout the ice age cycle. Clim. Past, 3, 423–438.

Abe-Ouchi, A., Saito, F., Kageyama, M., Braconnot, P., Harrison, S.P., Lambeck, K., Otto-Bliesner, B., Peltier, W.R., Tarasov, L., Peterschmitt, J.Y., Takahashi, K., 2015. Ice-sheet configuration in the CMIP5/PMIP3 Last Glacial Maximum experiments. Geosci. Model Dev. 8, 3621–3637.

Abe-Ouchi, A., Saito, F., Kawamura, K., Raymo, M.E., Okuno, J.I., Takahashi, K., Blatter, H., 2013. Insolation-driven 100,000-year glacial cycles and hysteresis of ice-sheet volume. Nature 500, 190–193.

Adkins, J.F., McIntyre, K., Schrag, D.P., 2002. The salinity, temperature, and $\delta^{18}O$ of the glacial deep ocean. Science 298, 1769–1773.

Ahn, J., Brook, E.J., 2014. Siple Dome ice reveals two modes of millennial CO_2 change during the last ice age. Nature Commun. 5, 3732, doi:10.1038/ncomms4723.

Aitken, M.J., 1998. An Introduction to Optical Dating. The Dating of Quaternary Sediments by the Use of Photon-Stimulated Luminescence. Oxford University Press, Oxford, 267 pp.

Argus, D.F., Peltier, W.R., Drummond, R., Moore, A.W., 2014. The Antarctica component of postglacial rebound model ICE-6G_C (VM5a) based upon GPS positioning, exposure age dating of ice thicknesses, and relative sea level histories. Geophys. J. Int. 198, 537–563.

Arndt, J.E., Niessen, F., Jokat, W., Dorschel, B., 2014. Deep water paleo-iceberg scouring on top of Hovgaard Ridge‐Arctic Ocean. Geophys. Res. Lett. 41, 5068–5074.

Arz, H.W., Lamy, F., Ganopolski, A., Nowaczyk, N., Pätzold, J., 2007. Dominant Northern Hemisphere climate control over millennial-scale glacial sea-level variability. Quat. Sci. Rev. 26, 312–321.

Arz, H.W., Pätzold, J., Müller, P.J., Moammar, M.O., 2003. Influence of Northern Hemisphere climate and global sea level rise on the restricted Red Sea marine environment during termination I. Paleoceanography 18, 1053, doi:10.1029/2002PA000864.

Astakhov, V., 2001. The stratigraphic framework for the Upper Pleistocene of the glaciated Russian Arctic: changing paradigms. Glob. Planet. Chang 31, 283–295.

Astakhov, V., 2011. Ice margins of Northern Russia revisited. *In* Ehlers, J., Gibbard, P.L. and Hughes, P.D. (Eds.). Quaternary Glaciations – Extent and Chronology: A Closer Look, Developments in Quaternary Science 15. Elsevier, Amsterdam, pp. 323–336.

Astakhov, V.I., 2013. Pleistocene glaciations of northern Russia–a modern view. Boreas 42, 1–24.

Astakhov, V., Shkatova, V., Zastrozhnov, A., Chuyko, M., 2016. Glaciomorphological map of the Russian Federation. Quat. Int. 420, 4–14.

Balson, S., Jeffery, D.H. ,1991. The glacial sequence of the southern North Sea. *In* Ehlers, J., Gibbard, P.L., Rose, J. (Eds.). Glacial Deposits in Great Britain and Ireland, A. A. Balkema, Rotterdam, pp. 245–254.

Bar-Or, R., Erlick, C., Gildor, H., 2008. The role of dust in glacial–interglacial cycles. Quat. Sci. Rev. 27, 201–208.

Bar-Matthews, M., Ayalon, A., Gilmour, M., Matthews, A., Hawkesworth, C.J., 2003. Sea–land oxygen isotopic relationships from planktonic foraminifera and speleothems in the Eastern Mediterranean region and their implication for paleorainfall during interglacial intervals. Geochim. Cosmochim. Acta 67, 3181–3199.

Bard, E., Hamelin, B., Arnold, M., Montaggioni, L., Cabioch, G., Faure, G., Rougerie, F., 1996. Deglacial sea-level record from Tahiti corals and the timing of global meltwater discharge. Nature 382, 241–244.

Bard, E., Hamelin, B., Delanghe-Sabatier, D., 2010. Deglacial meltwater pulse 1B and Younger Dryas sea levels revisited with boreholes at Tahiti. Science 327, 1235–1237.

Bard, E., Hamelin, B., Fairbanks, R.G., Zindler, A., 1990. Calibration of the 14C timescale over the past 30,000 years using mass spectrometric U-Th ages from Barbados corals. Nature 345, 405–410.

Barendregt, R.W., Duk-Rodkin, A., 2011. Chronology and extent of Late Cenozoic ice sheets in North America: a magnetostratigraphical assessment. *In* Ehlers, J., Gibbard, P.L. and Hughes, P.D. (Eds.). Quaternary Glaciations – Extent and Chronology: A Closer Look, Developments in Quaternary Science 15. Elsevier, Amsterdam, pp. 419–426.

Bazin, L., Landais, A., Lemieux-Dudon, B., Toyé Mahamadou Kele, H., Veres, D., Parrenin, F., Martinerie, P., Ritz, C., Capron, E., Lipenkov, V., Loutre, M.F., 2013. An optimized multi-proxy, multi-site Antarctic ice and gas orbital chronology (AICC2012): 120–800 ka. Clim. Past 9, 1715–1731.

Bintanja, R., van de Wal, R., Oerlemans, J., 2005. Modelled atmospheric temperatures and global sea levels over the past million years. Nature 437, 125–128.

Bond, G., Lotti, R., 1995. Iceberg discharges into the North Atlantic on millennial time scales during the last glaciation. Science 267, 1005–1010.

Braun, D.D., 2011. The Glaciation of Pennsylvania, USA. *In* Ehlers, J., Gibbard, P.L. and Hughes, P.D. (Eds.). Quaternary Glaciations – Extent and Chronology: A Closer Look, Developments in Quaternary Science 15. Elsevier, Amsterdam, pp. 521–529.

Briggs, R.D., Pollard, D., Tarasov, L., 2014. A data-constrained large ensemble analysis of Antarctic evolution since the Eemian. Quat. Sci. Rev. 103, 91–115.

Broecker, W.S., 1975. Floating glacial ice caps in the Arctic Ocean. Science 188, 1116–1118.

Buckley, M.W., Marshall, J., 2016 Observations, inferences, and mechanisms of the Atlantic Meridional Overturning Circulation: a review. Rev. Geophys. 54, 5–63.

Busschers, F.S., Van Balen, R.T., Cohen, K M., Kasse, C., Weerts, H.J.T., Wallinga, J., Bunnik, F.P.M., 2008. Response of the Rhine-Meuse fluvial system to Saalian ice-sheet dynamics. Boreas 37, 377–398.

Busschers, F.S., Weerts, H.J.T., Wallinga, J., Cleveringa, P., Kasse, C., Wolf, H.D., Cohen, K.M., 2005. Sedimentary architecture and optical dating of Middle and Late Pleistocene Rhine-Meuse deposits–fluvial response to climate change, sea-level fluctuation and glaciation. Geol. Mijnb. 84, 25–41.

Calov, R., Ganopolski, A., Kubatzki, C., Claussen, M., 2009. Mechanisms and time scales of glacial inception simulated with an Earth system model of intermediate complexity. Clim. Past 5, 245–258.

Carlson, A.E., Winsor, K., 2012. Northern Hemisphere ice-sheet responses to past climate warming. Nat. Geosci. 5, 607–613.

Carr, S.J., 2004. The North Sea Basin. *In* Ehlers, J. Gibbard, P.L. (Eds.). Quaternary Glaciations Extent and Chronology – Part I: Europe. Developments in Quaternary Sciences 2, Elsevier, Amsterdam, pp. 261–270.

Channell, J.E.T., Hodell, D.A., Romero, O., Hillaire-Marcel, C., de Vernal, A., Stoner, J.S., Mazaud, A., Röhl, U., 2012. A 750-kyr detrital-layer stratigraphy for the North Atlantic (IODP Site U1302-U1303, Orphan Knoll, Labrador Sea). Earth Planet. Sci. Lett. 317–318, 218–230.

Chappell, J., Shackleton, N., 1986. Oxygen isotopes and sea level. Nature 324, 137–140.

Clague, J.J., Ward, B., 2011. Pleistocene Glaciation of British Columbia. *In* Ehlers, J., Gibbard, P.L. and Hughes, P.D. (Eds.). Quaternary Glaciations – Extent and Chronology: A Closer Look, Developments in Quaternary Science 15. Elsevier, Amsterdam, pp. 419–426.

Clark, C.D., Evans, D.J., Khatwa, A., Bradwell, T., Jordan, C.J., Marsh, S.H., Mitchell, W.A., Bateman, M.D., 2004a. Map and GIS database of glacial landforms and features related to the last British Ice Sheet. Boreas 33, 359–375.

Clark, C.D., Gibbard, P.L., Rose, J., 2004b. Pleistocene glacial limits in England, Scotland and Wales. *In* Ehlers, J., Gibbard, P.L. (Eds). Quaternary Glaciations. Extent and Chronology Part I: Europe, Developments in Quaternary Sciences 2. Elsevier, Amsterdam, pp. 47–82.

Clark, P.U., Archer, D., Pollard, D., Blum, J.D., Rial, J.A., Brovkin, V., Mix, A.C., Pisias, N.G., Roy, M., 2006. The middle Pleistocene transition: characteristics, mechanisms, and implications for long-term changes in atmospheric pCO_2. Quat. Sci. Rev. 25, 3150–3184.

Clark, P.U., Dyke, A.S., Shakun, J.D., Carlson, A.E., Clark, J., Wohlfarth, B., Mitrovica, J.X., Hostetler, S.W., McCabe, A.M., 2009. The last glacial maximum. Science 325, 710–714.

Clark, P.U., Huybers, P., 2009. Interglacial and future sea level. Nature 462, 856–857.

Clark, P.U., Mix, A.C., 2002. Ice sheets and sea level of the Last Glacial Maximum. Quat. Sci. Rev. 21, 1–7.

Clark, P.U., Pollard, D., 1998. Origin of the middle Pleistocene transition by ice sheet erosion of regolith. Paleoceanography 13, 1–9.

Clark, P.U., Tarasov, L., 2014. Closing the sea level budget at the Last Glacial Maximum. Proc. Natl. Acad. Sci. USA 111, 15861–15862.

Colleoni, F., Krinner, G., Jakobsson, M., Peyaud, V., Ritz, C., 2009. Influence of regional parameters on the surface mass balance of the Eurasian ice sheet during the peak Saalian (140 kya). Glob. Planet. Change 68, 132–148.

Colleoni, F., Liakka, J., Krinner, G., Jakobsson, M., Masina, S., Peyaud, V., 2011. The sensitivity of the Late Saalian (140 ka) and LGM (21 ka) Eurasian ice sheets to sea surface conditions. Clim. Dyn. 37, 531–553.

Colleoni, F., Masina, S., Cherchi, A., Iovino, D., 2014. Impact of orbital parameters and greenhouse gas on the climate of MIS 7 and MIS 5 glacial inceptions. J. Clim. 27, 8918–8933.

Colleoni, F., Wekerle, C., Näslund, J.-O., Brandefelt, J., Masina, S., 2016. Constraint on the penultimate glacial maximum Northern Hemisphere ice topography (≈ 140 kyrs BP). Quat. Sci. Rev. 137, 97–112.

Cook, K.H., Held, I.M., 1988. Stationary waves of the ice age climate. J. Clim. 1, 807–819.

Cronin, T.M., Dwyer, G.S., Farmer, J., Bauch, H.A., Spielhagen, R.F., Jakobsson, M., Nilsson, J., Briggs Jr, W.M., Stepanova, A., 2012. Deep Arctic Ocean warming during the last glacial cycle. Nat. Geosci. 5, 631–634.

Curry, B.B., Grimley, D.A. and McKay III, E.D., 2011. *In* Ehlers, J., Gibbard, P.L. and Hughes, P.D. (Eds.). Quaternary Glaciations – Extent and Chronology: A Closer Look, Developments in Quaternary Science 15. Elsevier, Amsterdam, pp. 467–487.

Curry, W.B., Oppo, D.W., 1997. Synchronous, high-frequency oscillations in tropical sea surface temperatures and North Atlantic Deep Water production during the last glacial cycle. Paleoceanography 12, 1–14.

de Boer, B., Lourens, L., van de Wal, R.S., 2014. Persistent 400,000-year variability of Antarctic ice volume and the carbon cycle is revealed throughout the Plio-Pleistocene. Nature Commun. 5, 2999, doi: 10.1038/ncomms3999.

de Boer, B., Van de Wal, R.S.W., Bintanja, R., Lourens, L.J., Tuenter, E., 2010. Cenozoic global ice-volume and temperature simulations with 1-D ice-sheet models forced by benthic $\delta^{18}O$ records. Ann. Glaciol. 51, 23–33.

de Boer, B., van de Wal, R.S.W., Lourens, L.J., Bintanja, R., 2012. Transient nature of the Earth's climate and the implications for the interpretation of benthic $\delta^{18}O$ records. Palaeogeogr. Palaeoclimatol. Palaeoecol. 335–336, 4–11.

de Vernal, A., Gersonde, R., Goosse, H., Seidenkrantz, M.S., Wolff, E.W., 2013. Sea ice in the paleoclimate system: the challenge of reconstructing sea ice from proxies–an introduction. Quat. Sci. Rev. 79, 1–8.

DeConto, R.M., Pollard, D., 2016. Contribution of Antarctica to past and future sea-level rise. Nature 531, 591–597.

Demidov, 1998 (unpublished – see Svendsen, J.I., Astakhov, V.I., Bolshiyanov, D.Y., Demidov, I., Dowdeswell, J.A., Gataullin, V., Hjort, C., Hubberten, H.W., Larsen, E., Mangerud, J., Melles, M., Möller, P., Saarnisto, M., Siegert, M.J., 1999. Maximum extent of the Eurasian ice sheets in the Barents and Kara Sea region during the Weichselian. Boreas 28, 234–242.

Demidov, I.N., Houmark–Nielsen, M., Kjær, K.H., Funder, S., Larsen, E., Lysså, A., Lunkka, J.P., Saarnisto, M., 2004. Valdaian glacial maxima in the Arkhangelsk district of northwestern Russia. *In* Ehlers, J. Gibbard, P.L. (Eds.). Quaternary Glaciations - Extent and Chronology – Part I: Europe. Developments in Quaternary Sciences 2, Elsevier, Amsterdam, pp. 321–336.

Demidov, I.N., Houmark–Nielsen, M., Kjaer, K.H., Larsen, E., 2006. The last Scandinavian Ice Sheet in northwestern Russia: ice flow patterns and decay dynamics. Boreas 35, 425–443.

Demuro, M., Froese, D.G., Arnold, L.J., Roberts, R.G., 2012. Single-grain OSL dating of glaciofluvial quartz constrains Reid glaciation in NW Canada to MIS 6. Quat. Res. 77, 305–316.

Dendy, S., Austermann, J., Creveling, J.R., Mitrovica, J.X., 2017. Sensitivity of Last Interglacial sea-level high stands to ice sheet configuration during Marine Isotope Stage 6. Quat. Sci. Rev. 171, 234–244.

Denton, G.H., Hughes, T.J., 1981. Ch. 8 *in* Denton, G.H., Hughes, T.J. (Eds.) The Last Great Ice Sheets. Wiley Interscience, pp. 437–467.

Deschamps P., Durand N., Bard E., Hamelin B., Camoin G., Thomas A.L., Henderson G.M., Okuno J., Yokoyama Y. 2012. Ice-sheet collapse and sea-level rise at the Bolling warming 14600 years ago. Nature 483, 559–564.

Dove, D., Polyak, L., Coakley, B., 2014. Widespread, multi-source glacial erosion on the Chukchi margin, Arctic Ocean. Quat. Sci. Rev. 92, 112–122.

Dowdeswell, J.A., Jakobsson, M., Hogan, K.A., O'Regan, M., Backman, J., Evans, J., Hell, B., Löwemark, L., Marcussen, C., Noormets, R., Cofaigh, C.Ó., 2010. High-resolution geophysical observations of the Yermak Plateau and northern Svalbard margin: implications for ice-sheet grounding and deep-keeled icebergs. Quat. Sci. Rev. 29, 3518–3531.

Duk-Rodkin, A., Barendregt, R.W., Tarnocai, C., Phillips, F.M., 1996. Late Tertiary to late Quaternary record in the Mackenzie Mountains, Northwest Territories, Canada: stratigraphy, paleosols, paleomagnetism, and chlorine-36. Canadian J. Earth Sci. 33, 875–895.

Duplessy, J.C., Labeyrie, L., Juillet-Leclerc, A., Maitre, F., Duprat, J., Sarnthein, M., 1991. Surface salinity reconstruction of the North-Atlantic Ocean during the Last Glacial Maximum. Oceanol. Acta 14, 311–324.

Duplessy, J.C., Labeyrie, L., Arnold, M., Paterne, M., Duprat, J., van Weering, T.C., 1992. Changes in surface salinity of the North Atlantic Ocean during the last deglaciation. Nature 358, 485–488.

Duplessy, J.C., Labeyrie, L., Waelbroeck, C., 2002. Constraints on the ocean oxygen isotopic enrichment between the Last Glacial Maximum and the Holocene: paleoceanographic implications. Quat. Sci. Rev. 21, 315–330.

Dutton, A., Carlson, A.E., Long, A.J., Milne, G.A., Clark, P.U., DeConto, R., Horton, B.P., Rahmstorf, S., Raymo, M.E., 2015a. Sea-level rise due to polar ice-sheet mass loss during past warm periods. Science 349, doi: 10.1126/science.aaa4019.

Dutton, A., Lambeck, K., 2012. Ice volume and sea level during the last interglacial. Science 337, 216–219.

Dutton, A., Webster, J.M., Zwartz, D., Lambeck, K., Wohlfarth, B., 2015b. Tropical tales of polar ice: evidence of last interglacial polar ice sheet retreat recorded by fossil reefs of the granitic Seychelles islands. Quat. Sci. Rev. 107, 182–196.

Dyke, A.S., Andrews, J.T., Clark, P.U., England, J.H., Miller, G.H., Shaw, J., Veillette, J.J., 2002. The Laurentide and Innuitian ice sheets during the last glacial maximum. Quat. Sci. Rev. 21, 9–31.

Ehlers, J., Gibbard, P.L., 2007. The extent and chronology of Cenozoic global glaciation. Quat. Int. 164, 6–20.

Ehlers, J. Gibbard, P.L., Hughes P.D. (Eds.), 2011a. Quaternary Glaciations – Extent and Chronology, A Closer Look, Developments in Quaternary Science 15. Elsevier, Amsterdam. 1108 pp.

Ehlers, J., Grube, A., Stephan, H.J., Wansa, S., 2011b. Pleistocene glaciations of North Germany – new results. *In* Ehlers, J., Gibbard, P.L. and Hughes, P.D. (Eds.). Quaternary Glaciations – Extent and Chronology: A Closer Look, Developments in Quaternary Science 15. Elsevier, Amsterdam, pp. 149–162.

Ehlers, L., Eissmann, L., Lippstreu, L., Stephan, H.–J., Wansa, S., 2004. Pleistocene glaciations of North Germany. *In* J. Ehlers, P.L. Gibbard (Eds.). Quaternary Glaciations. Extent and Chronology Part I: Europe, Developments in Quaternary Science 2. Elsevier, Amsterdam, pp. 135–146.

Elderfield, H., Ferretti, P., Greaves, M., Crowhurst, S., McCave, I.N., Hodell, D., Piotrowski, A.M., 2012. Evolution of ocean temperature and ice volume through the Mid-Pleistocene Climate Transition. Science 337, 704–709.

Elderfield, H., Greaves, M., Barker, S., Hall, I.R., Tripati, A., Ferretti, P., Crowhurst, S., Booth, L., Daunt, C., 2010. A record of bottom water temperature and seawater $\delta^{18}O$ for the Southern Ocean over the past 440 kyr based on Mg/Ca of benthic foraminiferal *Uvigerina* spp. Quat. Sci. Rev. 29, 160–169.

Engels, J.L., Edwards, M.H., Polyak, L., Johnson, P.D., 2008. Seafloor evidence for ice shelf flow across the Alaska–Beaufort margin of the Arctic Ocean. Earth Surf. Proc. Landf. 33, 1047–1063.

Fabel, D., Harbor, J., 1999. The use of *in-situ* produced cosmogenic radionuclides in glaciology and glacial geomorphology. Ann. Glaciol. 28, 103–110.

Fairbanks, R.G., 1989. A 17,000-year glacio-eustatic sea level record: influence of glacial melting rates on the Younger Dryas event and deep-ocean circulation. Nature 342, 637–642.

Fairbanks, R.G., Mortlock, R.A., Chiu, T.C., Cao, L., Kaplan, A., Guilderson, T.P., Fairbanks, T.W., Bloom, A.L., Grootes, P.M., Nadeau, M.J., 2005. Radiocarbon calibration curve spanning 0 to 50,000 years BP based on paired $^{230}Th/^{234}U/^{238}U$ and ^{14}C dates on pristine corals. Quat. Sci. Rev. 24, 1781–1796.

Fenton, M., Geiselhart, S., Rohling, E.J., Hemleben, C., 2000. Aplanktonic zones in the Red Sea. Marine Micropal. 40, 277–294.

Ferguson, G., Jasechko, S., 2015. The isotopic composition of the Laurentide Ice Sheet and fossil groundwater. Geophys. Res. Lett. 42, 4856–4861.

Flower, B.P., 1997. Overconsolidated section on the Yermak Plateau, Arctic Ocean: ice sheet grounding prior to ca. 660 ka? Geology 25, 147–150.

Friedrich, T., Timmermann, A., Tigchelaar, M., Timm, O.E., Ganopolski, A., 2016. Nonlinear climate sensitivity and its implications for future greenhouse warming. Sci. Adv. 2, e1501923, doi:10.1126/sciadv.1501923.

Fugitt, F.L., Spahr, P.N., Pavey, R.R., Aden, D.J., Jones, M., Angle, M.P., 2016. Surfical geology of the Hillsboro 30 x 60-minute quadrangle in Ohio: Columbus, Ohio Department of Natural Resources, Division of Geological Survey Map SG-2-HIL, scale 1:100,000.

Gallimore, R.G., Kutzbach, J.E., 1996. Role of orbitally induced changes in tundra area in the onset of glaciation. Nature 381, 503–505.

Ganopolski, A., Calov, R., 2011 The role of orbital forcing, carbon dioxide and regolith in 100 kyr glacial cycles. Clim. Past 7, 1415–1425.

Gaunt, G.D., Fletcher, T.P., Wood, C.J., 1992: Geology of the Country Around Kingston upon Hull and Brigg. Brit. Geol. Surv. Mem. 172. HMSO, London.

Gebhardt, A.C., Jokat, W., Niessen, F., Matthießen, J., Geissler, W.H., Schenke, H.W., 2011. Ice sheet grounding and iceberg plow marks on the northern and central Yermak Plateau revealed by geophysical data. Quat. Sci. Rev. 30, 1726–1738.

Gemmell, A.M.D., 1988. Thermoluminescence dating of glacially transported sediments: some considerations. Quat. Sci. Rev. 7, 277–285.

Gey, V., Saarnisto, M., Lunkka, J.P., Demidov, I., 2001. Mikulino and Valdai palaeoenvironments in the Vologda area, NW Russia. Glob. Planet. Change 31, 347–366.

Gey, V.P., Kozlov, V.V., Malakhovsky, D.B., 2004. On the age and extent of the maximum Late Pleistocene ice advance along the Baltic–Caspian watershed. *In* J. Ehlers, Gibbard, P.L. (Eds.). Quaternary Glaciations Extent and Chronology – Part I: Europe. Developments in Quaternary Sciences 2, Elsevier, Amsterdam, pp. 355–358.

Gibbard, P.L., Cohen, K.M., 2008. Global chronostratigraphical correlation table for the last 2.7 million years. Episodes 31, 243–247.

Gibbard, P.L., Pasanen, A.H., West, R.G., Lunkka, J.P., Boreham, S., Cohen, K., Rolfe, C., 2009. Late Middle Pleistocene glaciation in East Anglia, England. Boreas 38, 504–528.

Gibbard, P.L., Clark, C.D., 2011. Pleistocene glaciation limits in Great Britain. *In* Ehlers, J., Gibbard, P.L. and Hughes, P.D. (Eds.). Quaternary Glaciations – Extent and Chronology: A Closer Look, Developments in Quaternary Science 15. Elsevier, Amsterdam, pp. 75–94.

Gibbard, P.L., West, R.G., Andrew, R., Pettit, M., 1992. The margin of a Middle Pleistocene ice advance at Tottenhill, Norfolk, England. Geol. Mag. 129, 59–76.

Glen, J.W., 1958. The flow law of ice: a discussion of the assumptions made in glacier theory, their experimental foundations and consequences. IASH Publ. 47, 171–183.

Gosse, J.C., Phillips, F.M., 2001. Terrestrial *in situ* cosmogenic nuclides: theory and application. Quat. Sci. Rev. 20, 1475–1560.

Grant, K.M., Rohling, E.J., Bar-Matthews, M., Ayalon, A., Medina-Elizalde, M., Ramsey, C.B., Satow, C., Roberts, A.P., 2012. Rapid coupling between ice volume and polar temperature over the past 150 kyr. Nature 491, 744–747.

Grant, K.M., Rohling, E.J., Ramsey, C.B., Cheng, H., Edwards, R.L., Florindo, F., Heslop, D., Marra, F., Roberts, A.P., Tamisiea, M.E., Williams, F., 2014. Sea-level variability over five glacial cycles. Nature Commun. 5, 5076.

Grosswald, M.G., 1980. Late Weichselian ice sheets of northern Eurasia. Quat. Res. 13, 1–32.

Grosswald, M.G., Hughes, T.J., 1999. The case for an ice shelf in the Pleistocene Arctic Ocean 1. Polar Geogr. 23, 23–54.

Guobyte, R., Satkunas, J., 2011. Pleistocene glaciations in Lithuania. *In* Ehlers, J., Gibbard, P.L. and Hughes, P.D. (Eds.). Quaternary Glaciations – Extent and Chronology: A Closer Look, Developments in Quaternary Science 15. Elsevier, Amsterdam, pp. 231–246.

Gurski B.N., Levkov E.A., Karabanov A.K., Bessarab D.A. 1990. New data about glaciations limits within the Belarus territory. Dokl. Akad. Nauk Belarusi 34, 345–348 (in Russian).

Hansen, J., Sato, M., Kharecha, P., Beerling, D., Berner, R., Masson-Delmotte, V., Pagani, M., Raymo, M., Royer, D.L., Zachos, J.C., 2008. Target atmospheric CO_2: where should humanity aim? Open Atmos. Sci. J. 2, 217–231.

Hansen, J., Sato, M., Kharecha, P., Russell, G., Lea, D.W., Siddall, M., 2007. Climate change and trace gases. Phil. Trans. R. Soc. Lond. A 365, 1925–1954.

Hansen, J., Sato, M., Russell, G., Kharecha, P., 2013. Climate sensitivity, sea level, and atmospheric carbon dioxide. Phil. Trans. R. Soc. A 371, 20120294, doi:10.1098/rsta.2012.0294.

Hansen, J., Sato, M., Kharecha, P., von Schuckmann, K., Beerling, D.J., Cao, J., Marcott, S.,

Masson-Delmotte, V., Prather, M.J., Rohling, E.J., Shakun, J., Smith, P., Lacis, A., Russell, G., Ruedy, R., 2017. Young people's burden: requirement of negative CO_2 emissions. Earth Syst. Dyn. 8, 577–616.

Harris, S.A., 2005. Thermal history of the Arctic Ocean environs adjacent to North America during the last 3.5 Ma and a possible mechanism for the cause of the cold events (major glaciations and permafrost events). Prog. Phys. Geogr. 29, 218–237.

Hatfield, R.G., Reyes, A.V., Stoner, J.S., Carlson, A.E., Beard, B.L., Winsor, K., Welke, B., 2016. Interglacial responses of the southern Greenland ice sheet over the last 430,000 years determined using particle-size specific magnetic and isotopic tracers. Earth Planet. Sci. Lett. 454, 225–236.

Hebbeln, D., Wefer, G., 1997. Late Quaternary paleoceanography in the Fram Strait. Paleoceanography 12, 65–78.

Hemming, S.R., 2004. Heinrich events: massive late Pleistocene detritus layers of the North Atlantic and their global climate imprint. Rev. Geophys. 42, RG1005, doi:10.1029/2003RG000128.

Hennekam, R., 2015. High-frequency climate variability in the late Quaternary eastern Mediterranean – associations of Nile discharge and basin overturning circulation dynamics. Utrecht Studies in Earth Sciences 78, 160 pp., ISBN 978-90-6266-390-3.

Hibbert, F.D., Rohling, E.J., Dutton, A., Williams, F.H., Chutcharavan, P.M., Zhao, C., Tamisiea, M.E., 2016. Corals as indicators of past sea-level change: a global repository of U-series dated benchmarks. Quat. Sci. Rev. 145, 1–56.

Hoffman, J.S., Clark, P.U., Parnell, A.C., He, F., 2017. Regional and global sea-surface temperatures during the last interglaciation. Science 355, 276–279.

Houmark–Nielsen, M., 2011. Pleistocene glaciations in Denmark: a closer look at chronology, ice dynamics and landforms. *In* Ehlers, J., Gibbard, P.L. and Hughes, P.D. (Eds.). Quaternary Glaciations – Extent and Chronology: A Closer Look, Developments in Quaternary Science 15. Elsevier, Amsterdam, pp. 47–58.

Hughes, T.J., Denton, G.H., Grosswald, M.G., 1977. Was there a late-Würm Arctic ice sheet? Nature 266, 596–602.

Hughes, P.D., Gibbard, P.L., Ehlers, J., 2013. Timing of glaciation during the last glacial cycle: evaluating the concept of a global 'Last Glacial Maximum' (LGM). Earth-Sci. Rev. 125, 171–198.

Huybers, P., 2006. Early Pleistocene glacial cycles and the integrated summer insolation forcing. Science 313, 508–511.

Huybrechts, P., 2002. Sea-level changes at the LGM from ice-dynamic reconstructions of the Greenland and Antarctic ice sheets during the glacial cycles. Quat. Sci. Rev. 21, 203–231.

Imbrie, J., Hays, J.D., Martinson, D.G., McIntyre, A., Mix, A.C., Morley, J.J., Pisias, N.G., Prell, W.L., Shackleton, N.J., 1984. The orbital theory of Pleistocene climate: support from a revised chronology of the marine $\delta^{18}O$ record. In: Berger, A. (Ed.), Milankovitch and Climate, Part I, pp. 269–305. New York, Springer.

Imbrie, J., Berger, A., Boyle, E.A., Clemens, S.C., Duffy, A., Howard, W.R., Kukla, G., Kutzbach, J., Martinson, D.G., McIntyre, A., Mix, A.C., Molfino, B., Morley, J.J., Peterson, L.C., Pisias, N.G., Prell, W.L., Raymo, M.E., Shackleton, N.J., Toggweiler, J.R., 1993. On the structure and origin of major glaciation cycles. 2, The 100,000-year cycle. Paleoceanography 8, 699–735.

Ivins, E.R., James, T.S., 2005. Antarctic glacial isostatic adjustment: a new assessment. Antarctic Sci. 17, 541–553.

Israelson, C., Wohlfarth, B., 1999. Timing of the last-interglacial high sea level on the Seychelles Islands, Indian Ocean. Quat. Res. 51, 306–316.

Jackson, L., Ward, B., Duk-Rodkin, A., Hughes, O., 1991. The last Cordilleran ice sheet in southern Yukon Territory. Géogr. Phys. Quat. 45, 341–354.

Jackson, L.E., Andriashek, L.D., Phillips, F.M., 2011. Limits of successive Middle and Late Pleistocene continental ice sheets, interior plains of southern and central Alberta and adjacent areas. *In* Ehlers, J., Gibbard, P.L. and Hughes, P.D. (Eds.). Quaternary Glaciations –

Extent and Chronology: A Closer Look, Developments in Quaternary Science 15. Elsevier, Amsterdam, pp. 575–590.

Jakobsson, M., 1999. First high-resolution CHIRP sonar profiles from the central Arctic Ocean reveal erosion of Lomonosov Ridge sediments. Mar. Geol. 158, 111–123.

Jakobsson, M., Polyak, L., Edwards, M., Kleman, J., Coakley. B., 2008. Glacial geomorphology of the Central Arctic Ocean: the Chukchi Borderland and the Lomonosov Ridge, Earth Surf. Proc. Landf. 33, 526–545.

Jakobsson, M., Nilsson, J., O'Regan, M., Backman, J., Löwemark, L., Dowdeswell, J.A., Mayer, L., Polyak, L., Colleoni, F., Anderson, L.G., Björk, G., 2010. An Arctic Ocean ice shelf during MIS 6 constrained by new geophysical and geological data. Quat. Sci. Rev. 29, 3505–3517.

Jakobsson, M., Andreassen, K., Bjarnadóttir, L.R., Dove, D., Dowdeswell, J.A., England, J.H., Funder, S., Hogan, K., Ingólfsson, Ó., Jennings, A., Larsen, N.K., 2014a. Arctic Ocean glacial history. Quat. Sci. Rev. 92, 40–67.

Jakobsson, M., Ingólfsson, Ó., Long, A.J., Spielhagen, R.F., 2014b. The dynamic Arctic. Quat. Sci. Rev. 92, 1–8.

Jakobsson, M., Nilsson, J., Anderson, L., Backman, J., Björk, G., Cronin, T.M., Kirchner, N., Koshurnikov, A., Mayer, L., Noormets, R., and O'Regan, M., 2016. Evidence for an ice shelf covering the central Arctic Ocean during the penultimate glaciation. Nat. Commun. 7, 10365.

Kageyama, M., Valdes, P.J., Ramstein, G., Hewitt, C., Wyputta, U., 1999. Northern Hemisphere storm tracks in present day and last glacial maximum climate simulations: a comparison of the European PMIP models. J. Clim. 12, 742–760.

Karabanov, A.K., Matveyev, A.V., 2011. The Pleistocene glaciations in Belarus. *In* Ehlers, J., Gibbard, P.L. and Hughes, P.D. (Eds.). Quaternary Glaciations – Extent and Chronology: A Closer Look, Developments in Quaternary Science 15. Elsevier, Amsterdam, pp. 29–35.

Kendall, R.A., Mitrovica, J.X., Milne, G.A., 2005. On post-glacial sea level – II. Numerical formulation and comparative results on spherically symmetric models. Geophys. J. Int. 161, 679–706.

Kirschner, N., Furrer, R., Jakobsson, M., Zwally, H.J., Robbins, J.W., 2013. Statistical modeling of a former Arctic Ocean ice shelf complex using Antarctic analogies. J. Geophys. Res 118, 1105–1117.

Knies, J., Spielhagen, R.F., 2016. A pan-Arctic ice shelf during late Marine Isotope Stage (MIS) 6: Fact or fiction? Abstracts, Past Gateways 4th International Conference, Trondheim, Norway, 23–27 May 2016, pp. 45–46.

Knies, J., Nowaczyk, N., Müller, C., Vogt, C., Stein, R., 2000. A multiproxy approach to reconstruct the environmental changes along the Eurasian continental margin over the last 150 000 years. Mar. Geol. 163, 317–344.

Knight, J., Coxon, P., McCabe, A.M., McCarron, S.G., 2004. Pleistocene glaciations in Ireland. *In* J. Ehlers, Gibbard, P.L. (Eds.). Quaternary Glaciations Extent and Chronology – Part I: Europe. Developments in Quaternary Sciences, 2, Elsevier, Amsterdam, pp. 183–191.

Köhler, P., Bintanja, R., 2008. The carbon cycle during the Mid Pleistocene Transition: the Southern Ocean decoupling hypothesis. Clim. Past 4, 311–332.

Köhler, P., Bintanja, R., Fischer, H., Joos, F., Knutti, R., Lohmann, G., Masson-Delmotte, V., 2010. What caused Earth's temperature variations during the last 800,000 years? Data-based evidence on radiative forcing and constraints on climate sensitivity. Quat. Sci. Rev. 29, 129–145.

Köhler, P., de Boer, B., von der Heydt, A. S., Stap, L.B., van de Wal, R., 2015. On the state dependency of the equilibrium climate sensitivity during the last 5 million years. Clim. Past 11, 1801–1823.

Krinner, G., Mangerud, J., Jakobsson, M., Crucifix, M., 2004. Enhanced ice sheet growth in Eurasia owing to adjacent ice-dammed lakes. Nature 427, 429–432.

Krinner, G., Boucher, O., Balkanski, Y., 2006. Ice-free glacial northern Asia due to dust deposition on snow. Clim. Dyn. 27, 613–625.

Kristoffersen, Y., Coakley, B., Jokat, W., Edwards, M., Brekke, H., Gjengedal, J., 2004. Seabed erosion on the Lomonosov Ridge, central Arctic Ocean: a tale of deep draft icebergs in the Eurasia Basin and the influence of Atlantic water inflow on iceberg motion? Paleoceanography 19. DOI: 10.1029/2003PA000985

Kuijpers, A., Dalhoff, F., Brandt, M.P., Hümbs, P., Schott, T., Zotova, A., 2007. Giant iceberg plow marks at more than 1 km water depth offshore West Greenland. Mar. Geol. 246, 60–64.

Laban, C., van der Meer, J. J. M., 2004. Pleistocene glaciation in the Netherlands. *In* J. Ehlers, Gibbard, P.L. (Eds.). Quaternary Glaciations Extent and Chronology – Part I: Europe. Developments in Quaternary Sciences, 2, Elsevier, pp. 251–260.

Laban, C., van der Meer, J.J., 2011. Pleistocene glaciation in the Netherlands. *In* Ehlers, J., Gibbard, P.L. and Hughes, P.D. (Eds.). Quaternary Glaciations – Extent and Chronology: A Closer Look, Developments in Quaternary Science 15. Elsevier, pp. 247–260.

Lambeck, K., Chappell, J., 2001. Sea level change through the last glacial cycle. Science 292, 679–686.

Lambeck, K., Purcell, A., Funder, S., Kjær, K., Larsen, E., Moller, P.E.R., 2006. Constraints on the Late Saalian to early Middle Weichselian ice sheet of Eurasia from field data and rebound modelling. Boreas 35, 539–575.

Lambeck, K., Purcell, A., Zhao, J., Svensson, N.O., 2010. The Scandinavian ice sheet: from MIS 4 to the end of the Last Glacial Maximum. Boreas 39, 410–435.

Lambeck, K., Purcell, A., Zhao, S., 2017. The North American Late Wisconsin ice sheet and mantle viscosity from glacial rebound analyses. Quat. Sci. Rev. 158, 172–210.

Landais, A., Dreyfus, G., Capron, E., Jouzel, J., Masson-Delmotte, V., Roche, D.M., Prié, F., Caillon, N., Chappellaz, J., Leuenberger, M., Lourantou, A., 2013. Two-phase change in CO_2, Antarctic temperature and global climate during Termination II. Nat. Geosci. 6, 1062–1065.

Larrasoaña, J.C., Roberts, A.P., Rohling, E.J., Winklhofer, M., Wehausen, R., 2003. Three million years of monsoon variability over the northern Sahara. Clim. Dyn. 21, 689–698.

Laskar, J., Robutel, P., Joutel, F., Gastineau, M., Correia, A.C.M., Levrard, B., 2004. A long-term numerical solution for the insolation quantities of the Earth. Astron. Astrophys. 428, 261–285.

Le Roy, I., 1994. Evolution des volcans en système de point chaud: île de Tahiti, Archipel de la Société (Polynésie Française). PhD thesis. University of Paris, 271 pp.

Lecavalier, B.S., Milne, G.A., Simpson, M.J., Wake, L., Huybrechts, P., Tarasov, L., Kjeldsen, K.K., Funder, S., Long, A.J., Woodroffe, S., Dyke, A.S., 2014. A model of Greenland ice sheet deglaciation constrained by observations of relative sea level and ice extent. Quat. Sci. Rev. 102, 54–84.

Liakka, J., Nilsson, J., Löfverström, M., 2012. Interactions between stationary waves and ice sheets: linear versus nonlinear atmospheric response. Clim. Dyn. 38, 1249–1262.

Liakka, J., Löverström, M., Colleoni, F., 2016. The impact of the North American glacial topography on the evolution of the Eurasian ice sheet over the last glacial cycle. Clim. Past 12, 1225–1241.

Licciardi, J.M., Clark, P.U., Jenson, J.W., Macayeal, D.R., 1998. Deglaciation of a soft-bedded Laurentide Ice Sheet. Quat. Sci. Rev. 17, 427–448.

Lippstreu, L., 2002 (unpublished – see Lippstreu, L., Brose, F., Marcinek, J., 1995. Brandenburg. Das Quartär Deutschlands, 116–147.)

Lisiecki, L.E., Raymo, M.E., 2005. A Pliocene-Pleistocene stack of 57 globally distributed benthic $\delta^{18}O$ records. Paleoceanography 20, PA1003, doi:10.1029/2004PA001071.

Litt, T., Behre, K.-E., Meyer, K.-D., Stephan, H.-J., Wansa, S., 2007. Stratigraphishe Begriffe für das Quartär des Norddeutschland Vereisungsgebietes. Quat. Sci. J. 56, 7–65.

Liverman, D.G., Catto, N.R., Rutter, N.W., 1989. Laurentide glaciation in west-central Alberta: a single (Late Wisconsinan) event. Canad. J. Earth Sci. 26, 266–274.

Lloyd, J.M., Kroon, D., Boulton, G.S., Laban, C., Fallick, A., 1996. Ice rafting history from the Spitsbergen ice cap over the last 200 kyr. Mar. Geol. 131, 103–121.

Loulergue, L., Schilt, A., Spahni, R., Masson-Delmotte, V., Blunier, T., Lemieux, B., Barnola, J.M., Raynaud, D., Stocker, T.F., Chappellaz, J., 2008. Orbital and millennial-scale features of atmospheric CH_4 over the past 800,000 years. Nature 453, 383–386.

Lourantou, A., Lavric, J.V., Koehler, P., Barnola, J.-M., Paillard, D., Michel, E., Raynaud, D., Chappellaz, J., 2010. Constraint of the CO_2 rise by new atmospheric carbon isotopic measurements during the last deglaciation. Global Biogeochem. Cycles 24, doi: 10.1029/2009GB003545.

Löfverström, M., Caballero, R., Nilsson, J., Kleman, J., 2014. Evolution of the large-scale atmospheric circulation in response to changing ice sheets over the last glacial cycle. Clim. Past 10, 1453–1471.

Löwemark, L., Chao, W.S., Gyllencreutz, R., Hanebuth, T.J.J., Chiu, P.Y., Yang, T.N., Su, C.C., Chuang, C.K., Dominguez, D.C., Jakobsson, M., 2016. Variations in glacial and interglacial marine conditions over the last two glacial cycles off northern Greenland. Quat. Sci. Rev. 147, 164–177.

Mangerud, J., Astakhov, V., Svendsen, J.I., 2002. The extent of the Barents–Kara ice sheet during the Last Glacial Maximum. Quat. Sci. Rev. 21, 111–119.

Mangerud, J., Jakobsson, M., Alexanderson, H., Astakhov, V., Clarke, G.K., Henriksen, M., Hjort, C., Krinner, G., Lunkka, J.P., Möller, P., Murray, A., 2004. Ice-dammed lakes and rerouting of the drainage of northern Eurasia during the Last Glaciation. Quat. Sci. Rev. 23, 1313–1332.

Marino, G., Rohling, E.J., Rodríguez-Sanz, L., Grant, K.M., Heslop, D., Roberts, A.P., Stanford, J.D., Yu, J., 2015. Bipolar seesaw control on last interglacial sea level. Nature 522, 197–201.

Marks, L., 2011. Quaternary glaciations in Poland. Developm. Quat. Sci. 15, 299–303.

Marks, L., 2012. Timing of the Late Vistulian (Weichselian) glacial phases in Poland. Quat. Sci. Rev. 44, 81–88.

Martin, P.A., Lea, D.W., Rosenthal, Y., Shackleton, N.J., Sarnthein, M., Papenfuss, T., 2002. Quaternary deep sea temperature histories derived from benthic foraminiferal Mg/Ca. Earth Planet. Sci. Lett. 198, 193–209.

Martinson, D.G., Pisias, N.G., Hays, J.D., Imbrie, J., Moore, T.C., Shackleton, N.J., 1987. Age dating and the orbital theory of the ice ages: development of a high-resolution 0 to 300,000-year chronostratigraphy. Quat. Res. 27, 1–29.

Martínez-Botí, M.A., Foster, G.L., Chalk, T.B., Rohling, E.J., Sexton, P.F., Lunt, D.J., Pancost, R.D., Badger, M.P.S., Schmidt, D.N., 2015. Plio-Pleistocene climate sensitivity evaluated using high-resolution CO_2 records. Nature 518, 49–54.

Marshall, S.J., Clark, P.U., 2002. Basal temperature evolution of North American ice sheets and implications for the 100-kyr cycle. Geophys. Res. Lett. 29, 671–674.

Marshall, S.J., James, T.S., Clarke, G.K., 2002. North American ice sheet reconstructions at the Last Glacial Maximum. Quat. Sci. Rev. 21, 175–192.

Matoshko, A.V., 2011. Chapter 31. Limits of the Pleistocene glaciation in the Ukraine: a closer look. *In* Ehlers, J., Gibbard, P.L. and Hughes, P.D. (Eds.). Quaternary Glaciations – Extent and Chronology: A Closer Look, Developments in Quaternary Science 15. Elsevier, Amsterdam, pp. 405–416.

Matoshko, A.V., Chugunny, Yu. G., 1993. The Dnieper glaciation of Ukraine (geological aspect). Naukova Dumka, Kiev, pp. 192 (In Russian).

Matoshko, A.V., Chugunny, Yu. G., 1995. Geological activity and dynamic evolution of the Dnieper glaciation. *In* Ehlers, J., Kozarski, S., Gibbard ,P.L. (Eds.). Glacial Deposits in North–East Europe, A.A. Balkema, Rotterdam, Brookfield, pp. 225–230.

Matthiessen, J., Knies, J., 2001. Dinoflagellate cyst evidence for warm interglacial conditions at the northern Barents Sea margin during marine oxygen isotope stage 5. J. Quat. Sci. 16, 727–737.

McKay, E.D., III, Berg, R.C., 2008. Optical ages spanning two glacial-interglacial cycles from deposits of the ancient Mississippi river, north-central Illinois. Geol. Soc. Am. Abstr. Progr. 40, 78.

McKay III, E.D., Berg, R.C., Hansel, A.K., Kemmis, T.J., Stumpf, A.J., 2008. Quaternary deposits and history of the ancient Mississippi river valley, north-central Illinois. Illinois State Geological Survey Guidebook 35, 106 pp.

McKay, N.P., Overpeck, J.T., Otto-Bliesner, B.L., 2011. The role of ocean thermal expansion in Last Interglacial sea level rise. Geophys. Res. Lett. 38, L14605, doi:10.1029/2011GL048280.

Mercer, J.H., 1970. A former ice sheet in the Arctic Ocean? Palaeogeogr. Palaeoclimatol. Palaeoecol. 8, 19–27.

Mitrovica, J.X., Wahr, J., Matsuyama, I., Paulson, A., 2005. The rotational stability of an ice-age earth. Geophys. J. Int. 161, 491–506.

Mix, A.C., Ruddiman, W.F., 1984. Oxygen-isotope analyses and Pleistocene ice volumes. Quat. Res. 21, 1–20.

Mix, A.C., Bard, E., Schneider, R., 2001. Environmental processes of the ice age: land, oceans, glaciers (EPILOG). Quat. Sci. Rev. 20, 627–657.

Mohr, K., 1993. Tertiär und Quartär. *In* Mohr, K. (Ed.). Geologie und Minerallagerstätten des Harzes. Schweizerbart Science Publications, Stuttgart, pp. 384.

Möller, P., Alexanderson, H., Funder, S., Hjort, C., 2015. The Taimyr Peninsula and the Severnaya Zemlya archipelago, Arctic Russia: a synthesis of glacial history and palaeo-environmental change during the Last Glacial cycle (MIS 5e–2). Quat. Sci. Rev. 107, 149–181.

Monnin, E., Indermühle, A., Dällenbach, A., Flückiger, J., Stauffer, B., Stocker, T.F., Raynaud, D., Barnola, J.M., 2001. Atmospheric CO_2 concentrations over the last glacial termination. Science 291, 112–114.

Monnin, E., Steig, E.J., Siegenthaler, U., Kawamura, K., Schwander, J., Stauffer, B., Stocker, T.F., Morse, D.L., Barnola, J.M., Bellier, B., Raynaud, D., Fischer, H., 2004. Evidence for substantial accumulation rate variability in Antarctica during the Holocene, through synchronization of CO_2 in the Taylor Dome, Dome C and DML ice cores. Earth Planet. Sci. Lett. 224, 45–54.

Montaggioni, L.F., 2005. History of Indo-Pacific coral reef systems since the last glaciation: development patterns and controlling factors. Earth Sci. Rev. 71, 1–75.

Naafs, B.D.A., Hefter, J., Acton, G., Haug, G.H., Martínez-Garcia, A., Pancost, R., Stein, R., 2012. Strengthening of North American dust sources during the late Pliocene (2.7 Ma). Earth Planet. Sci. Lett. 317, 8–19.

Niessen, F., Hong, J.K., Hegewald, A., Matthiessen, J., Stein, R., Kim, H., Kim, S., Jensen, L., Jokat, W., Nam, S.I., Kang, S.H., 2013. Repeated Pleistocene glaciation of the East Siberian continental margin. Nat. Geosci. 6, 842–846.

Nørgaard-Pedersen, N., Mikkelsen, N., Lassen, S.J., Kristoffersen, Y., Sheldon, E., 2007. Reduced sea ice concentrations in the Arctic Ocean during the last interglacial period revealed by sediment cores off northern Greenland. Paleoceanography 22, PA1218, doi:10.1029/2006PA001283.

Obrochta, S.P., Crowley, T.J., Channell, J.E.T., Hodell, D.A., Baker, P.A., Seki, A., Yokoyama, Y., 2014. Climate variability and ice-sheet dynamics during the last three glaciations. Earth Planet. Sci. Lett. 406, 198–212.

Oglesby, R.J., 1990. Sensitivity of glaciation to initial snow cover, CO_2, snow albedo, and oceanic roughness in the NCAR CCM. Clim. Dyn. 4, 219–235.

O'Regan, M., Jakobsson, M., Kirchner, N., 2010. Glacial geological implications of overconsolidated sediments on the Lomonosov Ridge and Yermak Plateau. Quat. Sci. Rev. 29, 3532–3544.

Osborne, A.H., Vance, D., Rohling, E.J., Barton, N., Rogerson, M., Fello, N., 2008. A humid corridor across the Sahara for the migration "Out of Africa" of early modern humans 120,000 years ago. Proc. Natl. Acad. Sci. USA 105, 16444–16447.

PALAEOSENS Project Members (Rohling, E.J., Sluijs, A., Dijkstra, H.A., Köhler, P., van de Wal, R.S.W., von der Heydt, A.S., Beerling, D., Berger, A., Bijl, P.K., Crucifix, M., deConto, R., Drijfhout, S.S., Fedorov, A., Foster, G., Ganopolski, A., Hansen, J., Hönisch, B., Hooghiemstra, H., Huber, M., Huybers, P., Knutti, R., Lea, D.W., Lourens, L.J., Lunt, D., Masson-Demotte, V., Medina-Elizalde, M., Otto-Bliesner, B., Pagani, M., Pälike, H., Renssen, H., Royer, D.L., Siddall, M., Valdes, P., Zachos, J.C., Zeebe, R.E.), 2012. Making sense of palaeoclimate sensitivity. Nature 491, 683–691.

Palienko V.P., 1982. Features of glacial relief of the Dnieper glacier marginal zone within Volyn' Polessie area. *In* Bondarchuk, V.G. (Ed.). Materialy po izucheniyu chetvertichnogo perioda na teritorii Ukrainy, Naukova dumka, Kiev, pp. 203–211.

Parrenin, F., Masson-Delmotte, V., Köhler, P., Raynaud, D., Paillard, D., Schwander, J., Barbante, C., Landais, A., Wegner, A., Jouzel, J., 2013. Synchronous change of atmospheric CO_2 and Antarctic temperature during the last deglacial warming. Science 339, 1060–1063.

Patton, H., Hubbard, A., Andreassen, K., Winsborrow, M., Stroeven, A.P., 2016. The build-up, configuration, and dynamical sensitivity of the Eurasian ice-sheet complex to Late Weichselian climatic and oceanic forcing. Quat. Sci. Rev. 153, 97–121.

Pattyn, F., 2010. Antarctic subglacial conditions inferred from a hybrid ice sheet/ice stream model. Earth Planet. Sci. Lett. 295, 451–461.

Pavey, R.R., Goldthwait, R.P., Brockman, C.S., Hull, D.N., Swinford, E.M., Van Horn, R.G., 1999. Quaternary geology of Ohio. Ohio Division of Geological Survey, Map No. 2.

Payne, A.J., 1995. Limit cycles in the basal thermal regime of ice sheets. J. Geophys. Res. 100, 4249–4263.

Peltier, W.R., 1996. Mantle viscosity and ice-age ice sheet topography. Science 273, 1359–1364.

Peltier, W.R., 2004. Global glacial isostasy and the surface of the ice-age Earth: the ICE-5G (VM2) model and GRACE. Ann. Rev. Earth Planet. Sci. 32, 111–149.

Peltier, W.R., Argus, D.F., Drummond, R., 2015. Space geodesy constrains ice-age terminal deglaciation: the global ICE-6G_C (VM5a) model. J. Geophys. Res. 120, 450–487.

Peyaud, V., 2006. Rôle de la dynamique des calottes glaciaires dans les grands changements climatiques des périodes glaciaires-interglaciaires. PhD thesis. Université Joseph-Fourier-Grenoble. 247 pp.

Polyak, L., Edwards, M. H., Coakley, B. J., Jakobsson M. 2001. Ice shelves in the Pleistocene Arctic Ocean inferred from glaciogenic deep-sea bedforms. Nature, 410, 453–457.

Polyak, L., Curry, W.B., Darby, D.A., Bischof, J., Cronin, T.M., 2004. Contrasting glacial/interglacial regimes in the western Arctic Ocean as exemplified by a sedimentary record from the Mendeleev Ridge. Palaeogeogr. Palaeoclimatol. Palaeoecol. 203, 73–93.

Polyak, L., Bischof, J., Ortiz, J.D., Darby, D.A., Channell, J.E.T., Xuan, C., Kaufman, D.S., Løvlie, R., Schneider, D.A., Eberl, D.D., Adler, R.E., 2009. Late Quaternary stratigraphy and sedimentation patterns in the western Arctic Ocean. Glob. Planet. Chang 68, 5–17.

Polyak, L., Alley, R.B., Andrews, J.T., Brigham-Grette, J., Cronin, T.M., Darby, D.A., Dyke, A.S., Fitzpatrick, J.J., Funder, S., Holland, M., Jennings, A.E., 2010. History of sea ice in the Arctic. Quat. Sci. Rev. 29, 1757–1778.

Potter, E.K., Lambeck, K., 2003. Reconciliation of sea-level observations in the Western North Atlantic during the last glacial cycle. Earth Planet. Sci. Lett. 217, 171–181.

Putkonen, J., Swanson, T., 2003. Accuracy of cosmogenic ages for moraines. Quat. Res. 59, 255–261.

Rabineau, M., Berné, S., Olivet, J.L., Aslanian, D., Guillocheau, F., Joseph, P., 2006. Paleo sea levels reconsidered from direct observation of paleoshoreline position during Glacial Maxima (for the last 500,000 yr). Earth Planet. Sci. Lett. 252, 119–137.

Raymo, M.E., Lisiecki, L.E., Nisancioglu, K.H., 2006. Plio-Pleistocene ice volume, Antarctic climate, and the global $\delta^{18}O$ record. Science 313, 492–495.

Reimer, P.J., Bard, E., Bayliss, A., Beck, J.W., Blackwell, P.G., Ramsey, C.B., Buck, C.E., Cheng, H., Edwards, R.L., Friedrich, M., Grootes, P.M., 2013. INTCAL13 and MARINE13 radiocarbon age calibration curves 0-50,000 years cal BP. Radiocarbon 55, 1869–1887.

Ringler, T.D., Cook, K.H., 1997. Factors controlling nonlinearity in mechanically forced stationary waves over orography. J. Atmos. Sci. 54, 2612–2629.

Roe, G.H., Lindzen, R.S., 2001. The mutual interaction between continental-scale ice sheets and atmospheric stationary waves. J. Clim. 14, 1450–1465.

Rohling, E.J., Cane, T.R., Cooke, S., Sprovieri, M., Bouloubassi, I., Emeis, K.C., Schiebel, R., Kroon, D., Jorissen, F.J., Lorre, A., Kemp, A.E.S., 2002. African monsoon variability during the previous interglacial maximum. Earth Planet. Sci. Lett. 202, 61–75.

Rohling, E.J., Fenton, M., Jorissen, F.J., Bertrand, P., Ganssen, G., Caulet, J.P., 1998. Magnitudes of sea-level lowstands of the past 500,000 years. Nature 394, 162–165.

Rohling, E.J., Foster, G.L., Grant, K.M., Marino, G., Roberts, A.P., Tamisiea, M.E., Williams, F., 2014. Sea-level and deep-sea-temperature variability over the past 5.3 million years. Nature 508, 477–482.

Rohling, E.J., Grant, K., Bolshaw, M., Roberts, A.P., Siddall, M., Hemleben, C., Kucera, M., 2009. Antarctic temperature and global sea level closely coupled over the past five glacial cycles. Nat. Geosci. 2, 500–504.

Rohling, E.J., Grant, K., Hemleben, C.H., Siddall, M., Hoogakker, B.A.A., Bolshaw, M., Kucera, M., 2008. High rates of sea-level rise during the last interglacial period. Nat. Geosci. 1, 38–42.

Rohling, E.J., Marino, G., Grant, K.M., 2015. Mediterranean climate and oceanography, and the periodic development of anoxic events (sapropels). Earth-Sci. Rev. 143, 62–97.

Rohling, E.J., Medina-Elizalde, M., Shepherd, J.G., Siddall, M., Stanford, J.D., 2012. Sea surface and high-latitude temperature sensitivity to radiative forcing of climate over several glacial cycles. J. Clim. 25, 1635–1656.

Rohling, E.J., Sprovieri, M., Cane, T., Casford, J.S., Cooke, S., Bouloubassi, I., Emeis, K.C., Schiebel, R., Rogerson, M., Hayes, A., Jorissen, F.J., 2004. Reconstructing past planktic foraminiferal

habitats using stable isotope data: a case history for Mediterranean sapropel S5. Mar. Micropal. 50, 89–123.

Rose, J., 2009. Early and Middle Pleistocene landscapes of eastern England. Proc. Geol. Assoc. 120, 3–33.

Rose, J., Candy, I., Moorlock, B.S.P., Wilkins, H., Lee, J.A., Hamblin, R.J.O., Lee, J.R., Riding, J.B., Morigi, A.N., 2002. Early and early Middle Pleistocene river, coastal and neotectonic processes, southeast Norfolk, England. Proc. Geol. Assoc. 113, 47–67.

Rovey, C.W., Balco, G., 2011. Summary of Early and Middle Pleistocene Glaciations in Northern Missouri, USA. *In* Ehlers, J., Gibbard, P.L., Hughes, P.D. (Eds.). Quaternary Glaciations – Extent and Chronology: A Closer Look, Developments in Quaternary Science 15. Elsevier, pp. 553–562.

Ruddiman, W.E., 1977. Late Quaternary deposition of ice-rafted sand in the sub-polar North Atlantic (40-60° N). Geol. Soc. Am. Bull. 88, 1813–1827.

Ruzicka, M., 2004. The Pleistocene glaciation of Czechia. *In* Ehlers, J., Gibbard, P.L. (Eds.). Quaternary Glaciations Extent and Chronology – Part I: Europe. Developments in Quaternary Sciences, 2, Elsevier, Amsterdam, pp. 27–34.

Schmitt, J., Schneider, R., Elsig, J., Leuenberger, D., Lourantou, A., Chappellaz, J., Köhler, P., Joos, F., Stocker, T.F., Leuenberger, M., Fischer, H., 2012. Carbon isotope constraints on the deglacial CO_2 rise from ice cores. Science 336, 711–714.

Schneider, R., Schmitt, J., Koehler, P., Joos, F., Fischer, H., 2013. A reconstruction of atmospheric carbon dioxide and its stable carbon isotopic composition from the penultimate glacial maximum to the last glacial inception. Clim. Past 9, 2507–2523.

Schott, F.A., Xie, S.-P., McCreary Jr., J.P., 2009. Indian Ocean circulation and climate variability. Rev. Geophys. 47, RG1002, doi:10.1029/2007RG000245.

Schrag, D.P., Adkins, J.F., McIntyre, K., Alexander, J.L., Hodell, D.A., Charles, C.D., McManus, J.F., 2002. The oxygen isotopic composition of seawater during the Last Glacial Maximum. Quat. Sci. Rev. 21, 331–342.

Scrivner, A.E., Vance, D., Rohling, E.J., 2004. New neodymium isotope data quantify Nile involvement in Mediterranean anoxic episodes. Geology 32, 565–568.

Seguinot, J., Khroulev, C., Rogozhina, I., Stroeven, A.P., Zhang, Q., 2014. The effect of climate forcing on numerical simulations of the Cordilleran ice sheet at the Last Glacial Maximum. Cryosphere 8, 1087–1103.

Seidel, G., 2003. Geologische Ubersichtskarte von Thüringen 1:200,000. *In* Seidel, G. (Ed.) Geologie von Thüringen. Schweizerbart Science Publishers, Stuttgart, pp. 548.

Sejrup, H.P., Hjelstuen, B.O., Dahlgren, K.T., Haflidason, H., Kuijpers, A., Nygård, A., Praeg, D., Stoker, M.S., Vorren, T.O., 2005. Pleistocene glacial history of the NW European continental margin. Mar. Petrol. Geol. 22, 1111–1129.

Shakun, J.D., Lea, D.W., Lisiecki, L.E., Raymo, M.E., 2015. An 800-kyr record of global surface ocean $\delta^{18}O$ and implications for ice volume-temperature coupling. Earth Planet. Sci. Lett. 426, 58–68.

Siani, G., Paterne, M., Arnold, M., Bard, E., Métivier, B., Tisnerat, N., Bassinot, F., 2000. Radiocarbon reservoir ages in the Mediterranean Sea and Black Sea. Radiocarbon 42, 271–280.

Siddall, M., Hönisch, B., Waelbroeck, C., Huybers, P., 2010. Changes in deep Pacific temperature during the mid-Pleistocene transition and Quaternary. Quat. Sci. Rev. 29, 170–182.

Siddall, M., Rohling, E.J., Almogi-Labin, A., Hemleben, C., Meischner, D., Schmelzer, I., Smeed, D.A., 2003. Sea-level fluctuations during the last glacial cycle. Nature 423, 853–858.

Siddall, M., Smeed, D.A., Hemleben, C., Rohling, E.J., Schmelzer, I., Peltier, W.R., 2004. Understanding the Red Sea response to sea level. Earth Planet. Sci. Lett. 225, 421–434.

Siegert, M.J., Dowdeswell, J.A., Hald, M., Svendsen, J.I., 2001. Modelling the Eurasian Ice Sheet through a full (Weichselian) glacial cycle. Glob. Planet. Change 31, 367–385.

Simpson, M.J.R., Milne, G.A., Huybrechts, P., Long, A.J. 2009. Calibrating a glaciological model of the Greenland ice sheet from the Last Glacial Maximum to present-day using field observations of relative sea level and ice extent. Quat. Sci. Rev. 28, 1631–1657.

Sivan, D., Sisma-Ventura, G., Greenbaum, N., Bialik, O.M., Williams, F.H., Tamisiea, M.E., Rohling, E.J., Frumkin, A., Avnaim-Katav, S., Shtienberg, G., Stein, M., 2016. Eastern Mediterranean sea levels through the last interglacial from a coastal-marine sequence in northern Israel. Quat. Sci. Rev. 145, 204–225.

Skinner, L.C., Shackleton, N.J., 2005. An Atlantic lead over Pacific deep-water change across Termination I: implications for the application of the marine isotope stage stratigraphy. Quat. Sci. Rev. 24, 571–580.

Snyder, C.W., 2016a. Bayesian hierarchical regression analysis of variations in sea surface temperature change over the past million years. Paleoceanography 31, 1283–1300.

Snyder, C.W., 2016b. Evolution of global temperature over the past two million years. Nature 538, 226–228.

Sosdian, S., Rosenthal, Y., 2009. Deep-sea temperature and ice volume changes across the Pliocene-Pleistocene climate transitions. Science 325, 306–310.

Spielhagen, R.F., Baumann, K.H., Erlenkeuser, H., Nowaczyk, N.R., Nørgaard-Pedersen, N., Vogt, C., Weiel, D., 2004. Arctic Ocean deep-sea record of northern Eurasian ice sheet history. Quat. Sci. Rev. 23, 1455–1483.

Stein, R., Fahl., K., Gierz, P., Niessen, F., Lohmann, G., 2017. Arctic Ocean sea ice cover during the penultimate glacial and the last interglacial. Nat. Commun. 8:373, doi: 10.1038/s41467-017-00552-1.

Stenni, B., Masson-Delmotte, V., Selmo, E., Oerter, H., Meyer, H., Röthlisberger, R., Jouzel, J., Cattani, O., Falourd, S., Fischer, H., Hoffmann, G., 2010. The deuterium excess records of EPICA Dome C and Dronning Maud Land ice cores (East Antarctica). Quat. Sci. Rev. 29, 146–159.

Stirling, C.H., Esat, T.M., McCulloch, M.T., Lambeck, K., 1995. High-precision U-series dating of corals from Western Australia and implications for the timing and duration of the Last Interglacial. Earth Planet. Sci. Lett. 135, 115–130.

Stocker, T.F., Qin, D., Plattner, G.K., Tignor, M., Allen, S.K., Boschung, J., Nauels, A., Xia, Y., Bex, V., Midgley, P.M., 2013. Climate Change 2013: The Physical Science Basis. Contribution of Working Group I to the Fifth Assessment Report of the Intergovernmental Panel on Climate Change. Cambridge University Press, Cambridge, UK, 1535 pp.

Straw, A., 1979. The Devensian glaciation. *In* Straw, A., Clayton, K.M. (Eds.), 1979. The Geomorphology of the British Isles: Eastern and Central England. Methuen, London, pp. 21–45.

Stokes, C.R., Tarasov, L., Blomdin, R., Cronin, T.M., Fisher, T.G., Gyllencreutz, R., Hättestrand, C., Heyman, J., Hindmarsh, R.C., Hughes, A.L., Jakobsson, M., 2015. On the reconstruction of palaeo-ice sheets: recent advances and future challenges. Quat. Sci. Rev. 125, 15–49.

Stroeven A.P., Fabel, D., Margold, M., Clague, J.J., Xu, S. 2014. Investigating absolute chronologies of glacial advances in the NW sector of the Cordilleran Ice Sheet with terrestrial in situ cosmogenic nuclides. Quat. Sci. Rev. 92, 429–443.

Stroeven A.P., Fabel, D., Codilean, A.T., Kleman, J., Clague, J.J., Miguens-Rodriguez, M., Xu., S., 2010. Investigating the glacial history of the northern sector of the Cordilleran Ice Sheet with cosmogenic 10Be concentrations in quartz. Quat. Sci. Rev. 29, 3630–3643.

Svendsen, J.I., Alexanderson, H., Astakhov, V.I., Demidov, I., Dowdeswell, J.A., Funder, S., Gataullin, V., Henriksen, M., Hjort, C., Houmark-Nielsen, M., Hubberten, H.W., 2004. Late Quaternary ice sheet history of Northern Eurasia. Quat. Sci. Rev. 23, 1229–1271.

Syverson, K.M., Colgan, P.M. 2011. The Quaternary of Wisconsin: an updated review of stratigraphy, glacial history and landforms. *In* Ehlers, J., Gibbard, P.L., Hughes, P.D. (Eds.). Quaternary Glaciations – Extent and Chronology: A Closer Look, Developments in Quaternary Science 15. Elsevier, Amsterdam, pp. 537–552.

Szabo, J.P., Totten, S.M., 1995. Multiple pre-Wisconsinan glaciations along the northwestern edge of the Allegheny Plateau in Ohio and Pennsylvania. Canad. J. Earth Sci. 32, 2081–2089.

Szabo, J.P., Angle, M.P., Eddy, A.M., 2011. Pleistocene Glaciation of Ohio, USA. *In* Ehlers, J., Gibbard, P.L., Hughes, P.D. (Eds.). Quaternary Glaciations – Extent and Chronology: A Closer Look, Developments in Quaternary Science 15. Elsevier, Amsterdam, pp. 521–529.

Tamisiea, M.E., 2011. Ongoing glacial isostatic contributions to observations of sea level change. Geophys. J. Int. 186, 1036–1044.

Tarasov, L., Dyke, A.S., Neal, R.M., Peltier, W.R., 2012. A data-calibrated distribution of deglacial chronologies for the North American ice complex from glaciological modeling. Earth Planet. Sci. Lett. 315, 30–40.

Thomas, A.L., Henderson, G.M., Deschamps, P., Yokoyama, Y., Mason, A.J., Bard, E., Hamelin, B., Durand, N., Camoin, G., 2009. Penultimate deglacial sea-level timing from uranium/thorium dating of Tahitian corals. Science 324, 1186–1189.

Toucanne, S., Zaragosi, S., Bourillet, J.F., Cremer, M., Eynaud, F., Van Vliet-Lanoë, B., Penaud, A., Fontanier, C., Turon, J.L., Cortijo, E., Gibbard, P.L., 2009. Timing of massive 'Fleuve Manche' discharges over the last 350kyr: insights into the European ice-sheet oscillations and the European drainage network from MIS 10 to 2. Quat. Sci. Rev. 28, 1238–1256.

Turner, D.G., Ward, B.C., Bond, J.D., Jensen, B.J., Froese, D.G., Telka, A.M., Zazula, G.D., Bigelow, N.H., 2013. Middle to Late Pleistocene ice extents, tephrochronology and paleoenvironments of the White River area, southwest Yukon. Quat. Sci. Rev. 75, 59–77.

Turney, C.S.M., Jones, R.T., 2010. Does the Agulhas Current amplify global temperatures during super-interglacials? J. Quat. Sci. 25, 839–843.

Ullman, D.J., LeGrande, A.N., Carlson, A.E., Anslow, F.S., Licciardi, J.M., 2014. Assessing the impact of Laurentide Ice Sheet topography on glacial climate. Clim. Past 10, 487–507.

Van Den Berg, J., van de Wal, R., Oerlemans, H., 2008. A mass balance model for the Eurasian Ice Sheet for the last 120,000 years. Glob. Planet. Change 61, 194–208

Velichko, A.A., Faustova, M.A., Pisareva, V.V., Gribchenko, Y.N., Sudakova, N.G. and Lavrentiev, N.V., 2011. Glaciations of the East European Plain: distribution and chronology. *In* Ehlers, J., Gibbard, P.L., Hughes, P.D. (Eds.). Quaternary Glaciations – Extent and Chronology: A

Closer Look, Developments in Quaternary Science 15. Developments in Quaternary Science 15. Elsevier, Amsterdam, pp. 337–359.

Veres, D., Bazin, L., Landais, A., Toyé Mahamadou Kele, H., Lemieux-Dudon, B., Parrenin, F., Martinerie, P., Blayo, E., Blunier, T., Capron, E., Chappellaz, J., 2013. The Antarctic ice core chronology (AICC2012): an optimized multi-parameter and multi-site dating approach for the last 120 thousand years. Clim. Past 9, 1733–1748.

Vogt, P.R., Crane, K., Sundvor, E., 1994. Deep Pleistocene iceberg plowmarks on the Yermak Plateau: sidescan and 3.5 kHz evidence for thick calving ice fronts and a possible marine ice sheet in the Arctic Ocean. Geology 22, 403–406.

Waelbroeck, C., Labeyrie, L., Michel, E., Duplessy, J.C., McManus, J.F., Lambeck, K., Balbon, E., Labracherie, M., 2002. Sea-level and deep water temperature changes derived from benthic foraminifera isotopic records. Quat. Sci. Rev. 21, 295–305.

Ward, B.C., Bond, J.D., Froese, D., Jensen, B., 2008. Old Crow tephra (140±10ka) constrains penultimate Reid glaciation in central Yukon Territory. Quat. Sci. Rev. 27, 1909–1915.

Webb, N.D., Grimley, D.A., Phillips, A.C., Fouke, B.W., 2012. Origin of glacial ridges (OIS 6) in the Kaskaskia Sublobe, southwestern Illinois, USA. Quat. Res. 78, 341–352.

Wekerle, C., Colleoni, F., Naslund, J.-O., Brandefelt, J., Masina, S., 2016. Numerical reconstructions of the penultimate glacial maximum Northern Hemisphere ice sheets: sensitivity to climate forcing and model parameters. J. Glaciol. 62, 607–622.

Weldeab, S., Emeis, K.C., Hemleben, C., Schmiedl, G., Schulz, H., 2003. Spatial productivity variations during formation of sapropels S5 and S6 in the Mediterranean Sea: evidence from Ba contents. Palaeogeogr. Palaeoclimatol. Palaeoecol. 191, 169–190.

Weldeab, S., Siebel, W., Wehausen, R., Emeis, K.C., Schmiedl, G., Hemleben, C., 2003. Late Pleistocene sedimentation in the Western Mediterranean Sea: implications for productivity changes and climatic conditions in the catchment areas. Palaeogeogr. Palaeoclimatol. Palaeoecol. 190, 121–137.

Whitehouse, P.L., Bentley, M.J., Le Brocq, A.M., 2012. A deglacial model for Antarctica: geological constraints and glaciological modelling as a basis for a new model of Antarctic glacial isostatic adjustment. Quat. Sci. Rev. 32, 1–24.

Wainer, K.A.I., Rowe, M.P., Thomas, A.L., Mason, A.J., Williams, B., Tamisiea, M.E., Williams, F.H., Düsterhus, A., Henderson, G.M., 2017. Speleothem evidence for MIS 5c and 5a sea level above modern level at Bermuda. Earth Planet. Sci. Lett. 457, 325–334.

Williams, D.F., Moore, W.S., Fillon, R.H., 1981. Role of glacial Arctic Ocean ice sheets in Pleistocene oxygen isotope and sea level records. Earth Planet. Sci. Lett. 56, 157–166.

Williams, F.H., 2016. A geophysical approach to reconstructing past global mean sea levels using highly resolved sea-level records. PhD Thesis, University of Southampton, UK, 503 pp.

Yamane, M., Yokoyama, Y., Abe-Ouchi, A., Obrochta, S., Saito, F., Moriwaki, K., Matsuzaki, H., 2015. Exposure age and ice-sheet model constraints on Pliocene East Antarctic ice sheet dynamics. Nat. Commun. 6, 7016, doi:10.1038/ncomms8016.

Yokoyama, Y., Esat, T.M., 2011. Global climate and sea level – enduring variability and rapid fluctuations over the past 150,000 years. Oceanography 24, 54–69.

Young, R.R., Burns, J.A., Smith, D.G., Arnold, L.D., Rains, R.B., 1994. A single, late Wisconsin, Laurentide glaciation, Edmonton area and southwestern Alberta. Geology 22, 683–686.

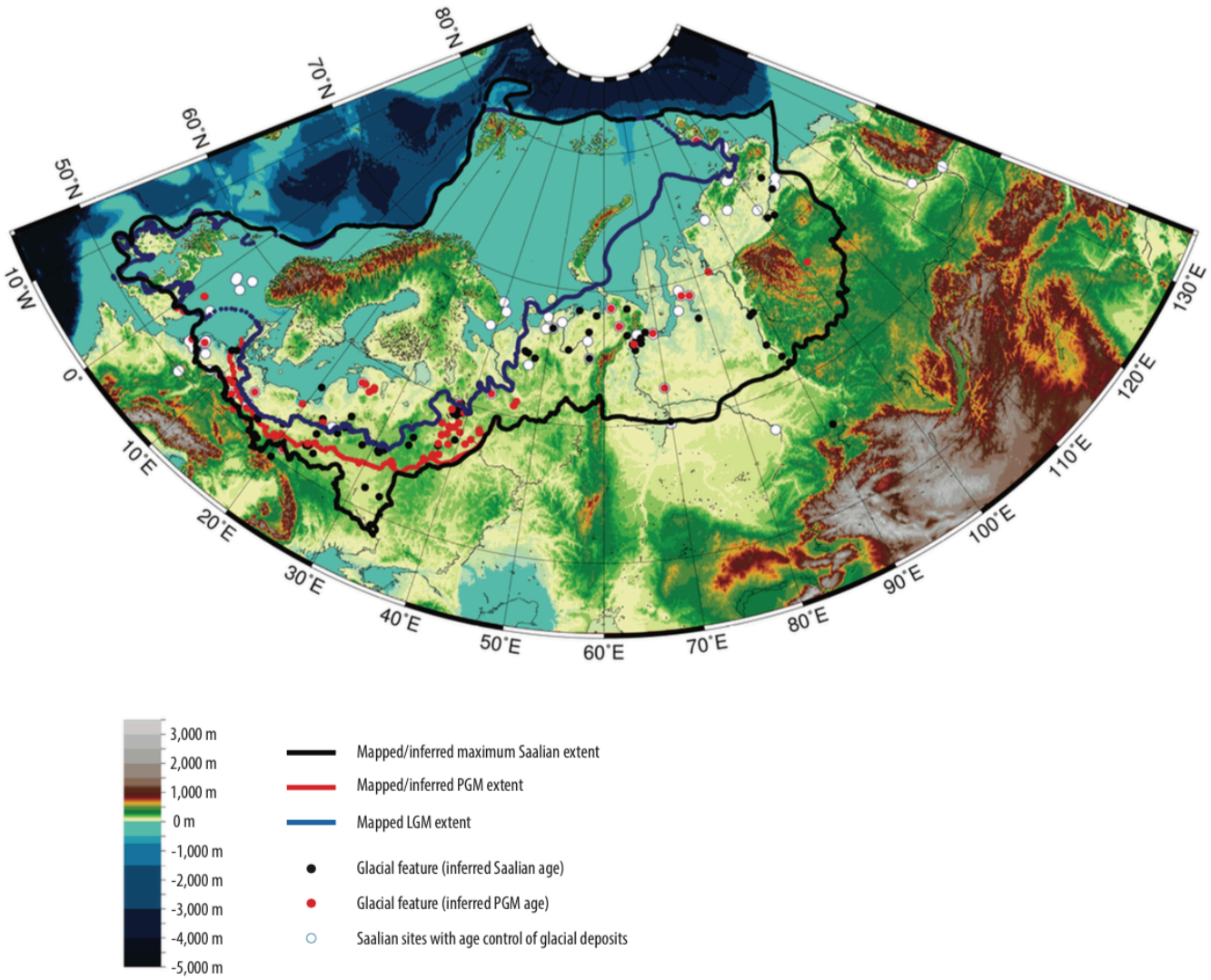

Figure 1. Maximum mapped extents of the former Eurasian ice sheets. Ice extents are in blue for the LGM (Weichselian); black for the maximum of the Saalian glacial complex (or local equivalent); and red for the PGM. Black dots denote locations of glacial features of inferred Saalian age; red dots denote locations of glacial features of inferred PGM/MIS 6 age; and white dots are Saalian sites with age control, where material dated is not necessarily of glacial origin. For site details, including age determinations and references, see Appendix I. References for the mapped/inferred Saalian, PGM, and LGM ice extents are as follows. LGM: Astakhov, 2011; Balson and Jeffery, 1991; Carr, 2004; Clark et al., 2004 a, b; Demidov, 1998 (unpublished), 2004, 2006; Ehlers et al., 2004, 2011 a, b; Gaunt et al., 1992; Gey et al., 2001, 2004; Guobyte and Satkunas, 2011; Houmark-Nielsen, 2011; Karabanov and Matveyev, 2011; Knight et al., 2004; Lippstreu, 2002 (unpublished); Mangerud et al., 2002; Marks, 2012; Straw, 1979;

Svendsen et al., 2004; Velichko et al., 2011. Saalian maximum: Astakhov, 2001, 2011; Astakhov et al., 2016; Ehlers et al., 2011 a, b; Gibbard and Clark, 2011; Gibbard et al., 1992, 2009; Gurski et al., 1990; Mohr, 1993; Seidel, 2003; Knight et al., 2004; Marks, 2012; Matoshko, 2011; Matoshko and Chugunny, 1993, 1995; Palienko, 1982; Rose et al., 2002; Rose, 2009; Ruzicka, 2004; Svendsen et al., 2004; Velichko et al., 2011. PGM/MIS 6: Astakhov, 2011; Astakhov et al., 2016; Ehlers et al., 2011 a, b; Gurski et al., 1990; Mohr, 1993; Karabanov and Matveyev, 2011; Rose, 2009; Rose et al., 2002, Ruzicka, 2004; Velichko et al., 2011.

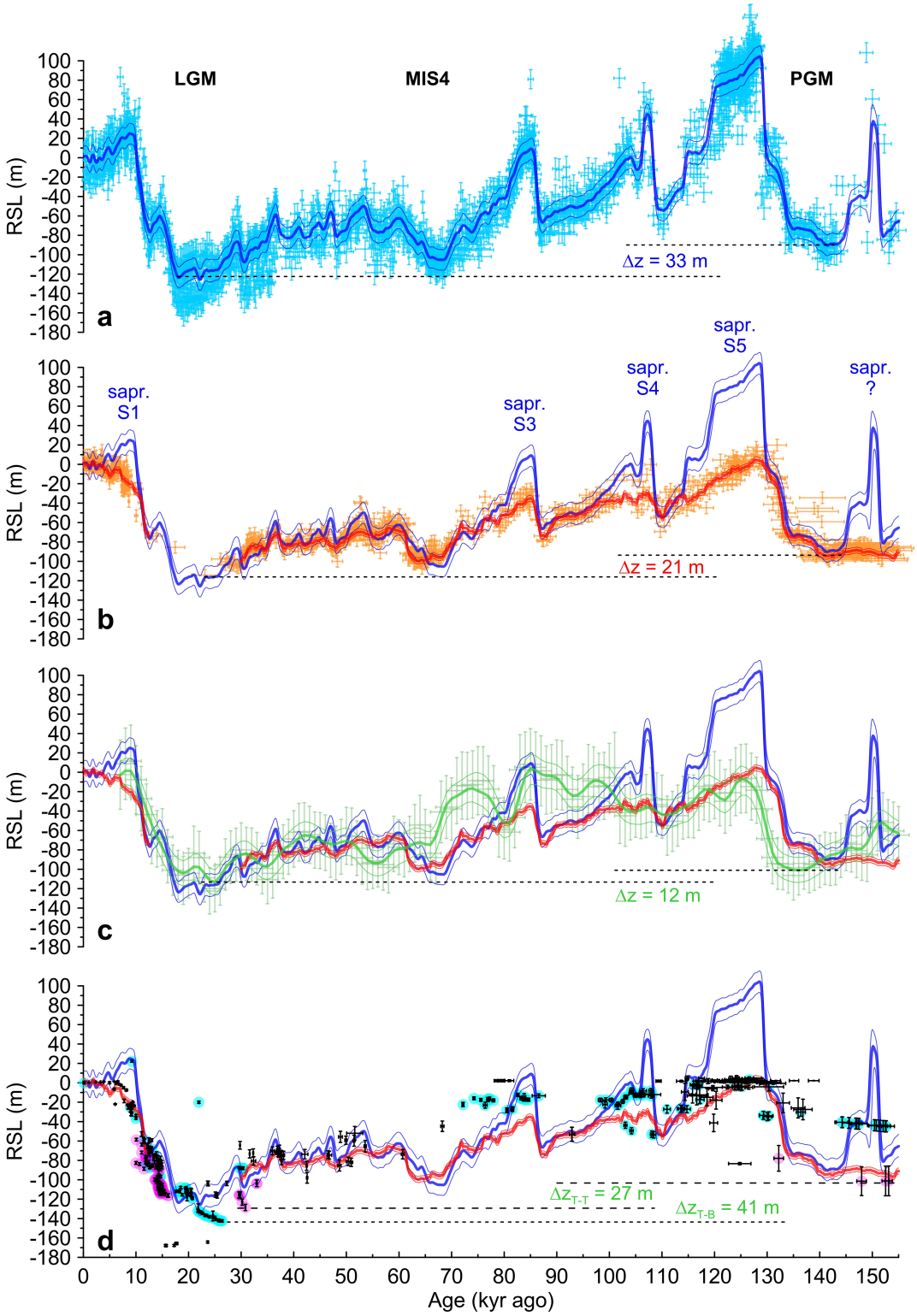

Figure 2. Compilation of relative sea-level records. Δz is the inferred PGM–LGM sea-level difference. **a.** Mediterranean relative sea-level data (for the Strait of Gibraltar) from a new highly resolved planktonic foraminiferal $\delta^{18}O$ stack (Figure 3). The ~1900 individual values are shown after conversion into relative sea level with 1σ age and RSL uncertainties (light blue) (Rohling et al., 2014), with the probabilistically determined maximum (thick blue line) with 95% bounds (thin blue lines) (Grant et al., 2012; Rohling et al., 2014). **b.** Comparison

between probabilistic results from **a** for the Mediterranean (blue) with (~800) individual data points with 1σ uncertainties (orange), and probabilistic results (red lines, 95% bounds) from the Red Sea method for the Bab-el-Mandab Strait (Grant et al., 2012). "Sapr." indicates sapropels that resulted from African monsoon flooding into the Mediterranean (Rohling et al., 2015). "?" is a "missing sapropel"; section 2.1. The LGM gap in the Red Sea data-series represents the prominent LGM aplanktonic zone discussed in the text. **c.** Results from **a** and **b** compared with SW Pacific deep-sea δ_{sw} sea-level estimates with 1σ uncertainties (Elderfield et al., 2012), and its probabilistic assessment (Rohling et al., 2014). **d.** As **c**, but compared with fossil coral positions (Zcp) (Hibbert et al., 2016) with 95% uncertainties. Magenta: Tahiti. Cyan: Barbados. No species-specific habitat depth uncertainties are indicated (Hibbert et al., 2016), but the deepest PGM and LGM Tahiti values are both based on *Porites* sp. from Tiarei, deep LGM values from Barbados are also based on *Porites* sp., but possess wider depth ranges. Hence, we focus on the PGM_{Tahiti}–LGM_{Tahiti} comparison (Table 2).

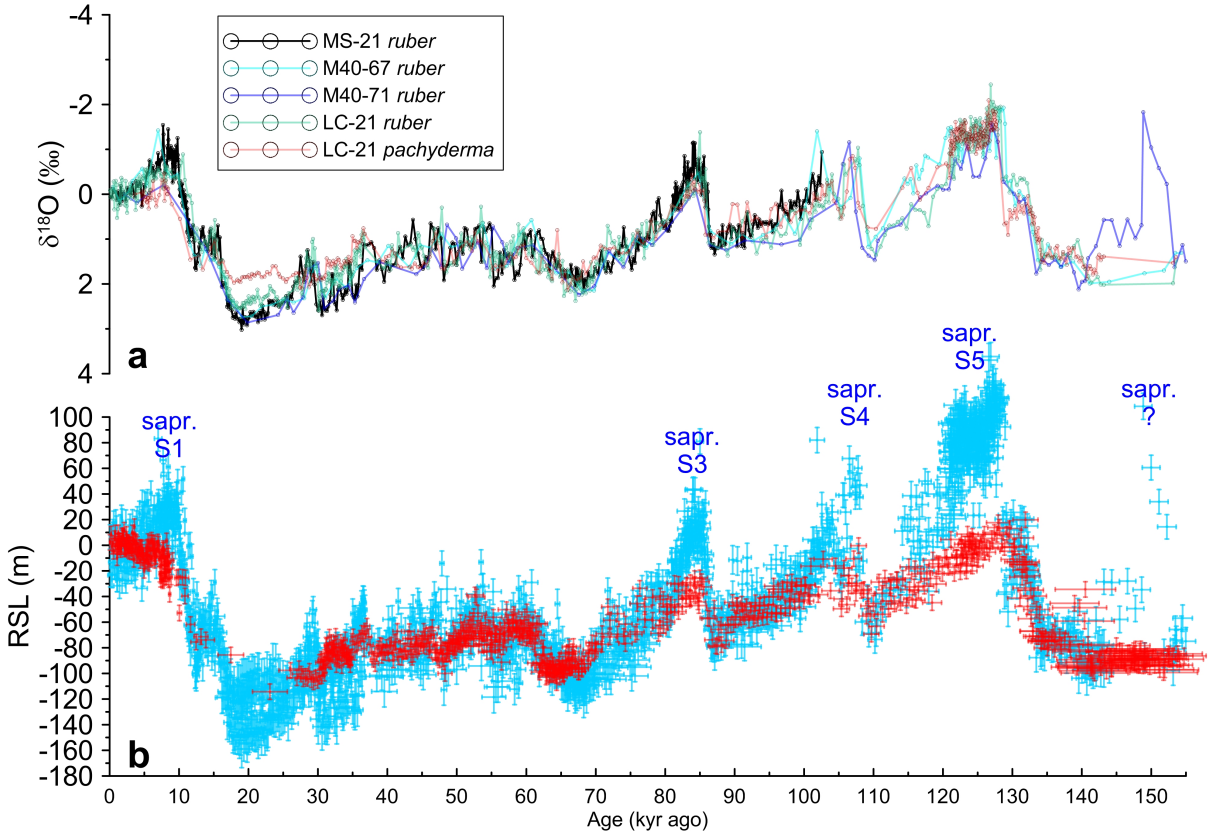

Figure 3. Mediterranean relative sea-level stack. a. Mediterranean planktonic foraminiferal $\delta^{18}O$ records on the Grant et al. (2012) chronology. **b.** Combined Mediterranean RSL dataset (blue) after transformation of $\delta^{18}O$ data for *Globigerinoides ruber* (white) and *Neogloboquadrina pachyderma* (dextral) into RSL (Rohling et al., 2014). Individual datapoints are shown with relative sea level with 1σ age and RSL uncertainties. Sapropel intervals (Rohling et al., 2014) with anomalous values are indicated. We include Red Sea RSL data (red, Figure 2) for comparison of full data ranges between the two marginal-basin RSL records. The LGM gap in the Red Sea data-series represents the prominent LGM aplanktonic zone discussed in the text.

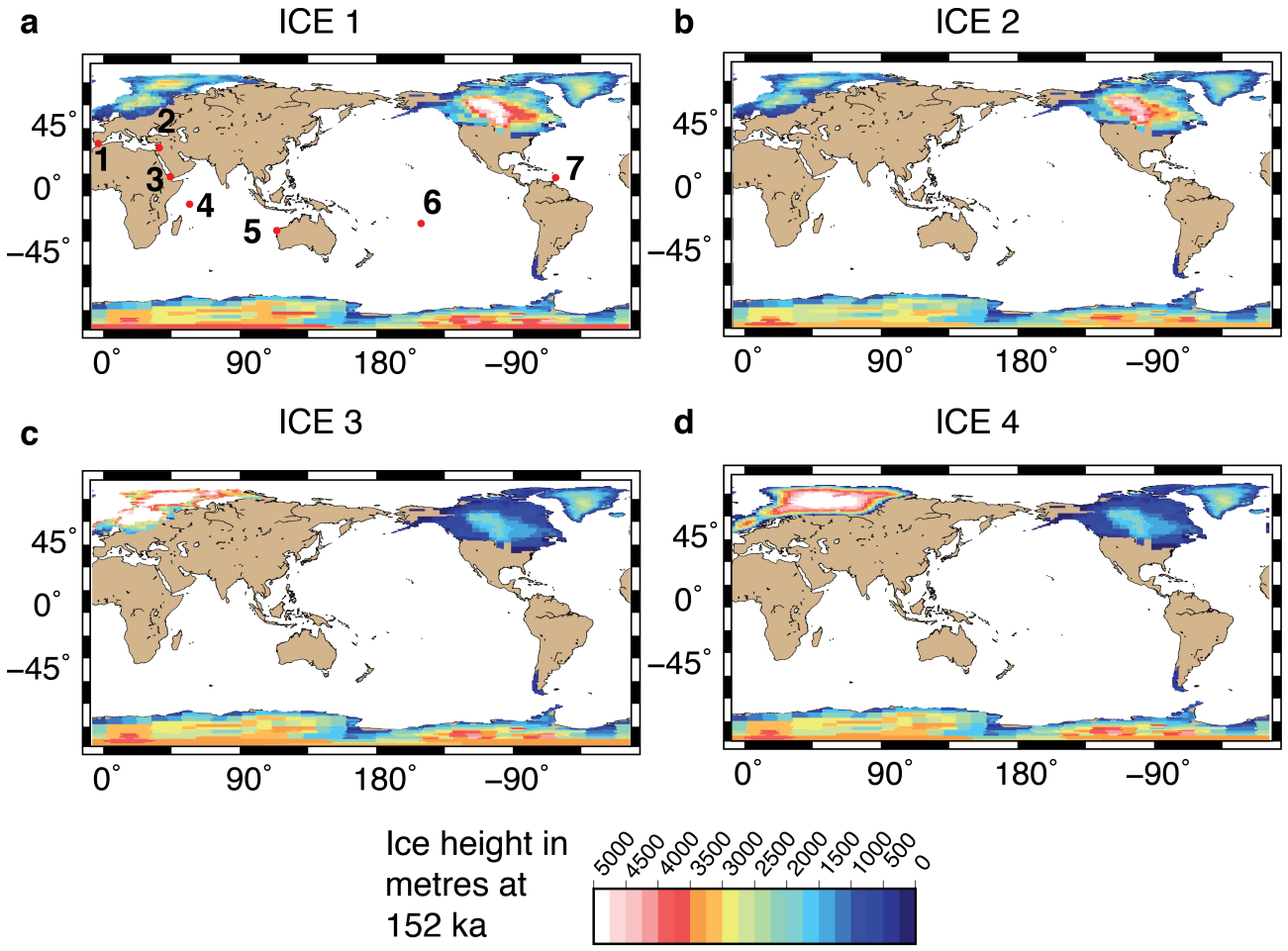

Figure 4. Hypothetical scenarios of PGM ice-mass distribution used to explore GIA implications. For details, see text, Figure 5, and Table 5. **a.** ICE-1 scenario. Numbered sites are locations modelled here: 1. Camarinal Sill, 2. Rosh Hanikra, 3. Hanish Sill, 4. Seychelles, 5. Western Australia, 6. Tahiti, 7. Barbados. **b.** ICE-2 scenario. **c.** ICE-3 scenario. Note the switch in ice heights compared to ICE-2. **d.** ICE-4 scenario. Note the different geographical boundaries of the EIS, relative to other scenarios.

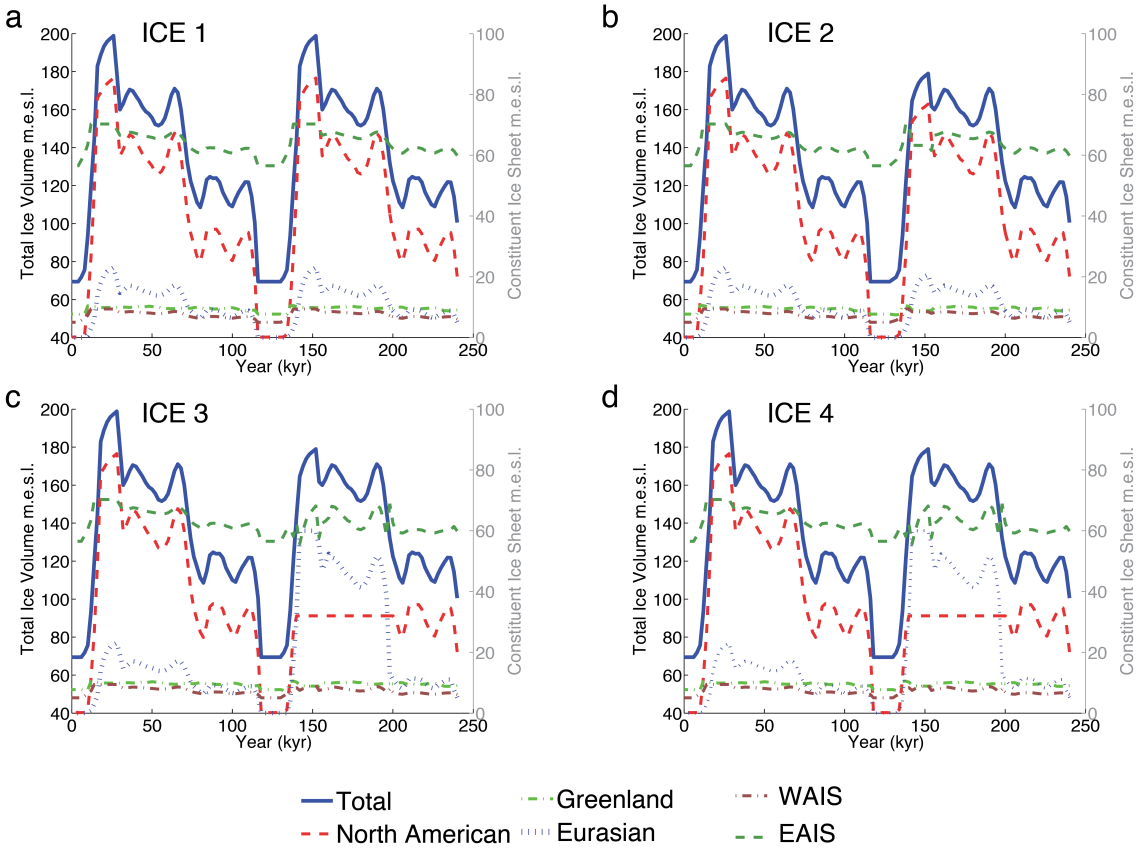

Figure 5. Total ice volume and constituent ice-sheet volumes for each hypothetical ice history. a. ICE-1, **b.** ICE-2, **c.** ICE-3, and **d.** ICE-4 scenarios (for details, see text and Table 5).

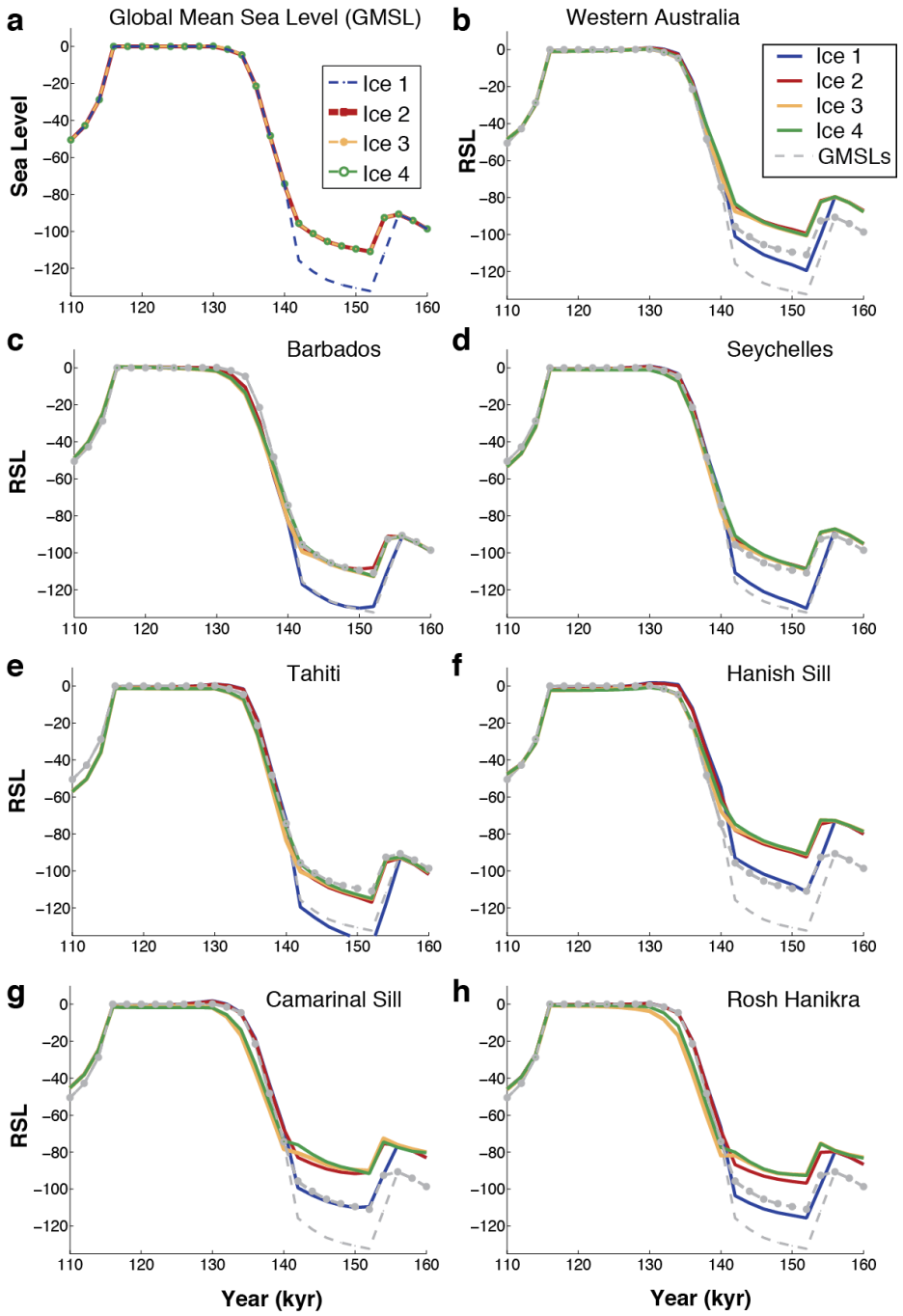

Figure 6. Glacioisostatic adjustment results between 160 and 110 kyr ago. a. Global mean sea level (GMSL) results for the four ice histories (Table 5, and Figures 4, 5). **b-h.** Relative sea-level (RSL) results for key sea-level reconstruction locations for the four simulated ice histories (Table 5, and Figures 4, 5). In each panel, corresponding GMSL results are repeated in grey for reference. Results are shown for the VM2-like Earth Model as part of a wider suite of 495 Earth models (Table 6). Note that the GMSL output derived from ICE-1 tracks a different ice volume, relative to GMSL outputs from scenarios ICE-2, -3, and -4, which over-plot one another.

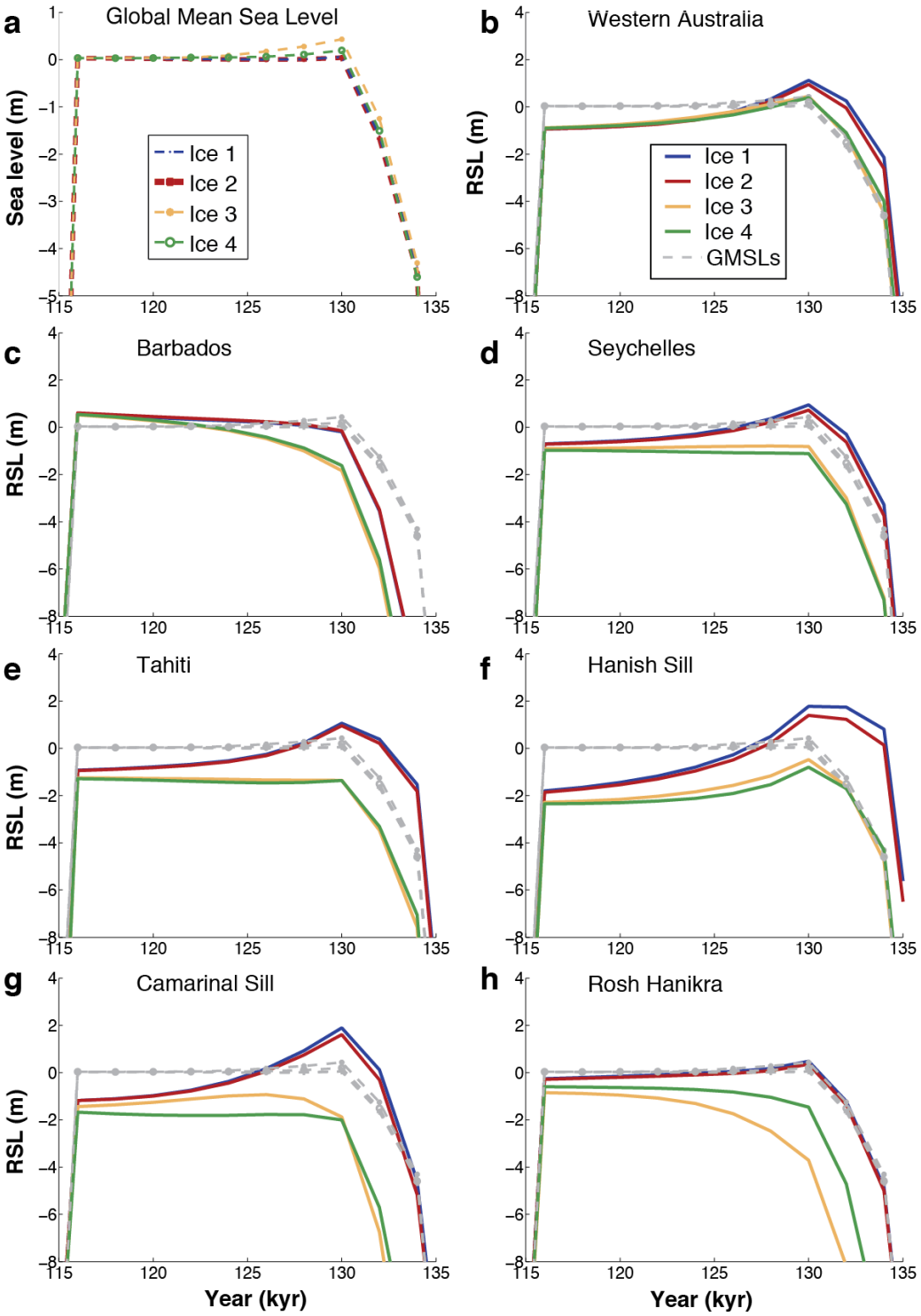

Figure 7. As Figure 6, but magnified for the interval between 135 and 115 kyr ago. a. Global mean sea-level (GMSL) results for the four ice histories (Table 5, and Figures 4, 5). **b-h.** Relative sea level (RSL) results for key sea-level reconstruction locations for the four ice histories (Table 5, and Figures 4, 5). In each panel, corresponding GMSL results are repeated

in grey, for reference. Results are shown for the VM2 Earth Model, as part of a wider suite of 495 Earth models (Table 6). Note that GMSL values for all ice scenarios (ICE-1 to -4) are virtually indistinguishable through the interglacial period because they track the same global ice volume.

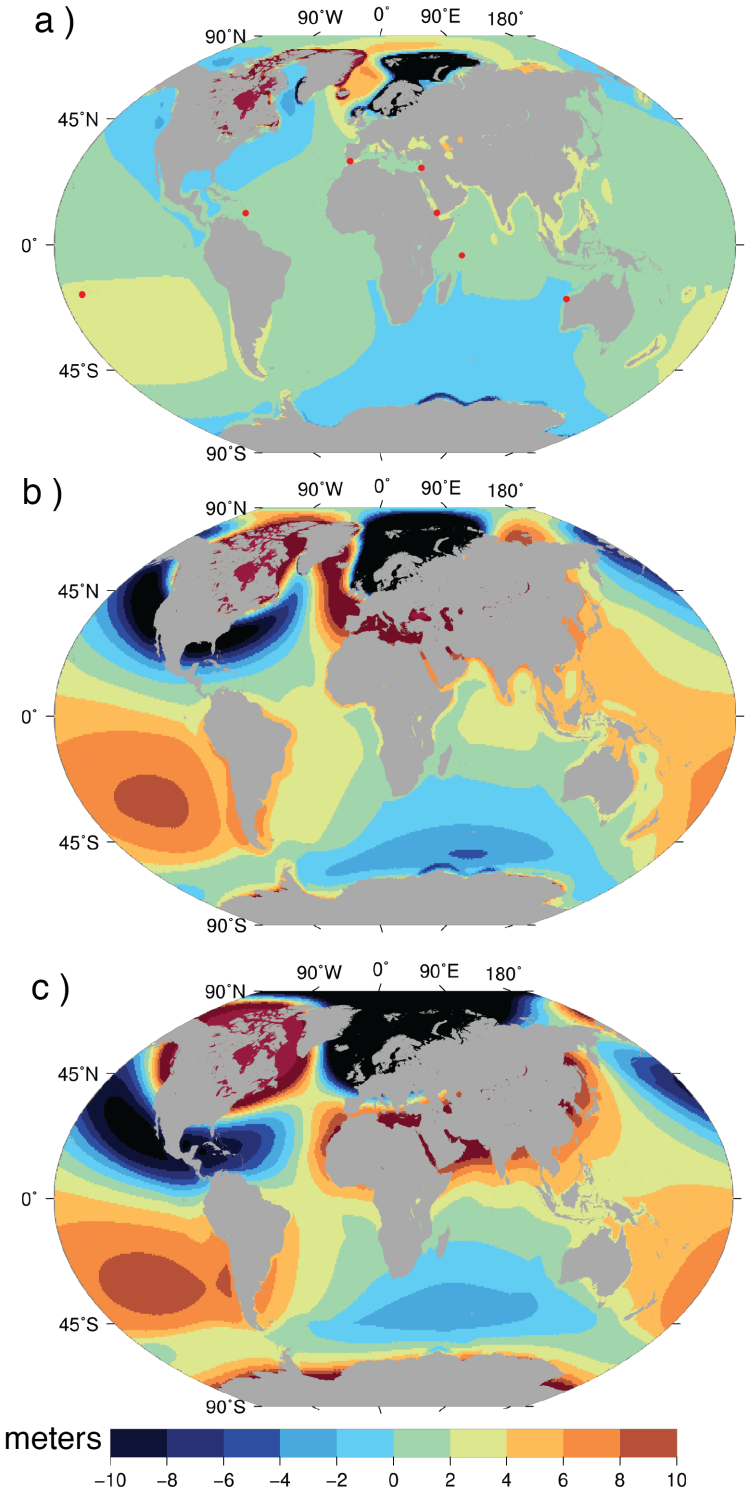

Figure 8. Differences between peak (maximum) LIG RSL values for ice histories ICE-1 and ICE-3, for three different representative Earth models (Table 7). The analysis includes results from the entire LIG, between 116 and 130 ka. **a.** Using Earth model E1. **b.** Based on E2.

c. For E3 (Table 7). Red dots in **a** represent key sites referenced in this study. Positive values indicate that the ICE-3 scenario generates lower peak (maximum) MIS 5e RSL values than the ICE-1 scenario.

Table 1. Previously modelled ice-volume changes (excess ice compared to present in m sea-level equivalent) for the Eurasian, North American, Greenland and Antarctic ice sheets.

Study	Eurasia		North America		Greenland		Antarctica		TOTAL	
	LGM	**PGM**	**LGM**	**PGM**	**LGM**	**PGM**	**LGM**	**PGM**	**LGM**	**PGM**
Colleoni et al., 2016										
(PGM centred on 140 ka)										
Topo1	*n/r*	70[a,b]	*n/r*	78[a,d]	*n/r*	2[c]	*n/r*	17[a]	*n/r*	~175[b]
Topo2	*n/r*	70[a,b]	*n/r*	30[a,c,d]	*n/r*	2[c]	*n/r*	17[a]	*n/r*	~120[b]
Wekerle et al., 2016										
(PGM centred on 140 ka)										
K140_Topo1	*n/r*	71[a]	*n/r*	80[c,d]	*n/r*	2[c]	*n/r*	17	*n/r*	167
K140_Topo2	*n/r*	71[a]	*n/r*	36[c,d]	*n/r*	2[c]	*n/r*	17	*n/r*	123
REF_Topo1 (GRISLI)	*n/r*	52	*n/r*	84[d]	*n/r*	2[c]	*n/r*	17	*n/r*	163
REF_Topo2 (GRISLI)	*n/r*	50	*n/r*	59[d]	*n/r*	2[c]	*n/r*	17	*n/r*	149
Lambeck et al., 2006, 2010, 2017 [g]	18.25[e]	52.5[e]	85[f]	68[f]	[f]	[f]	*n/r*	*n/r*	130	130
(PGM centred on 150 ka)										
de Boer et., 2014 [h]	33.5	33.2	49.8	58.3	0.9	2.7	12.6	12.6	98.0	107.7
(PGM centred on 144 ka)										
this study										
(PGM centred on 152 ka)										
ICE-1	23[c]	23[c]	85.2[c]	85.2[c]	2[c]	2[c]	18.1[c]	18.1[c]	129.5	129.5
ICE-2	23[c]	20.7	85.2[c]	76.7	2[c]	1.1	18.1[c]	10.2[c]	129.5	109.5
ICE-3	23[c]	60	85.2[c]	32	2[c]	1.1	18.1[c]	15.8[c]	129.5	109.5
ICE-4	23[c]	60	85.2[c]	32	2[c]	1.1	18.1[c]	15.8[c]	129.5	109.5
CMIP5/PMIP3 composite (Abe-Ouchi et al., 2015)	16.6	*n/r*	78.6	*n/r*		*n/r*	22.3	*n/r*	121.5	*n/r*
ICE-4G (Peltier, 1994, 1996) (LGM at 21 ka) [i]	24.86 [j]	*n/r*	64.24	*n/r*	6.38 [k]	*n/r*	18.09	*n/r*	114.12	*n/r*
ICE-5G v.1.2 (Peltier, 2004) (LGM at 26 ka) [i]	22.73 [j]	*n/r*	83.71	*n/r*	2.45 [k]	*n/r*	18.04	*n/r*	127.48	*n/r*
ICE-6G v.2 (Argus et al 2014; Peltier et al., 2015) (LGM at 26 ka) [i]	22.23 [j]	*n/r*	88.14	*n/r*	2.34 [k]	*n/r*	13.23	*n/r*	126.81	*n/r*
Siegert et al., 2002 (LGM at ~20 ka)	14	*n/r*	*n/r*	*n/r*	*n/r*	*n/r*	*n/r*	*n/r*	*n/r*	*n/r*
van den Berg, 2008 (LGM at ~25 ka)	~22	*n/r*	*n/r*	*n/r*	*n/r*	*n/r*	*n/r*	*n/r*	*n/r*	*n/r*
Patton et al., 2017 (LGM at ~22 ka)	17	*n/r*	*n/r*	*n/r*	*n/r*	*n/r*	*n/r*	*n/r*	*n/r*	*n/r*
Marshall et al., 2002	*n/r*	*n/r*	69 to 94	*n/r*	*n/r*	*n/r*	*n/r*	*n/r*	*n/r*	*n/r*
Tarasov et al., 2012 (LGM at ~20 ka)	*n/r*	*n/r*	70.1 ± 2	*n/r*	*n/r*	*n/r*	*n/r*	*n/r*	*n/r*	*n/r*
Denton and Hughes, 2002	*n/r*	*n/r*	*n/r*	*n/r*	*n/r*	*n/r*	14	*n/r*	*n/r*	*n/r*
Irvin and James, 2005 (LGM at ~21 ka)	*n/r*	*n/r*	*n/r*	*n/r*	*n/r*	*n/r*	10.12	*n/r*	*n/r*	*n/r*
Whitehouse et al., 2012 (LGM at ~20 ka)	*n/r*	*n/r*	*n/r*	*n/r*	*n/r*	*n/r*	9 ± 1.5	*n/r*	*n/r*	*n/r*
Briggs et al., 2014. (LGM at ~24 ka)	*n/r*	*n/r*	*n/r*	*n/r*	*n/r*	*n/r*	5.6 to 14.3	*n/r*	*n/r*	*n/r*
Argus et al., 2014. (ICE-6G)	*n/r*	*n/r*	*n/r*	*n/r*	*n/r*	*n/r*	13.6	*n/r*	*n/r*	*n/r*
Huybrechts, 2002 (LGM at ~21 ka)	*n/r*	*n/r*	*n/r*	*n/r*	2 to 3	*n/r*	14 to 18	*n/r*	*n/r*	*n/r*
Huy2 (Simpson et al., 2009)	*n/r*	*n/r*	*n/r*	*n/r*	4.1	*n/r*	*n/r*	*n/r*	*n/r*	*n/r*
Huy3 (Lecavalier et al., 2014)	*n/r*	*n/r*	*n/r*	*n/r*	> 4.7	*n/r*	*n/r*	*n/r*	*n/r*	*n/r*
Range (excepting ICE-1 to ICE-4 values and any initial, offline boundary estimates)	14 to 29	33.2 to 52.5	50.6 to 88.14	32 to 84	2 to ~6	2	9 to 22.3	10.2 to 17	98 to 130	107 to 163

[a] Initial volumes used as boundary conditions for offline GCM climate modelling, rather than modelled ice-volume estimates *per se*.

[b] Peyaud (2006), based on the Lambeck et al. (2006) PGM model estimate of 140 m_{SLE} total ice volume, of which the EIS constitutes 50 %.

[c] Values based on LGM ICE-5G files made available by R. Peltier at atnwww.atmosp.physics.utoronto.ca/~peltier/data.php, which differ slightly from the published ICE-5G reconstruction of Peltier (2004).

[d] Laurentide only.

[e] Eurasian = Fennoscandian in this reconstruction.

(f) North American estimates include Greenland Ice Sheet.
(g) Values used in the most recent iteration of the ANU model (values from A. Purcell, pers. comm.).
(h) Values used were obtained from ice files provided by de Boer (pers. comm., and now available in slightly different format on http://www.staff.science.uu.nl/~boer0160/data.php), re-gridded and assuming ice/water density constants of 1000/920 kg/m^3, to translate values to m_{SLE}.
(i) Values based on ICE-5G version 1.2. of R. Drummond, available at https://wiki.lsce.ipsl.fr/pmip3/doku.php/pmip3:design:21k:icesheet:index
(j) Eurasian = Fennoscandian, Barents/Kara Seas, and British-Irish Ice Sheets.
(k) These values, provided by R. Drummond (see note *i*), are combined volumes for the Greenland and Iceland Ice Sheets, although each ice sheet is modelled separately in ICE-4G, -5G, -6G.
n/r Not reconstructed.

Table 2. Results of PGM–LGM sea-level comparisons.

	Mean z_{LGM}	95% bounds	Mean z_{PGM}	95% bounds	Δz	95% bounds to Δz	df	Probability that means are *equal*
Mediterranean Sea	–124	11	–90	11	34	15	3998	P << 0.0001
Red Sea	(–116)	6	–96	3	20	7	999	P << 0.0001
Elderfield et al. (2012)	–113	13	–101	13	12	18	1998	P = 0.09
Corals (Tahiti only)	–129	3	(–101)	15	28	15	3	P = 0.02
Corals (PGM_{Tahiti} – $LGM_{Barbados}$)	–142	1	(–101)	15	41	15	8	P = 0.0003
Rabineau et al. (2006)*	–102	6	–92	7	10	9	n/a	n/a

Over the five main estimates (i.e., without the PGM_{Tahiti} –$LGM_{Barbados}$ coral estimate), mean $\Delta z_{PGM-LGM}$ = 21 ± 14 m (95% probability). Parentheses indicate values based on small numbers of observations. Probabilities of means being equal were assessed with a one-tailed *t*-test, where $t = \Delta z/se$, where se is the standard error of the mean (the reported 95% probability bounds are equivalent to 2se, and df = degrees of freedom for the combined means). * = 95% bounds on western Mediterranean palaeoshorelines are highly unlikely to overlap between LGM and PGM because both depend systematically on regional subsidence rate (if uncertainty is positive in one estimate, it is positive in the other); hence, the *t*-test is not applicable, as it assumes random-normal distributions instead of systematically related uncertainties.

Table 3. Results of PGM–MIS4 sea-level comparisons.

	Mean z_{MIS4}	95% bounds	Mean z_{PGM}	95% bounds	Δz	95% bounds (2 se equi-valent)	df	Probability that means are *equal*
Mediterranean Sea	–105	11	–90	11	15	15	3998	P = 0.02
Red Sea	–100	3	–96	3	4	5	1998	P = 0.06
Elderfield et al. (2012)	–93	13	–101	13	–8	18	1998	P = 0.19

Over the three estimates, mean $\Delta z_{PGM-MIS4}$ = 4 ± 14 m (95% probability). NB: the third record has a reversed sign. Omitting this only changes the overall result to $\Delta z_{PGM-MIS4}$ = 10 ± 11 m (95% probability). Probabilities of means being equal were assessed as in Table 2.

Table 4. PGM–LGM comparisons between important climate parameters.

	LGM	95% bounds	PGM	95% bounds	$\Delta_{PGM-LGM}$	95% bounds
Insolation (W m^{-2}) [1]	464.34		463.97		-0.37	
Summer energy (Ga-Joules m^{-2}) [2]	2.89		2.97		0.08	
CO_2 (p.p.m.v.) [3-8]	182.17(181.59)	4.27(1.45)	188.79(188.32)	6.72(1.41)	6.62(6.74)	7.96(2.02)
ΔF_{CO2} (W m^{-2}) [3-8,10]	-2.41(-2.43)	0.16(0.06)	-2.11(-2.12)	0.20(0.05)	0.30(0.32)	0.26(0.08)
CH_4 (p.p.b.v.) [9]	354.20(356.49)	18.24(17.45)	354.04(350.02)	42.63(7.59)	-0.16(-6.47)	46.37(19.03)
ΔF_{CH4} (W m^{-2}) [9,10]	-0.25(-0.25)	0.02(0.01)	-0.25(-0.25)	0.04(0.01)	0.00(-0.01)	0.05(0.02)
ΔF_{GHG} (W m^{-2}) [10]	-3.03(-3.03)	0.36(0.09)	-2.74(-2.73)	0.38(0.09)	0.29(0.30)	0.52(0.13)
Antarctic Temperature (°C) [11]	-9.60(-9.61)	3.24(0.77)	-9.03(-9.03)	3.24(0.72)	0.57(0.58)	4.58(1.05)
Antarctic Temperature (°C) [12]	-9.18(-9.21)	3.25(0.78)	-8.49(-8.50)	3.33(0.87)	0.69(0.71)	4.65(1.17)
$\Delta\delta^{18}O_{benthic}$ stack [13]	1.78	0.10	1.77	0.10	-0.01	0.14

Insolation is calculated at 65°N on June 21st. Summer energy is calculated at 65°N, for τ = 400 W m^{-2}. For CO_2, ΔF_{CO2}, CH_4, ΔF_{CH4}, ΔF_{GHG}, and Antarctic temperatures both median and probability maximum (latter in parenthesis) values and their 95% bounds are reported. The standard error associated to the $\Delta\delta^{18}O_{benthic}$ stack is 0.05‰. References: 1. Laskar et al., 2004; 2. Huybers, 2006; 3. Monnin et al., 2001; 4. Monnin et al., 2004; 5. Schmitt et al., 2012; 6. Schneider et al., 2013; 7. Landais et al., 2013; 8. Ahn and Brook, 2014; 9. Loulergue et al., 2008; 10. Köhler et al., 2010; 11. Stenni et al., 2010; 12. Parrenin et al., 2013; 13. Lisiecki and Raymo, 2005.

Table 5. Characteristics of hypothetical ice histories for GIA modelling.

	Scenario Features			
Ice History	**Contains a 14-kyr LIG highstand**	**Reduced ice volume through PGM relative to LGM**	**Small NAIS, large EIS at PGM**	**Changed extent of PGM EIS**
ICE 1	**X**			
ICE 2	**X**	**X**		
ICE 3	**X**	**X**	**X**	
ICE 4	**X**	**X**	**X**	**X**

Table 6. RSL at each study site for each ice-history scenario.

PGM (152 ka)	**ICE 2 – ICE1**		**ICE 3 – ICE 1**		**ICE 4 – ICE 1**	
Location	Mean Difference	Standard Deviation	Mean Difference	Standard Deviation	Mean Difference	Standard Deviation
Western Australia	19.8	0.4	18.1	0.7	17.9	0.8
Hanish Sill	19.2	0.6	22.1	1.9	22.2	1.7
Camarinal Sill	18.0	0.3	18.1	3.5	17.9	1.9
Rosh Hanikra	19.2	0.2	24.1	4.3	24.8	3.9
Tahiti	23.9	0.5	26.4	1.5	26.5	1.3
Barbados	20.6	0.3	15.6	0.9	15.3	1.2

Seychelles	21.1	0.6	20.9	0.7	21.1	0.7

Start of LIG (130 ka)	**ICE 2 – ICE1**		**ICE 3 – ICE 1**		**ICE 4 – ICE 1**	
Location	Mean Difference	Standard Deviation	Mean Difference	Standard Deviation	Mean Difference	Standard Deviation
Western Australia	-0.4	0.2	-1.3	0.7	-1.1	0.8
Hanish Sill	-0.7	0.3	-5.5	2.5	-5.1	2.1
Camarinal Sill	-0.1	0.2	-12.7	5.2	-7.5	3.0
Rosh Hanikra	-0.2	0.1	-15.8	7.2	-11.0	6.3
Tahiti	-0.5	0.3	-5.4	1.9	-5.3	1.9
Barbados	0.1	0.2	-0.2	1.9	0.0	2.1
Seychelles	-0.3	0.3	-2.2	1.0	-2.5	1.1

End of LIG (116 ka)	**ICE 2 – ICE1**		**ICE 3 – ICE 1**		**ICE 4 – ICE 1**	
Location	Mean Difference	Standard Deviation	Mean Difference	Standard Deviation	Mean Difference	Standard Deviation
Western Australia	-0.1	0.1	-0.2	0.6	-0.1	0.7
Hanish Sill	-0.2	0.2	-2.3	1.7	-2.1	1.4
Camarinal Sill	0.0	0.1	-5.2	4.4	-2.6	2.0
Rosh Hanikra	-0.1	0.1	-7.2	5.4	-5.5	4.5
Tahiti	-0.2	0.2	-2.2	1.4	-2.2	1.4
Barbados	0.0	0.1	0.6	1.6	0.7	1.9
Seychelles	-0.1	0.1	-0.6	0.3	-0.7	0.5

Across the range of 495 Earth Models, we take the difference between RSL values calculated at the same time point, and present the mean and standard deviation of the distribution of values across the 495 Earth models.

Table 7. Summary of three representative Earth models used in Figure 8.

Earth Model	Parameterisations	Rationale
E1	96 km thick lithosphere 5 x 10^{20} Pa s upper mantle viscosity 2.5 x 10^{21} Pa s lower mantle viscosity	VM2-like (Peltier et al., 2004).
E2	120 km thick lithosphere 5 x 10^{20} Pa s upper mantle viscosity 1.3 x 10^{22} Pa s lower mantle viscosity	Closest within suite of earth models to a recent preferred earth model for North American ice history (Lambeck et al., 2017).
E3	71 km thick lithosphere 1.6 x10^{20} Pa s upper mantle viscosity 5 x 10^{22} Pa s lower mantle viscosity	Closest within suite of earth models to recent preferred earth model for the last deglaciation (Lambeck et al., 2014).

APPENDIX I.

Appendix 1a. Details and references for the new glaciogeomorphological database

The database contains locations and dates of PGM glaciogenic sediments, or other dated deposits (not necessarily of glacial origin) that directly over- or under-lie glacial deposits relating to the PGM. The database is available directly via the URL listed in the main-text acknowledgements (doi: 0.6084/m9.figshare.5131963). The field descriptors for the database are given in the table below.

Column	Identifier	Description
A	Identifier	Numerical database entry number
B	Location	Geographic location
C	Site	Local site name
D	Latitude	Decimal latitude
E	Longitude	Decimal longitude
F	Lat/Long estimated?	Whether the latitude or longitude of the site is estimated
G	Unit designation	Stratigraphic unit (as determined by the original authors), e.g., Saalian, Warthe etc.
H	Feature	Type of deposit
I	Reference	Publication source
J	Dating method	Dating method
K	Material dated	The type of material dated
L	Reported age (ka)	Calculated age as originally reported
M	Age uncertainty	Age uncertainty as originally reported
N	Interpretation	Palaeo-environmental interpretation of the deposit (by the original authors)

Appendix Ib. Complete references for the glaciogeomorphological database

Arkhipov, S.A., 1990. Explanatory Note to the Regional Stratigraphic Scheme of the Quaternary of the West Siberian Plain. Institute of Geology and Geophysics, Siberian Branch of Academy of Sciences of USSR, Novosibirsk, pp. 95 (in Russian).

Arkhipov, S.A., 1989. A chronostratigraphic scale of the glacial Pleistocene of the West Siberian North. *In* Skabichevskaya, N.A.(Ed.). Pleistotsen Sibiri. Stratigrafia i mezhregionalnye korrelatsii. Nauka, Novosibirsk (in Russian).

Arkhipov, S.A., Levchuk, L.K., Shelkoplyas, V.N., 1994. Stratigraphy and geological structure of Quaternary cover in the lower-Ob-Yamal-Taz region, West Siberia. Russ. J. Geol. Geophys. 35, 74-89 (in Russian).

Arkhipov, S.A., Levchuk, L.K., Shelkoplyas, V.N., 1992. Marine Quaternary sediments of the lower Ob. *In* Murzayeva, V.E., Punning, J.-M.K., Chichagova, O.A. (Eds.). Geokhronolohgia Chetvertichnogo Perioda, Nauka, Moscow. pp. 90–101 (in Russian).

Arkhipov, S.A., Panychev, V.A., Shelekhova, T.G., Shelkoplyas, V.N., 1978. Glacial Geology of the Belogorsk Upland, the West Siberian Plain, the Lower Ob region. Siberian Branch of Academy of Sciences of the USSR, Novosibirsk, pp.132.

Armstrong, J.E., 1981. Post-Vashon Wisconsin glaciation, Fraser Lowland, British Columbia (No. 322). Geological Survey of Canada. Ottawa, ON Paper. pp.34.

Armstrong, J.E., 1975. Quaternary geology, stratigraphic studies and revaluation of terrain inventory maps, Fraser Lowland, British Columbia. Geological Survey of Canada, Ottawa. ON Paper. Number 75-1A, 377–380.

Arslanov, K.A., Maksimov, F.E., Kuznetsov, V.Y., Chernov, S.B., Velichkevich, F.Y., Razina, V.V., Kuzmin, G.F., Baranova, N.G., 2005. U-Th age and paleobotanical characteristics of the interglacial peat in the Rodionovo key section. *In* Yushkin, N.P. (Ed.). Proceedings of the IV All-Russia Quaternary Congress, Geoprint, Syktyvkar. pp. 21–23 (in Russian).

Arslanov, K.A., Yevzerov, V.Y., Tertichnyi, N.I., Gerasimov, S.A., Lokshin, N.V., 1981. Kvoprocu o vozraste otlozhenii borealnoi transgressii (ponoiskikh sloev) na Kolskom poluostrove (On the age of deposits (Ponoi layers) Boreal transgression in the Kola Peninsula). In Pleistotsenovye oledeneniya Vostochno-Evropeiskoi ravniny (Pleistocene Glaciations at the East European Plain). Nauka, Moscow, pp. 28–37 (in Russian).

Astakhov, V.I., 2013. Pleistocene glaciations of northern Russia–a modern view. Boreas, 42(1), 1–24.

Astakhov, V., 2011. Ice margins of Northern Russia revisited. *In* Ehlers, J., Gibbard, P.L., Hughes, P.D. (Eds.), Quaternary Glaciations – Extent and Chronology, A Closer Look, Developments in Quaternary Science 15. Elsevier, Amsterdam, pp. 323–336.

Astakhov, V.I., 2006. Evidence of Late Pleistocene ice-dammed lakes in West Siberia. Boreas 35, 607–621.

Astakhov, V.I., 2004. Middle Pleistocene glaciations of the Russian North. Quat. Sci. Rev. 23, 1285–1311.

Astakhov, V., Mangerud, J., 2007. The geochronometric age of Late Pleistocene terraces on the lower Yenisei. Doklady Earth Sciences, 416, 1022–1026.

Astakhov, V., Nazarov, D., 2010. Correlation of Upper Pleistocene sediments in northern West Siberia. Quat. Sci. Rev. 29, 3615–3629.

Astakhov, V.I., Mangerud, J., Svendsen, J.I., 2007. Trans-Uralian correlation of the northern Upper Pleistocene. Regionalnaya Geologia i Metallogenia 30/31, 190–206 (in Russian).

Astakhov, V.I., Arslanov, K.A., Maksimov, F.E., Kuznetsov, V.Y., Razina, V.V. Nazarov, D.V., 2005. The age of interglacial peat on the Lower Ob. Doklady Earth Sciences 401, 298–302.

Ballantyne, C.K., Hall, A.M., 2008. The altitude of the last ice sheet in Caithness and east Sutherland, northern Scotland. Scott. J. Geol. 44(2), 169–181.

Ballantyne, C.K., Stone, J.O., Fifield, L.K., 2009. Glaciation and deglaciation of the SW Lake District, England: implications of cosmogenic 36 Cl exposure dating. Proc. Geol. Assoc. 120, 139–144.

Baltrūnas, V., Šeirienė, V., Molodkov, A., Zinkutė, R., Katinas, V., Karmaza, B., Kisielienė, D., Petrošius, R., Taraškevičius, R., Piličiauskas, G., Schmölcke, U., 2013. Depositional environment and climate changes during the late Pleistocene as recorded by the Netiesos section in southern Lithuania. Quat. Int. 292, 136–149.

Bardeyeva, M.A., 1986. The key sections of Quaternary deposits in the Central Siberian Upland. *In* Velichko, A.A., Isayeva, L.L. (Eds.). Chetvertichnye Oledeneniya Srednei Sibiri, Nauka, Moscow. pp. 35–52 (in Russian).

Bardeyeva, M.A., Isayeva, L.L., Andreyeva, S.M., Kind, N.V., Nikolskaya, M.V., Pirumova, L.G., Sulerzhitsky, L.D., Cherkasova, N.N., 1980. Stratigraphy, geochronology and palaeogeography of the Pleistocene and Holocene of the northern Central Siberian Upland. Geokhronologia chetvertichnogo perioda. Nauka, Moscow. 198-207.

Barendregt, R.W., 2011. Magnetostratigraphy of Quaternary sections in eastern Alberta. In Ehlers, J., Gibbard, P.L., Hughes P.D. (Eds.). Quaternary Glaciations – Extent and Chronology, A Closer Look, Developments in Quaternary Science 15. Elsevier, Amsterdam, pp. 591–600.

Ber, A., 2006. Pleistocene interglacials and glaciations of northeastern Poland compared to neighbouring areas. Quat. Int.149, 12–23.

Berg, R.C., McKay III, E.D., Stiff B.J., 2012. Elevation of the Basal Sand and Gravel of the Middle Illinois River Valley, Bureau, LaSalle, Marshall, Peoria, Putnam, and Woodford Counties, Illinois. Illinois State Geological Survey. Illinois Map 17. Scale 1:62,500.

Bobrowsky, P., 1987. Quaternary stratigraphy of the northern Canadian Cordillera based on new evidence from the Finlay River of northeastern British Columbia. International Quaternary Association, Xllth International Congress, Ottawa. 132.

Bobrowsky, P., Rutter, N.W., 1992. The Quaternary geologic history of the Canadian Rocky Mountains. Géographie physique et Quaternaire, 46, 5–50.

974 Bolshiyanov, D., Molodkov, A., 1999. Marine Pleistocene deposits of the Taymyr Peninsula and their age
975 from ESR dating. *In* Kassens, H., Bauch, H.A., Dmitrenko, I.A., Eicken, H., Hubberten, H.-W., Melles, M.,
976 Thiede, J., Timochov, L.A. (Eds.). Land-Ocean Systems in the Siberian Arctic: Dynamics and History.
977 Springer-Verlag, Berlin, pp. 469– 475.
978 Börner, A., Hrynowiecka, A., Kuznetsov, V., Stachowicz-Rybka, R., Maksimov, F., Grigoriev, V., Niska, M.,
979 Moskal-del Hoyo, M., 2015. Palaeoecological investigations and 230 Th/U dating of Eemian interglacial
980 peat sequence of Banzin (Mecklenburg-Western Pomerania, NE-Germany). Quat. Int. 386, 122–136.
981 Brzezina, R., 2000. Detailed Geological Map of Poland at 1:50000 Scale, Sheet Krzesk. Polish Geological
982 Institute, Warszawa.
983 Busschers, F.S., van Balen, R.T., Cohen, K.M., Kasse, C., Weerts, H.J.T., Wallinga, J., Bunnik, F.P.M., 2008.
984 Response of the Rhine-Meuse fluvial system to Saalian ice sheet dynamics. Boreas 37, 377–398.
985 Busschers, F.S., Kasse, C., Van Balen, R.T., Vandenberghe, J., Cohen, K.M., Weerts, H.J.T., Wallinga, J.,
986 Johns, C., Cleveringa, P., Bunnik, F.P.M., 2007. Late Pleistocene evolution of the Rhine-Meuse system
987 in the southern North Sea basin: imprints of climate change, sea-level oscillation and glacio-isostacy.
988 Quat. Sci. Rev. 26, 3216–3248.
989 Busschers, F.S., Weerts, H.J.T., Wallinga, J., Cleveringa, P., Kasse, C., Wolf, H.D., Cohen, K.M., 2005.
990 Sedimentary architecture and optical dating of Middle and Late Pleistocene Rhine-Meuse deposits–
991 fluvial response to climate change, sea-level fluctuation and glaciation. Geol. Mijnb. 84, 25–41.
992 Catt, J.A., 2007. The Pleistocene glaciations of eastern Yorkshire: a review. Proc. Yorkshire Geol. Soc. 56,
993 177–207.
994 Counts, R.C., Murari, M.K., Owen, L.A., Mahan, S.A., Greenan, M., 2015. Late Quaternary
995 chronostratigraphic framework of terraces and alluvium along the lower Ohio River, southwestern
996 Indiana and western Kentucky, USA. Quat. Sci. Rev. 110, 72–91.
997 Curry, B.B., 1998. Evidence at Lomax, Illinois, for Mid-Wisconsin (~40,000 yr BP) position of the Des Moines
998 Lobe and for diversion of the Mississippi River by the Lake Michigan Lobe (20,350 yr BP). Quat. Res. 50,
999 128–138.
1000 Curry, B.B., Baker, R.G., 2000. Palaeohydrology, vegetation, and climate since the late Illinois Episode
1001 (~130 ka) in south-central Illinois. Palaeogeogr. Palaeoclimatol. Palaeoecol. 155, 59–81.
1002 Curry, B.B., Pavich, M.J., 1996. Absence of glaciation in Illinois during marine isotope stages 3 through 5.
1003 Quat. Res. 46, 19–26.

1004 Curry, B.B., Troost, K.G., Berg, R.C., 1994. Quaternary geology of the Martinsville alternative site, Clark
1005 County, Illinois, a proposed low level radioactive waste disposal site. Illinois State Geological Survey
1006 Circular 556, 85.
1007 Demuro, M., Froese, D.G., Arnold, L.J., Roberts, R.G., 2012. Single-grain OSL dating of glaciofluvial quartz
1008 constrains Reid glaciation in NW Canada to MIS 6. Quat. Res. 77, 305–316.
1009 Duk-Rodkin, A., Barendregt, R.W., 2011. Stratigraphical record of glacials/interglacials in northwest Canada.
1010 In Ehlers, J. Gibbard, P.L., Hughes P.D. (Eds.). Quaternary Glaciations – Extent and Chronology, A
1011 Closer Look, Developments in Quaternary Science 15. Elsevier, Amsterdam, pp. 661–698.
1012 Duk-Rodkin, A., Barendregt, R.W., White, J.M., 2010. An extensive late Cenozoic terrestrial record of
1013 multiple glaciations preserved in the Tintina Trench of west-central Yukon: stratigraphy, paleomagnetism,
1014 paleosols, and pollen. Can. J. Earth Sci. 47, 1003–1028.
1015 Duk-Rodkin, A., Barendregt, R.W., White, J.M., Singhroy, V.H., 2001. Geologic evolution of the Yukon River:
1016 implications for placer gold. Quat. Int. 82, 5–31.
1017 Duk-Rodkin, A., Barendregt, R.W., Tarnocai, C., Phillips, F.M., 1996. Late Tertiary to late Quaternary record
1018 in the Mackenzie Mountains, Northwest Territories, Canada: stratigraphy, paleosols, paleomagnetism,
1019 and chlorine-36. Can. J. Earth Sci. 33(6), 875–895.
1020 Ehlers, J., Grube, A., Stephan, H.J., Wansa, S., 2011b. Pleistocene glaciations of North Germany–new
1021 results. *In* Ehlers, J., Gibbard, P.L., Hughes, P.D. (Eds.). Quaternary Glaciations – Extent and
1022 Chronology, A Closer Look, Developments in Quaternary Science 15. Elsevier, Amsterdam, pp. 149–162.
1023 Ehlers, L. Eissmann, L. Lippstreu, H.-J. Stephan, S. Wansa., 2004. Pleistocene glaciations of North
1024 Germany. *In*, J. Ehlers, P.L. Gibbard (Eds.). 2004. Quaternary Glaciations. Extent and Chronology Part I:
1025 Europe, Developments in Quaternary Science 2. Elsevier, Amsterdam, pp. 135–146.
1026 Elias, S.A., Hamilton, T.D., Edwards, M.E., Begét, J.E., Krumhardt, A.P., Lavoie, C., 1999. Late Pleistocene
1027 environments of the western Noatak basin, northwestern Alaska. Geol. Soc. Am. Bull. 111, 769–789.
1028 Fard, A.M., Gruszka, B., 2007. Subglacial conditions in a branching Saalian esker in north-central Poland.
1029 Filonowicz, P., 1980. Objaśnienia do Mapy geologicznej Polski w skali 1:200000, ark. Kielce
1030 [Explanations to the Geological Map of Poland 1: 200 000, Kielce sheet]. Warszawa, 143 pp.
1031 Filonowicz, P., 1980. Objaśnienia do Mapy geologicznej Polski w skali 1:200000, ark. Kielce [Explanations to
1032 the Geological Map of Poland 1: 200 000, Kielce sheet]. Warszawa, 143 pp.
1033 Follmer, L.R., Nelson, W.J., 2010. Surfical geology of Johnston City Quadrangle. Willliamson and Franklin
1034 Counties, Illinois. Illinois State Geological Survey, Illinois Quadrangle Map. IGQ Pittsburg, SG, 1: 24,000.

1035 Fugitt, F.L., Spahr, P.N., Pavey, R.R., Aden, D.J., Jones, M., Angle, M.P., 2016. Surfical geology of the
1036 Hillsboro 30 x 60-mintue quadrangle in Ohio: Columbus, Ohio Department of Natural Resources,
1037 Division of Geological Survey Map SG-2-HIL, scale 1:100,000.
1038 Fulton, R.J., Irving, E., Wheadon, P.M., 1992. Stratigraphy and paleomagnetism of Brunhes and Matuyama
1039 (> 790 ka) Quaternary deposits at Merritt, British Columbia. Can. J. Earth Sci. 29, 76–92.
1040 Gaigalas, A., Arslanov, K.A., Maksimov, F.E., Kuznetsov, V.Y., Chernov, S.B., 2007. Uranium-Thorium
1041 isochron dating results of penultimate (Late Mid-Pleistocene) Interglacial in Lithuania from Mardasavas
1042 site. Geologija 57, 21–29.
1043 Gallagher, C., Thorp, M., 1997. The age of the Pleistocene raised beach near Fethard, County Wexford,
1044 using infrared stimulated luminescence (IRSL). Irish Geography, 30, 68–89.
1045 Gemmell, A.M.D., Murray, A.S., Connell, E.R., 2007. Devensian glacial events in Buchan (NE Scotland): A
1046 progress report on new OSL dates and their implications. Quat. Geochronol. 2, 237–242.
1047 Gey, V.P., Kozlov, V.V., Malakhovsky, D.B., 2004. On the age and extent of the maximum Late Pleistocene
1048 ice advance along the Baltic-Caspian watershed. *In* Ehlers, J., Gibbard, P.L., (Eds.). Quaternary
1049 Glaciations – Extent and Chronology. Part 1: Europe. Developments in Quaternary Sciences, 2, pp. 355-
1050 358.
1051 Gey, V., Saarnisto, M., Lunkka, J.P., Demidov, I., 2001. Mikulino and Valdai palaeoenvironments in the
1052 Vologda area, NW Russia. Glob. Planet. Change 31, 347-366.
1053 Gibbard P.L., Pasanen, A.H., West, R.G., Lunkka, J.P., Boreham, S., Cohen, K., Rolfe C., 2009. Late Middle
1054 Pleistocene glaciation in East Anglia, England. Boreas 38, 504–528.
1055 Gibbard, P.L., West, R.G., Andrew, R., Pettit, M., 1992. The margin of a Middle Pleistocene ice advance at
1056 Tottenhill, Norfolk, England. Geol. Mag. 129, 59–76.
1057 Gibbard P.L., West, R.G., Andrew, R., Pettit, M., 1991. Tottenhill, Norfolk (TF 636115). 1991. *In* Lewis, S.G.,
1058 Whiteman, C.A., Bridgland, D.R. (Eds.), Central East Anglia and The Fen Basin – Field Guide,
1059 Quaternary Research Association, London, pp. 131–144.
1060 Gillespie, A.R., Clark, D.H., 2011. Glaciations of the Sierra Nevada, California, USA. *In* Ehlers, J., Gibbard,
1061 P.L., Hughes P.D. (Eds.), 2011, Quaternary Glaciations – Extent and Chronology, A Closer Look,
1062 Developments in Quaternary Science 15. Elsevier, Amsterdam, pp. 447–462.
1063 Glapa, H., 1971. Warthezeitliche Eisrandlagen im Gebiet der Letzlinger Heide. Geologie 20, 1087–1110.
1064 Godlewska, A., 2014. Dynamics of the Younger Saalian Ice-sheet in the Marginal Zone in the Krzna and Bug
1065 Interfluve in the Light of Lithofacies Analysis. Maria Curie-Sklodowska University Press, Lublin (in Polish,
1066 with English summary).

1067 Godlewska, A., Terpiłowski, S., 2012. Transverse, supraglacially derived crevasse infillings in a Pleistocene
1068 ice-sheet margin zone (eastern Poland): genesis and sedimentary record. Geomorphology 161, 73–81.
1069 Grichuk, V.P., Zaklinskaya, E.D., Mizerov, B.V., 1971. Excursion Guide on Silts of Cenozoic Deposits of
1070 Tomskoe Priob'ye. IGiG SO AN SSSR, Novosibirsk, 1–64 (in Russian).
1071 Grimley, D.A., McKay, E.D., 2004. Surficial Geology of French Village Quadrangle, St. Clair County, IL:
1072 Illinois State Geological Survey, Illinois Geologic Quadrangle Map, IGQ French Village-SG, 1:24,000.
1073 Grimley, D.A., Phillips, A.C., 2011. Surficial Geology of St. Clair County, Illinois: Illinois State Geological
1074 Survey, Illinois County Geologic Map, ICGM St. Clair-SG, 2 sheets, 1:62,500.
1075 Grimley, D.A., Phillips, A.C., 2006, Surficial Geology of Grantfork Quadrangle, Madison County, Illinois:
1076 Illinois State Geological Survey, Illinois Geologic Quadrangle Map, IGQ Grantfork-SG, 1:24,000.
1077 Grimley, D.A., Webb, N.D., 2009. Surficial Geology of New Athens East Quadrangle, St. Clair County,
1078 Illinois: Illinois State Geological Survey, Illinois Geologic Quadrangle Map, IGQ New Athens East-SG,
1079 1:24,000, report, 12 pp.
1080 Grimley, D.A., Phillips, A.C., Follmer, L.R., Wang, H., Nelson, R.S., 2001. Quaternary and environmental
1081 geology of the St. Louis Metro East area. *In* Malone, D. (Ed.). Guidebook for field trip for the 35th annual
1082 meeting of the North-Central Section of the Geological Society of America. Illinois State Geological
1083 Survey, Guidebook 33, pp. 21–73.
1084 Grimley, D.A., Follmer, L.R., McKay, E.D., 1998. Magnetic susceptibility and mineral zonations controlled by
1085 provenance in loess along the Illinois and central Mississippi River valleys. Quat. Res. 49, 24–36.
1086 Grüger, E., 1972. Late Quaternary vegetation development in south-central Illinois. Quat. Res. 2, 217–231.
1087 Gruszka, B., Van Loon, A.J., Zielinski, T., 2006. Bridging the gap in Quaternary geology between East and
1088 West: the Brodzikowski heritage. Sediment. Geol. 193, 1–5.
1089 Guobyte, R., Satkunas, J., 2011. Pleistocene glaciations in Lithuania. *In* Ehlers, J., Gibbard, P.L. (Eds).
1090 Quaternary Glaciations – Extent and Chronology. Part 1: Europe. Developments in Quaternary Sciences
1091 2, Elsevier, Amsterdam, pp. 231–246.
1092 Hamblin, R.J.O., Moorlock, B.S.P., Rose, J., Lee, J.R., Riding, J.B., Booth, S.J., Pawley, S.M., 2005.
1093 Revised Pre-Devensian glacial stratigraphy in Norfolk, England, based on mapping and till provenance.
1094 Geol. Mijnb. 84, 77–85.
1095 Hicock, S.R., 1990. Last Interglacial Muir Point Formation, Vancouver Island, British Columbia. Géographie
1096 physique et Quaternaire 44, 337–340.
1097 Hicock, S.R., Lian, O.B., 1995. The Sisters Creek Formation: Pleistocene sediments representing a
1098 nonglacial interval in southwestern British Columbia at about 18 ka. Can. J. Earth Sci. 32, 758–767.

1099 Hjort C., Funder S., 2008. Mountain-derived versus shelf-based glaciations on the western Taymyr Peninsula,
1100 Siberia. Polar Res. 27, 273–279.
1101 Höfle, H.C., Lade, U., 1983. The stratigraphic position of the Lamstedter Moraine within the Younger Drenthe
1102 substage (middle Saalian). *In* Muller, E.H. (Ed.). Glacial deposits in North-West Europe. AA Balkema
1103 Rotterdam. pp. 343–346.
1104 Houmark-Nielsen, M., Demidov, I., Funder, S., Grøsfjeld, K., Kjær, K.H., Larsen, E., Lavrova, N., Lyså, A.,
1105 Nielsen, J.K., 2001. Early and Middle Valdaian glaciations, ice-dammed lakes and periglacial
1106 interstadials in northwest Russia: new evidence from the Pyoza River area. Glob. Planet. Change 31,
1107 215–237.
1108 Huscroft, C.A., 2002. Late Cenozoic history of the Yukon River Valley, Fort Selkirk to the Stevenson Ridge
1109 map area. PhD thesis, Simon Fraser University. Burnaby, British Columbia.
1110 Huscroft, C.A., Ward, B.C., Barendregt, R.W., Jackson Jr, L.E., Opdyke, N.D., 2004. Pleistocene volcanic
1111 damming of Yukon River and the maximum age of the Reid Glaciation, west-central Yukon. Can. J.
1112 Earth Sci. 41, 151–164.
1113 Isayeva, L.L., Kind, N.V., Laukhin, S.A., Kolpakov, V.V., Shofman, I.L., Fainer, Y.B., 1986. The stratigraphic
1114 scheme of the Quaternary of Central Siberia. Chetvertichnye oledeneniya Srednei Sibiri. Nauka, Moscow,
1115 4–17.
1116 Jackson, L.E., Andriashek, L.D., Phillips, F.M., 2011. Limits of successive Middle and Late Pleistocene
1117 continental ice sheets, interior plains of southern and central Alberta and adjacent areas. In Ehlers, J.
1118 Gibbard, P.L., Hughes, P.D. (Eds.), 2011, Quaternary Glaciations – Extent and Chronology, A Closer
1119 Look, Developments in Quaternary Science 15. Elsevier, Amsterdam, pp. 575–590.
1120 Johnson, W.H., Follmer, L., Gross, D.L., Jacobs, A.M., 1972. Pleistocene stratigraphy of the east-central
1121 Illinois. Illinois State Geological Survey Guidebook Series, 9, Illinois State Geological Survey. 1–97.
1122 Kajak, K., 1995. Map of the Quaternary Deposits of Estonia 1:2500000. Eesti Geoloogiakeskus. Tallinn. pp.
1123 26 (In Estonian).
1124 Kajak K., Raukas A., Hütt G., 1981. Experience in dating different-aged tills using thermoluminescence
1125 method. *In* Gaigalas, A., Jevzerov, V., Ivanova, L., Raukas, A., Ruhina, E. (Eds.). Pleistocene geology in
1126 northwestern part of the USSR, Kola Branch of the USSR Academy of Sciences, Apatity, pp. 3–11 (in
1127 Russian).
1128 Kalm, V., Raukas, A., Rattas, M., Lasberg, K., 2011. Pleistocene glaciations in Estonia. *In* Ehlers, J., Gibbard,
1129 P.L., Hughes, P.D. (Eds.). Quaternary Glaciations – Extent and Chronology, A Closer Look,
1130 Developments in Quaternary Science 15, Elsevier, Amsterdam, pp. 95–104.

Karabanov, A.K., Matveyev, A.V., 2011. The Pleistocene glaciations in Belarus. *In* Ehlers, J., Gibbard, P.L. and Hughes, P.D., 2011. Quaternary Glaciations – Extent and Chronology: A Closer Look, Developments in Quaternary Science 15. Elsevier, Amsterdam, pp. 29–35.

Kaufman, D.S., Manley, W.F., Forman, S.L., Layer. P.W., 2001a. Pre-late-Wisconsin glacial history, coastal Ahklun Mountains, southwestern Alaska – new amino acid, thermoluminescence, and 40Ar/39Ar results. Quat. Sci. Rev. 20, 337–352.

Kaufman, D.S., Manley, W.F., Wolfe, A.P., Hu, F.S., Preece, S.J., Westgate, J.A., Forman, S.L., 2001b. The last interglacial to glacial transition, Togiak Bay, southwestern Alaska. Quat. Res. 55, 190–202.

Kind, N.V. 1974. Late Quaternary Geochronology According to Isotopes Data. Nauka, Moscow, pp. 255 (in Russian).

Kind, N.V., Leonov, B.N., 1982. The Anthropocene of Taimyr (Antropogen Taimyra). Nauke, Moscow, 184 pp. (in Russian).

King, J.E., Saunders, J.J., 1986. Geochelone in Illinois and the Illinoian-Sangamonian vegetation of the type region. Quat. Res. 25, 89–99.

Kjaer, K.H., Larsen, E., Funder, S., Demidov, I., Jensen, M., Hakansson, L., Murray, A., 2006. Eurasian ice-sheet interaction in northwestern Russia throughout the late Quaternary. Boreas 35, 444–475.

Korsakova O.P., 2009. Pleistocene marine deposits in the coastal areas of Kola Peninsula (Russia). Quat. Int. 206, 3–15.

Krebetschek, M.R., Degering, D., Alexowsky, W., 2008. Ifrarot-Radiofluoreszenz-Alter (IR-RF) unter-saalezeitlicher Sedimente Mittel-und Ostdeutschlands. Zeitschrift der Deutschen Gesellschaft für Geowissenschaften 159, S.133–140.

Krzyszkowski, D., 2002. Sedimentary successions in ice-marginal fans of the Late Saalian glaciation, southwestern Poland. Sediment. Geol. 149, 93–109.

Lang, J., Winsemann, J., Steinmetz, D., Polom, U., Pollok, L., Böhner, U., Serangeli, J., Brandes, C., Hampel, A., Winghart, S., 2012. The Pleistocene of Schöningen, Germany: a complex tunnel valley fill revealed from 3D subsurface modelling and shear wave seismics. Quat. Sci. Rev. 39, 86–105.

Larsen, E., Kjær, K.H., Jensen, M., Demidov, I., Håkansson, L., Paus, A., 2006. Early Weichselian palaeoenvironments reconstructed from a mega-scale thrust-fault complex, Kanin Peninsula, northwestern Russia. Boreas 35, 476–492.

Lauhkin, S., Gaigalas, A., 2008. On the palaeoclimatic structure of MIS-5 analogues in the midland part of Siberia (palaeobotanical and U/Th dating data). Geologija 50,176–187.

Leonard, A.B., Frye, J.C., 1960. Wisconsinan molluscan faunas of the Illinois Valley region Ill. Geol. Surv. Circ. 304, 32.

Leonard, A.B., Frye, J.C., Johnson, W.H., 1971. Illinoian and Kansan molluscan faunas of Illinois Ill. State Geol. Surv. Circ. 461, 23.

Levina, T.P., 1964. Quaternary pollen spectra from the proglacial zone of the Samarovo ice sheet (the Yenissei catchment). Sistematika i metody izucheniya iskopayemykh pyltsy i spor. Nauka, Moscow, pp. 208–217.

Lewis, S.G., Rose, J. 1991. Tottenhill, Norfolk (TF 639 120). *In* Lewis, S.G., Whiteman, C.A., Bridgland D.R. (Eds.). Central East Anglia and the Fen Basin, Field Guide, Quaternary Research Association, London, pp. 145–148.

Lian, O.B., Hu, J., Huntley, D.J., Hicock, S.R., 1995. Optical dating studies of Quaternary organic-rich sediments from southwestern British Columbia and northwestern Washington State. Can. J. Earth Sci. 32, 1194–1207.

Lindner, L., Astapova, S.D., 2000. The age and geological setting of Pleistocene glacigenic beds around the border between Poland and Belarus. Geol. Quart. 44, 187–198.

Lindner L., Marks L., 1994. Pleistocene glaciations and interglacials in the Vistula, the Oder, and the Elbe drainage basins (Central European Lowland). Acta Geologica Polonica 44, 153–165.

Lindner, L., Marciniak, B., Sanko, A.A., Khursevich, G.K., 2001. The age of the oldest Scandinavian glaciations in mid-eastern Poland and southwestern Belarus. Geol. Quart. 45, 373–386.

Lippstreu, L., Brose, F., Marcinek, J., 1995. Brandenburg. Das Quartär Deutschlands, 116–147.

Litt, T., Behre, K.-E., Meyer, K.-D., Stephan, H.-J., Wansa, S., 2007. Stratigraphische Begriffe für das Quartär des norddeutschen Vereisungsgebietes. Eiszeitalter und Gegenwart 56, 7–65.

Loseva, E.I., Duryagina, D.A., 1983. Palaeobotanic evidence for stratigraphy of Cenozoic sediments of the central Pai-Hoi. Trudy Inst. Geol. Komi Branch Acad. Sci. Syktyvkar, USSR 43, pp. 56–68 (in Russian).

Ludwikowska-Kędzia, M., Pawelec, H., Adamiec, G., 2015. Sedimentological interpretation and stratigraphical position of glacigenic deposits in the Napęków area (Holy Cross Mountains, Poland). Geologos 21, 261–284.

Lunkka, J.P., Saarnisto, M., Gey, V., Demidov, I., Kiselova, V., 2001. Extent and age of the Last Glacial Maximum in the southeastern sector of the Scandinavian Ice Sheet. Glob. Planet. Change 31, 407–425.

Luethgens, C., Boese, M., Preusser, F., 2011. Age of the Pomeranian ice‐marginal position in northeastern Germany determined by Optically Stimulated Luminescence (OSL) dating of glaciofluvial sediments. Boreas 40, 598–615.

Lüthgens, C., Böse M., Krbetschek M., 2010a. On the age of the young morainic morphology in the area ascribed to the maximum extent of the Weichselian glaciation in north-eastern Germany. Quat. Int. 222, 72–79.

Lüthgens, C., Krbetschek, M.R., Böse, M., Fuchs, M.C., 2010b. Optically stimulated luminescence dating of fluvioglacial (sandur) sediments from north-eastern Germany. Quat. Geochron. 5, 237–243.

Lüthgens, C., Böse, M., Lauer, T., Krbetschek, M., Strahl, J., Wenske, D., 2010c. Timing of the last interglacial in Northern Europe derived from Optically Stimulated Luminescence (OSL) dating of a terrestrial Saalian–Eemian–Weichselian sedimentary sequence in NE-Germany. Quat. Int. 241, 79–96.

Maksimov, F.E., Laukhin, S.A., Arslanov, K.A., Kuznetsov, V.-Y., Shilova, G.N., Chernov, S.B., Zherebtsov, I.E., Levchenko, S.B., 2010. The first Uranium-Thorium dating of the Middle Neopleistocene peat in West Siberia. Doklady Earth Sciences 433, 915–919.

Mangerud, J., Gosse, J., Matiouchkov, A., Dolvik, T., 2008. Glaciers in the Polar Urals, Russia, were not much larger during the Last Global Glacial Maximum than today. Quat. Sci. Rev. 27, 1047–1057.

Mangerud, J., Astakhov, V., Svendsen, J.I., 2002. The extent of the Barents–Kara ice sheet during the Last Glacial Maximum. Quat. Sci. Rev. 21, 111–119.

Mangerud, J., Astakhov, V.I., Murray, A., Svendsen, J.I. 2001. The chronology of a large ice-dammed lake and the Barents-Kara Ice Sheet advances, Northern Russia. Glob. Planet. Change 31, 321–336.

Mangerud, J., Svendsen, J. I., Astakhov, V. I., 1999. Age and extent of the Barents and Kara ice sheets in Northern Russia. Boreas 28, 46–80.

McClenaghan, B., Seaman, A., Parkhill, M., Pronk, A., 2014. Till geochemical signatures associated with the Sisson W-Mo deposit, New Brunswick, Canada. Atlantic Geology 50, 116–137.

McCarroll, D., Stone, J.O., Ballantyne, C.K., Scourse, J.D., Fifield, L.K., Evans, D.J., Hiemstra, J.F., 2010. Exposure-age constraints on the extent, timing and rate of retreat of the last Irish Sea ice stream. Quat. Sci. Rev. 29, 1844–1852.

McKay, D., Berg, R.C., 2008, April. Optical ages spanning two glacial-interglacial cycles from deposits of the ancient Mississippi River, north-central Illinois. *In* Geol. Soc. Am. Abstr. 40, 78.

McKay, E.D., Berg, R.C., Hansel, A.K., Kemmis, T.J., Stumpf, A.J., 2008. Quaternary deposits and history of the ancient Mississippi River valley, north-central Illinois. Illinois State Geological Survey Guidebook, 35, Illinois State Geological Survey. Champaign, Illinois. 1–98.

Meng, S., Wansa, S., 2008. Sedimente und Prozesse am Außenrand der Saale-Vereisung südwestlich von Halle (Saale) [Sediments and processes at the borderline of Saalian glaciation southwest of Halle (Saale)]. Zeitschrift der Deutschen Gesellschaft für Geowissenschaften 159, 205–220.

1226 Mirecki, J.E., Miller, B.B., 1994. Aminostratigraphic correlation and geochronology of two Quaternary loess
1227 localities, central Mississippi Valley. Quat. Res. 41, 289–297.
1228 Möller, P., Hjort, C., Alexanderson, H., Sallaba, F., 2011. Glacial History of the Taymyr Peninsula and the
1229 Severnaya Zemlya Archipeligo, Arctic Russia. *In* J Ehlers, J., Gibbard, P.L., Hughes, P.D. (Eds.).
1230 Quaternary Glaciations – Extent and Chronology, A Closer Look, Developments in Quaternary Science
1231 15. Elsevier, Amsterdam, pp. 373–384.
1232 Möller, P., Fedorov, G., Pavlov, M., Seidenkrantz, M.-S., Sparrenbom, C., 2008. Glacial and
1233 palaeoenvironmental history of the Cape Chelyuskin area, Arctic Russia. Polar Res. 27, 222–248.
1234 Möller, P., Lubinski, D.J., Ingólfsson, O., Forman, S.L, Seidenkrantz, M.-S., Bolshiyanov, D.Y., Lokrantz, H.,
1235 Antonov, O., Pavlov, M., Ljung, K., Zeeberg, J.J., Andreev, A., 2007. Erratum to: Severnaya Zemlya,
1236 Arctic Russia: a nucleation area for Kara Sea ice sheets during the Middle to Late Quaternary [Quat. Sci.
1237 Rev. 25, 2894–2936]. Quat. Sci. Rev. 26, 1149–1191.
1238 Möller, P., Lubinski, D.J., Ingólfsson, Ó., Forman, S.L., Seidenkrantz, M.-S., Bolshiyanov, D.Y., Lokrantz, H.,
1239 Antonov, O., Pavlov, M., Ljung, K., Zeeberg, J.J., Andreev, A., 2006. Severnaya Zemlya, Arctic Russia: a
1240 nucleation area for Kara Sea ice sheets during the Middle to Late Quaternary. Quat. Sci. Rev. 25,
1241 2894–2936.
1242 Molodkov, A., 2001. ESR dating evidence for early man at a Lower Palaeolithic cave-site in the Northern
1243 Caucasus as derived from terrestrial mollusc shells. Quat. Sci. Rev. 20, 1051–1055.
1244 Molodkov A.N., Bolikhovskaya N.S., 2009. Climate change dynamics in Northern Eurasia over the last 200
1245 ka: evidence from mollusc-based ESR-chronostratigraphy and vegetation sucessions of the loess-
1246 palaeosol records. Quat. Int. 201, 67–76.
1247 Molodkov, A.N., Bolikhovskaya N.S., 2002. Eustatic sea-level and climate changes over the last 600 ka as
1248 derived from mollusc-based ESR-chronostratigraphy and pollen evidence in Northern Eurasia. Sediment.
1249 Geol. 150, 185–201.
1250 Murray, A., Buylaert, J.-P., Henriksen, M., Svendsen, J.-I., Mangerud, J., 2008. Testing the reliability of
1251 quartz OSL ages beyond the Eemian. Radiation Measurements 43, 776–780.
1252 Murray, A.S., Svendsen, J.I., Mangerud, J., Astakhov, V.I., 2007. Quartz OSL age of an Eemian site on the
1253 Sula River, northern Russia. Quat. Geochron. 2, 102–109.
1254 Nazarov, D.V., 2007. New data on Quaternary sediments in the central part of the West Siberian Arctic.
1255 Regionalnaya Geologia i Metallogenia 30/31, 213–221 (in Russian).
1256 Nazarov, D., Henriksen, M., 2010. New data on Quaternary stratigraphy of the Lower Yenissei area, Arctic
1257 Siberia. APEX Fourth International Conference and Workshop, University of Iceland, Höfn. pp. 62.

1258 Nelson, W.J., 2013, Surficial Geology of Carbondale Quadrangle, Jackson and Williamson Counties, Illinois:
1259 Illinois State Geological Survey, Illinois Geologic Quadrangle Map, IGQ Carbondale-SG, 1:24,000.
1260 O'Cofaigh, C.Ó., Telfer, M.W., Bailey, R.M., Evans, D.J., 2012. Late Pleistocene chronostratigraphy and ice
1261 sheet limits, southern Ireland. Quat. Sci. Rev. 44, 160–179.
1262 Occhietti, S., Long, B., Clet, M., Boespflug, X., Sabeur, N., 1995. Séquence de la transition Illinoien-
1263 Sangamonien: forage IAC-91 de l'île aux Coudres, estuaire moyen du Saint-Laurent, Québec. Can. J.
1264 Earth Sci. 32, 1950–1964.
1265 Pavlovskaya, I.E.P., 2000. The Middle and Late Pleistocene glacial-interglacial succession of eastern
1266 Belarus. Geol. Quart. 44, 199–204.
1267 Peeters, J., Busschers, F.S., Stouthamer, E., Bosch, J.H.A., Van den Berg, M.W., Wallinga, J., Versendaal,
1268 A.J., Bunnik, F.P.M., Middelkoop, H., 2016. Sedimentary architecture and chronostratigraphy of a late
1269 Quaternary incised-valley fill: a case study of the late Middle and Late Pleistocene Rhine system in the
1270 Netherlands. Quat. Sci. Rev. 131, 211–236.
1271 Philips, A.C., 2008. Surfical geology of New Athens West Quadrangle. Munroe and St. Claire Counties,
1272 Illinois. Illinois State Geological Survey. 1:10,000 (2 sheets).
1273 Phillips, A.C., 2004 Surficial Geology of Collinsville Quadrangle, Madison and St. Clair Counties, Illinois.
1274 Illinois State Geological Survey. Illinois Preliminary Geologic Map, IPGM Collinsville-SG, scale 1:24,000.
1275 Phillips, F.M., Zreda, M., Plummer, M.A., Elmore, D., Clark, D.H., 2009. Glacial geology and chronology of
1276 Bishop Creek and vicinity, eastern Sierra Nevada, California. Geol. Soc. Am. Bull. 121, 1013–1033.
1277 Phillips, W.M., Hall, A.M., Mottram, R., Fifield, L.K., Sugden, D.E., 2006. Cosmogenic 10 Be and 26 Al
1278 exposure ages of tors and erratics, Cairngorm Mountains, Scotland: timescales for the development of a
1279 classic landscape of selective linear glacial erosion. Geomorphology 73, 222–245.
1280 Preece, S.J., Pearce, N.J., Westgate, J.A., Froese, D.G., Jensen, B.J.L., Perkins, W.T., 2011. Old Crow
1281 tephra across eastern Beringia: a single cataclysmic eruption at the close of Marine Isotope Stage 6.
1282 Quat. Sci. Rev. 30, 2069–2090.
1283 Rattas, M., Kalm, V., Kihno, K., Liivrand, E., Tinn, O., Tänavsuu-Milkeviciene, K., Sakson, M., 2010.
1284 Chronology of Late Saalian and Middle Weichselian episodes of ice-free lacustrine sedimentation
1285 recorded in the Arumetsa section, southwestern Estonia. Estonian J. Earth Sci. 59, 125–140.
1286 Raukas, A., 1995. Properties, origin and stratigraphy of Estonian tills. Glacial Deposits in North-East Europe,
1287 93–101.
1288 Raukas, A., Kajak, K., 1997. Quaternary cover. Geology and mineral resources of Estonia, 125–136.
1289 Rose, J., 2009. Early and Middle Pleistocene landscapes of eastern England. Proc. Geol. Assoc. 120, 3–33.

Roskosch, J., Winsemann, J., Polom, U., Brandes, C., Tsukamoto, S., Weitkamp, A., Bartholomäus, W.A., Henningsen, D., Frechen, M., 2015. Luminescence dating of ice-marginal deposits in northern Germany: evidence for repeated glaciations during the Middle Pleistocene (MIS 12 to MIS 6). Boreas 44, 103–126.

Salamon, T., 2014. Basal till and subglacial conditions at the base of the Upper Odra ice lobe (southern Poland) during the Odranian (Saalian) Glaciation. Geol. Quart. 58, 779–794.

Scourse, J.D., Evans, D.J.A., Hiemstra, J., McCarroll, D., Rhodes, E., 2004. Late Devensian glaciation of the Isles of Scilly. Quat. Res. Assoc. Research Fund Report. Quaternary Newsletter 102, 49–54.

Sier, M.J., Peeters, J., Dekkers, M.J., Parés, J.M., Chang, L., Busschers, F.S., Cohen, K.M., Wallinga, J., Bunnik, F.P., Roebroeks, W., 2015. The Blake Event recorded near the Eemian type locality - a diachronic onset of the Eemian in Europe. Quat. Geochron. 28, 12–28.

Stauch, G., Gualtieri, L., 2008. Late Quaternary glaciations in northeastern Russia. J. Quat. Sci. 23, 545–558.

Stauch, G., Lehmkuhl, F., 2011. Extent and Timing of Quaternary Glaciations in the Verkhoyansk Mountains. *In* Ehlers, J., Gibbard, P.L., Hughes, P.D. (Eds.). Quaternary Glaciations – Extent and Chronology, A Closer Look, Developments in Quaternary Science 15. Elsevier, Amsterdam, pp. 877–881.

Stauch, G., Lehmkuhl F., 2010. Quaternary glaciations in the Verkhoyansk Mountains, Northeast Siberia. Quat. Res. 74, 145–155.

Stauch, G., Lehmkuhl, F., Frechen, M., 2007. Luminesence chronology from the Verkhoyansk Mountains (North-Eastern Siberia). Quat. Geochron. 2, 255–259.

Stea, R.R., Seaman, A.A., Pronk, T., Parkhill, M.A., Allard, S., Utting, D., 2011. The Appalachian Glacier Complex in Maratime Canada. *In* Ehlers, J., Gibbard, P.L., Hughes, P.D., (Eds.). Quaternary Glaciations – Extent and Chronology, A Closer Look, Developments in Quaternary Science 15. Elsevier, Amsterdam, pp. 631–660.

Stea, R.R., Piper, D.J.W., Fader, G.B.J., Boyd, R., 1998. Wisconsinan glacial and sea-level history of Maritime Canada and the adjacent continental shelf: a correlation of land and sea events. Geol. Soc. Am. Bull. 110, 821–845.

Stea, R.R., Mott, R.J., Belknap, D.F., Radtke, U., 1992. The pre–late Wisconsinan chronology of Nova Scotia, Canada. *In* Clark, P.U., Lea, P.D., (Eds.). The last interglaciation/glaciation transition in North America: Geol. Soc. Am. Spec. Pap. 270, pp. 185–206.

Stepanov, A.N., 1974. Stratigraphy and Sedimentary Environments of the Upper Cenozoic of the Pechora-Kama Interfluve. Resume of PhD thesis. Geological Faculty of Moscow University, 34 pp. (in Russian).

Stephan, H.J., 1980. Glazialgeologische Untersuchungen im südlichen Geestgebiet Dithmarschens.

Stroeven, A.P., Fabel, D., Margold, M., Clague, J.J., Xu, S., 2014. Investigating absolute chronologies of glacial advances in the NW sector of the Cordilleran Ice Sheet with terrestrial ß cosmogenic nuclides. Quat. Sci. Rev. 92, 429–443.

Stroeven A.P., Fabel, D., Codilean, A.T., Kleman, J., Clague, J.J., Miguens-Rodriguez ,M., Xu, S., 2010. Investigating the glacial history of the northern sector of the Cordilleran Ice Sheet with cosmogenic 10Be concentrations in quartz. Quat. Sci. Rev. 29, 3630–3643.

Stumpf, A.J., Dey, W.S., 2012. Understanding the Mahomet Aquifer: Geological, Geophysical, and Hydrogeological Studies in Champaign County and Adjacent Areas. Prairie Research Institute, Illinois State Geological Survey. Champaign, Illinois. 350 pp.

Svendsen, J.I., Alexanderson, H., Astakhov, V.I., Demidov, I., Dowdeswell, J.A., Funder, S., Gataullin, V., Henriksen, M., Hjort, C., Houmark-Nielsen, M., Hubberten, H.W., 2004. Late Quaternary ice sheet history of northern Eurasia. Quat. Sci. Rev. 23, 1229–1271.

Szabo, J.P., Totten, S.M., 1995. Multiple pre-Wisconsian glaciations along the northwestern edge of the Allegheny Plateau in Ohio and Pennsylvania. Can. J. Earth Sci. 32, 2081–2089.

Teed, R., 2000. A > 130,000-year-long pollen record from Pittsburg Basin, Illinois. Quat. Res. 54, 264–274.

Thomas, J.P., Murray, A.S., Kjaer, H., Funder, S., Larsen, E., 2006. Optically Stimulated Luminescence (OSL) dating of glacial sediments from Arctic Russia - depositional bleaching and methodological aspects. Boreas 35, 587–599.

Törnqvist, T.E., Wallinga, J., Busschers, F.S., 2003. Timing of the last sequence boundary in a fluvial setting near the highstand shoreline – insights from optical dating. Geology 31, 279–282.

Törnqvist, T.E., Wallinga, J., Murray, A.S., De Wolf, H., Cleveringa, P., De Gans, W., 2000. Response of the Rhine–Meuse system (west-central Netherlands) to the last Quaternary glacio-eustatic cycles: a first assessment. Glob. Planet. Change. 27, 89–111.

Van Gijssel, K., 1987. A lithostratigraphic and glaciotectonic reconstruction of the Lamstedt Moraine, Lower Saxony (FRG). *In* Houmark-Nielsen, M. (Ed.). Tills and glaciotectonics. Boreas 18, 145–155.

Velichko, A.A., Faustova, M.A., Pisareva, V.V., Gribchenko, Y.N., Sudakova, N.G., Lavrentiev, N.V., 2011. Glaciations of the East European Plain: distribution and chronology. *In* J Ehlers, J., Gibbard, P.L., Hughes, P.D., (Eds.). Quaternary Glaciations – Extent and Chronology, A Closer Look, Developments in Quaternary Science 15. Elsevier, Amsterdam, pp. 337–359.

von Poblozki, B., 1995. Quaternary geology of the Altmark region. *In* Ehlers, J., Kozarski, S., Gibbard, P.L. (Eds.), 1995. Glacial deposits in North-East Europe, Balkema, Rotterdam, Brookfield, pp. 473–484.

Wallinga, J., Törnqvist, T.E., Busschers, F.S., Weerts, H.J., 2004. Allogenic forcing of the late Quaternary Rhine‐Meuse fluvial record: the interplay of sea-level change, climate change and crustal movements. Basin Res. 16, 535–547.

Wang, H., Follmer, L.R., Liu, J.C.L., 2000. Isotope evidence of paleo–El Niño–Southern Oscillation cycles in loess-paleosol record in the central United States. Geology 28, 771–774.

Ward, B.C., Bond, J.D., Froese, D.G., Jensen, B., 2008. Old Crow tephra (140 ± 10 ka) constrains penultimate Reid glaciation in central Yukon Territory. Quat. Sci. Rev. 27, 1909–1915.

Waythomas, C.F., Lea, P.D., Walter, R.C., 1993. Stratigraphic context of Old Crow tephra, Holitna Lowland, interior southwest Alaska. Quat. Res. 40, 20–29.

Webb, N.D., Grimley, D.A., Phillips, A.C., Fouke, B.W., 2012. Origin of glacial ridges (OIS 6) in the Kaskaskia Sublobe, southwestern Illinois, USA. Quat. Res. 78, 341–352.

Westgate, J.A., Hamilton, T.D., Gorton, M.P., 1983. Old Crow tephra: a new late Pleistocene stratigraphic marker across north-central Alaska and western Yukon Territory. Quat. Res. 19, 38–54.

Włodarski, W., Godlewska, A., 2016. Sedimentary and structural evolution of a Pleistocene small-scale push moraine in eastern Poland: new insight into paleoenvironmental conditions at the margin of an advancing ice lobe. Quat. Sci. Rev. 146, 300–321.

Wood, J.R., Forman, S.L., Pierson, J., Gomez, J., 2010. New insights on Illinoian deglaciation from deposits of Glacial Lake Quincy, central Indiana. Quat. Res. 73, 374–384.

Zarkhidze, V.S., 1981. Stratigraphy and correlation of Pliocene and Pleistocene deposits. *In* Kamaletdinov, M.A., Yakhimovich, V.L., (Eds.). Pliotsen i pleistotsen Volgo-Uralskoi oblasti. Nauka, Moscow, pp. 7–28.

Zarkhidze, V.S., 1972. The Padimei formation of the western and central Timan-Uralian Region. *In* Yakhimovich, V. L., (Ed.). Voprosy Stratigrafii i Korrelatsii Pliotsenovykh i Pleistotsenovykh Otlozheniy Ssevernoi i Yuzhnoi Chastei Preduralya, 1, Bashkir Branch of Academy of Sciences of USSR, Ufa. pp. 56–66 (in Russian).

Zech, M., Andreev, A., Zech, R., Müller, S., Hambach, U., Frechen, M., Zech, W., 2010. Quaternary vegetation changes derived from a loess-like permafrost palaosol sequence in northeast Siberia using alkane biomarker and pollen analyses. Boreas 39, 540–555.

Zech, M., Zech, R., Zech, W., Glaser, B., Brodowski, S., Amelung, W., 2008. Characterisation and palaeoclimate of the loess-like permafrost palaeosol sequence in NE Siberia. Geoderma 143, 281–295.

Zhu, H., Baker, R.G., 1995. Vegetation and climate of the last glacial-interglacial cycle in southern Illinois, USA. J. Paleolim. 14, 337–354.

1383 Zubakov, V.A., 1972a. Recent Sediments of the West Siberian Lowland. Nedra, Leningrad. 312 pp. (in
1384 Russian).
1385 Zubakov, V.A. 1972b. Anthropogene Deposits of the West Siberian Lowland. Nedra, Leningrad, 312 pp. (in
1386 Russian).

Appendix 1c. Further detail on the GIA analysis

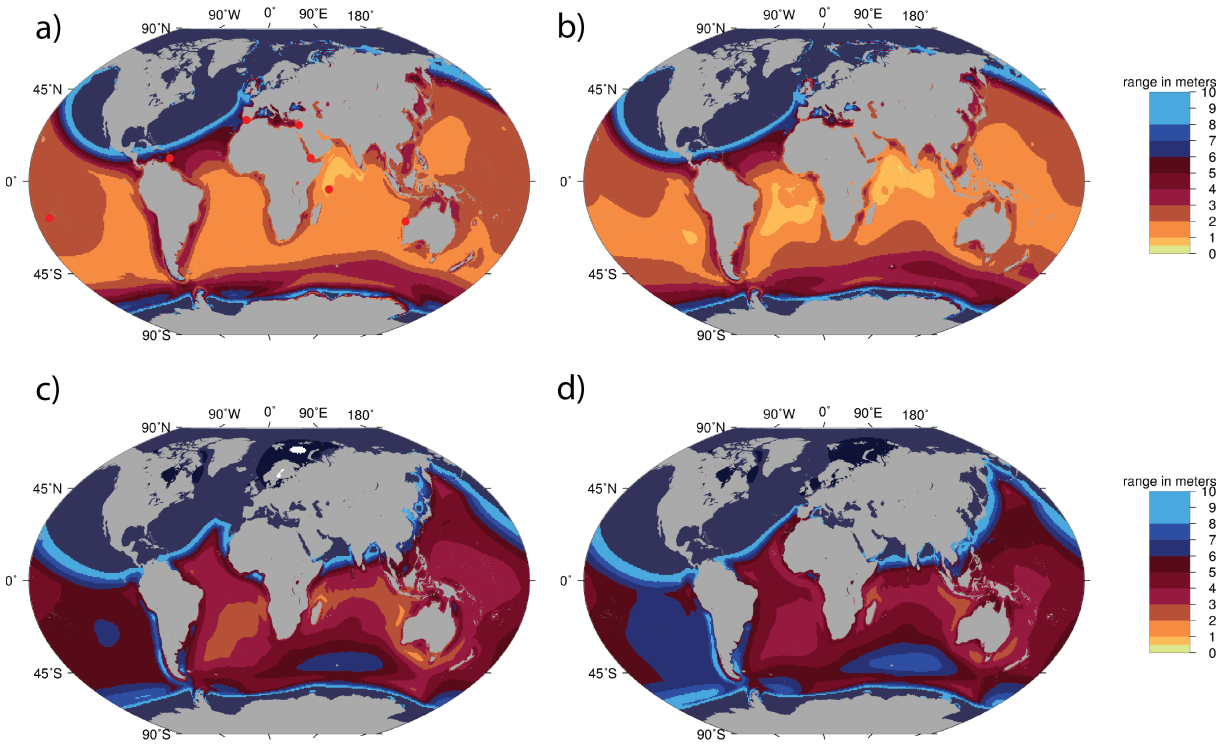

Figure A1. Range of peak MIS 5e interglacial relative sea levels due to choice of Earth model, for each modelled ice history. a. Output for ICE-1, **b.** for ICE-2, **c.** for ICE-3, and **d.** for ICE-4. Red dots in **a** indicate sea-level reconstruction sites referenced within this study. Each panel illustrates the range of sensitivity of sea-level reconstruction at any given location to the choice of Earth model, for each ice history. A far greater range of sensitivity exists for choice of Earth model during the LIG for ice histories that contain a larger EIS through the PGM (ICE-3 and ICE-4) than for ICE histories that infer an LGM-like PGM (ICE-1 and ICE-2).